Chemosphere 339 (2023) 139659

Contents lists available at ScienceDirect

Chemosphere

journal homepage: www.elsevier.com/locate/chemosphere

Generation and engineering applications of sulfate radicals in environmental remediation

Jun Xie [a], Chunping Yang [a,b,c,*], Xiang Li [b], Shaohua Wu [b,**], Yan Lin [a]

[a] College of Environmental Science and Engineering, Hunan University and Key Laboratory of Environmental Biology and Pollution Control (Hunan University), Ministry of Education, Changsha, Hunan, 410082, China
[b] Academy of Environmental and Resource Sciences, School of Environmental Science and Engineering, Guangdong University of Petrochemical Technology, Maoming, Guangdong, 525000, China
[c] School of Environmental and Chemical Engineering, Nanchang Hangkong University, Nanchang, Jiangxi, 330063, China

HIGHLIGHTS

- Various methods and mechanisms for activation of persulfate and sulfite were summarized.
- Reactivity of $SO_4.^{\bullet-}$ for degradation of various organic pollutants was described.
- Detection methods of $SO_4.^{\bullet-}$ were reviewed and commented.
- Applications of $SO_4.^{\bullet-}$-AOPs in various environmental remediation were discussed.

GRAPHICAL ABSTRACT

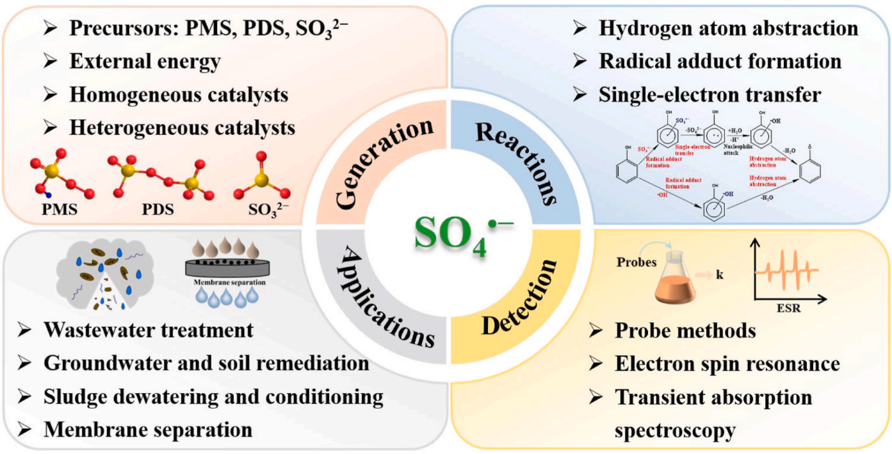

ARTICLE INFO

Handling Editor: Y Yeomin Yoon

Keywords:
Free radical
Reaction rate constant
Detection
Persulfate
Sulfite
Advanced oxidation process

ABSTRACT

Sulfate radical ($SO_4^{\bullet-}$)-based advanced oxidation processes (AOPs) have become promising alternatives in environmental remediation due to the higher redox potential (2.6–3.1 V) and longer half-life period (30–40 μs) of sulfate radicals compared with many other radicals such as hydroxyl radicals (•OH). The generation and mechanisms of $SO_4^{\bullet-}$ and the applications of $SO_4^{\bullet-}$-AOPs have been examined extensively, while those using sulfite as activation precursor and their comparisons among various activation precursors have rarely reviewed comprehensively. In this article, the latest progresses in $SO_4^{\bullet-}$-AOPs were comprehensively reviewed and commented on. First of all, the generation of $SO_4^{\bullet-}$ was summarized via the two activation methods using various oxidant precursors, and the generation mechanisms were also presented, which provides a reference for guiding

---

* Corresponding author. College of Environmental Science and Engineering, Hunan University and Key Laboratory of Environmental Biology and Pollution Control (Hunan University), Ministry of Education, Changsha, Hunan, 410082, China.
** Corresponding author.
E-mail addresses: yangc@hnu.edu.cn (C. Yang), wushaohua@hnu.edu.cn (S. Wu).

https://doi.org/10.1016/j.chemosphere.2023.139659
Received 10 June 2023; Received in revised form 20 July 2023; Accepted 25 July 2023

researchers to better select two precursors. Secondly, the reaction mechanisms of $SO_4^{\bullet -}$ were reviewed for organic pollutant degradation, and the reactivity was systematically compared between $SO_4^{\bullet -}$ and •OH. Thirdly, methods for $SO_4^{\bullet -}$ detection were reviewed which include quantitative and qualitative ones, over which current controversies were discussed. Fourthly, the applications of $SO_4^{\bullet -}$-AOPs in various environmental remediation were summarized, and the advantages, challenges, and prospects were also commented. At last, future research needs for $SO_4^{\bullet -}$-AOPs were also proposed consequently. This review could lead to better understanding and applications of $SO_4^{\bullet -}$-AOPs in environmental remediations.

1. Introduction

Recently, environmental problems including various industrial wastewater pollution, soil and groundwater pollution, and air pollution have not been solved satisfactorily, while pollution from many emerging contaminants has attracted close attention worldwide. There are many emerging contaminants including endocrine disruptors, pharmaceuticals and personal care products, disinfection by-products, microplastics, and antibiotics, most of which are characterized by toxicity, biological tolerance, or persistence (Luo et al., 2023; Zou et al., 2023). Usually, traditional biological and chemical treatment technologies such as the activated sludge process, biofilm-based process, and chemical coagulation could not achieve an accepted removal efficiency (Giannakis et al., 2021; Wang et al., 2023a). Therefore, the development of more efficient environmental remediation strategies has become a research focus.

Advanced oxidation processes (AOPs) are such a group of technologies of which the Fenton or Fenton-like reactions and persulfate-AOPs are the most frequently used. In these AOPs, various highly active species such as hydroxyl radicals (•OH) and sulfate radicals ($SO_4^{\bullet -}$) are generated which could degrade emerging contaminants into harmless or low-toxic products, including carbon dioxide and water (Lee et al., 2020; Lin et al., 2022). •OH are produced by the Fenton or Fenton-liked reaction, that is activating H_2O_2 precursors through conditions such as sound, light, electricity, and catalysts, but its short-lived, low selectivity, and pH dependence limit its effectiveness in environmental remediation (Wu et al., 2018b). Sulfate radicals-based advanced oxidation processes ($SO_4^{\bullet -}$-AOPs) have received increasing attention in recent years as a more efficient and stable environmental remediation technology (Ushani et al., 2020; Wu et al., 2022). $SO_4^{\bullet -}$ have strong oxidation ability and are widely used in environmental remediation, including wastewater treatment (Chen et al., 2020b), sludge dewatering and conditioning (Zhen et al., 2018), water disinfection (Wen et al., 2017), and membrane separation (Ye et al., 2021b).

The precursors of $SO_4^{\bullet -}$ are persulfate and sulfite, and various methods to activate them have been proposed. Energy-based activation methods such as heat, microwave, ultrasound, and ultraviolet can directly apply energy to break the peroxide bond to generate $SO_4^{\bullet -}$ (Chen and Huang, 2015; Zrinyi and Pham, 2017; Chen et al., 2020d). However, its high equipment investment and power cost decide that it can only play an auxiliary role in $SO_4^{\bullet -}$-AOPs. Cost-effective catalysts have gradually become the mainstream in the activation of persulfate and sulfite. Homogeneous catalysts have the advantages of fast reaction and high utilization rate. The use of non-toxic transition metal ions such as Fe^{2+} to activate persulfate and sulfite to generate $SO_4^{\bullet -}$ has been widely used in the treatment of actual wastewater (Liang et al., 2008). To improve the recovery and stability of catalysts, more and more heterogeneous catalysts, such as biochar, zero-valent metals, metal oxides, metal-organic framework derivatives, and single-atom catalysts have been developed, which have high catalytic efficiency. So far, the published reviews related to this content tend to describe the activation method and formation mechanism of persulfate, and lack the discussion on the activation mechanism of sulfite, another precursor of $SO_4^{\bullet -}$, especially the difference between the two precursors in $SO_4^{\bullet -}$-AOPs. Meanwhile, their mechanisms and specific applications in the process of $SO_4^{\bullet -}$ generation are rarely compared. In addition, systematic descriptions of the reactivity of $SO_4^{\bullet -}$ and its application status in various fields of environmental remediation have been poorly reported.

Based on the above gaps, this review summarizes the latest progress in the activation of persulfate and sulfite by external energy, homogeneous and heterogeneous catalysts, and compares the differences in the generation mechanism of $SO_4^{\bullet -}$ under different activation conditions. This provides a reference for researchers to choose the two precursors better. At the same time, the reactivity of $SO_4^{\bullet -}$ and •OH with pollutants was systematically compared, and the quantitative and qualitative detection methods of $SO_4^{\bullet -}$ were summarized. The existing disputes are also discussed. In addition, we also focused on the application status of $SO_4^{\bullet -}$ in environmental remediation, including industrial wastewater treatment, groundwater and soil remediation, sludge dewatering and conditioning, water disinfection, membrane separation, and air purification, and proposed the main challenges and solutions of $SO_4^{\bullet -}$-AOPs in future applications.

2. Characteristics of sulfate radicals

$SO_4^{\bullet -}$ are a kind of highly active free radical produced by persulfate or sulfite as a precursor under the activation condition of external energy or catalyst. Table 1 shows a comparison of redox potentials of $SO_4^{\bullet -}$ with other common reactive species. It can be seen that $SO_4^{\bullet -}$ is a strong oxidant compared to other reactive species, with a redox potential of 2.6–3.1 V (Lee et al., 2020). The half-life of $SO_4^{\bullet -}$ is 30–40 μs, which is higher than that of •OH whose half-life is less than 1 μs (Oh et al., 2016). A longer half-life means better interaction with the target pollutant and higher free radical utilization (Ushani et al., 2020). $SO_4^{\bullet -}$ are more selective and tends to preferentially react with electron-rich compounds. The reaction rate constant with compounds containing electron-donating groups (amino, hydroxyl, etc.) is four orders of magnitude larger than that with compounds containing electron-withdrawing groups (nitro, carboxyl, etc.), and its reaction rate range with aromatic compounds is much greater than •OH (the reaction rate constant of aromatic compounds with •OH ranges from 2.0×10^9 to 1.0×10^{10} $M^{-1}s^{-1}$, while the reaction rate constant with $SO_4^{\bullet -}$ ranges from 1.0×10^6 $M^{-1}s^{-1}$ to 6.0-8.0 $\times 10^9$ $M^{-1}s^{-1}$) (Wojnarovits and Takacs, 2019). •OH is pH-dependent, and its reactivity decreases with increasing pH, but the reactivity of $SO_4^{\bullet -}$ is independent of pH, which means that it has better environmental adaptability. In addition, when $pH > 9$, the main oxidant will be converted from $SO_4^{\bullet -}$ to •OH through single-electron oxidation ($k = 6.5 \times 10^7$ $M^{-1}s^{-1}$), and this change may make $SO_4^{\bullet -}$-AOPs better for the degradation of organic pollutants due to the low selectivity of •OH (Oh et al., 2016; Lee et al., 2020). $SO_4^{\bullet -}$ has a lower reaction rate with dissolved organic matter (DOM) than •OH ($k_{SO4\bullet -+DOM} = 6.8 \times 10^3$ $mgC^{-1}s^{-1}$ and $k_{\bullet OH\ +\ DOM} = 1.4 \times 10^4$

Table 1
Redox potentials of common reactive species.

Reactive species	Redox potentials, E^0 (V)	References
$SO_4^{\bullet -}/SO_4^{2-}$	2.6–3.1	Lee et al. (2020)
$SO_3^{\bullet -}/SO_3^{2-}$	0.75	Das et al. (1999)
$SO_5^{\bullet -}/SO_5^{2-}$	0.12	Das et al. (1999)
$\bullet OH/H_2O$	2.7	Schwarz and Dodson (1984)
$^{\bullet}O_2^-/H_2O_2$	0.89	Wood (1988)
$^1O_2/^{\bullet}O_2^-$	0.83	Stanbury (1989)
$\bullet HO_2^-/H_2O_2$	1.44	Stanbury (1989)
$Fe_{aq}^{IV}O^{2+}/Fe$ (III)	1.95	Wang et al. (2022b)

$mgC^{-1}s^{-1}$), so $SO_4^{\bullet-}$ has a higher contaminant removal efficiency in the presence of NOM (Lutze et al., 2015). However, compared with •OH, common anions (especially halogen ions) have a greater scavenging effect on $SO_4^{\bullet-}$, which is due to the by-products generated by the reaction of •OH with halogen ions are reconverted to •OH under neutral conditions. Although halogen anions react with $SO_4^{\bullet-}$ to form halogen radicals with a lower redox potential ($E^0(Cl^{\bullet}/Cl^-) = 2.5V$; $E^0(Cl_2^{\bullet-}/Cl^-) = 2.2$ V; $E^0(Br^{\bullet}/Br^-) = 2.0$ V; $E^0(Br_2^{\bullet-}/Br^-) = 1.7$ V), the higher selectivity of these halogen radicals can lead to efficient degradation of specific pollutants in complex circumstances (Zhang and Parker, 2018).

3. Generation of sulfate radicals

3.1. Production from persulfate

Persulfate are similar to hydrogen peroxide in that both have peroxide bonds, with sulfonic acid groups ($-SO_3$) replacing one hydrogen atom in H_2O_2 to form HSO_5^- and two hydrogen atoms in H_2O_2 to form $S_2O_8^{2-}$. Therefore, persulfate can be divided into permonosulfate (PMS) and perdisulfate (PDS) based on the number of sulfonic acid groups connected by their peroxide bonds. External energy and electron transfer can break the O–O bond in persulfate, resulting in the production of highly reactive $SO_4^{\bullet-}$ and/or •OH (Fig. 1). However, different activation methods have a great influence on the free radical yield of PMS and PDS. This difference is due to their different molecular structures (Oh et al., 2016; Lee et al., 2020), On the one hand, compared with PDS, the molecular structure of PMS is asymmetric, resulting in uneven charge distribution, which makes PMS more easily activated by the catalyst to generate $SO_4^{\bullet-}$. On the other hand, the two sulfonic groups in the PDS further elongate the O–O bond, resulting in a longer bond than a PMS with only one sulfonic group, which makes the PDS easier to activate by external energy. Therefore, different activation methods will lead to different effects of PMS and PDS in environmental remediation. In this section, we will discuss the specific mechanisms of activation of persulfates by external energy (heat, microwave, ultrasound, and ultraviolet), homogeneous and heterogeneous catalysts, summarize the advantages and limitations of various activation methods, and make some suggestions for further investigation.

3.1.1. Activation of persulfate by external energy

The activation of persulfates by external energy is mainly achieved by breaking their peroxide bonds. The activation effect mainly depends on the bond energy of the peroxide bond. As shown in Table 2, among the three peroxides, the O–O bond energy of PDS is the smallest and the bond energy of H_2O_2 is the largest, which means that PDS and PMS are more easily activated by external energy. External energies include heat, microwaves, ultrasound, and ultraviolet light. Next, we will briefly introduce the various external energy activation mechanisms of persulfate and the status of their application in persulfate activation alone.

Thermal activation causes the peroxide bonds of PMS and PDS to break to form $SO_4^{\bullet-}$ and/or •OH by increasing the solution temperature and inputting energy in the form of heat (Li et al., 2022b). Many industrial wastewaters, such as desulfurization wastewater, have a large amount of waste heat, which can be used for thermal activation persulfate, with higher feasibility and practical operation. PDS has good pollutant removal efficiency even at lower temperatures (>50 °C), while PMS is hardly activated. Even if the temperature rises to 80 °C, the degradation efficiency of acid orange 7 is still very low (Yang et al., 2010). This may be due to the higher O–O bond energy of PMS than PDS. The oxidation efficiency of thermal activation is highly dependent on temperature. The higher the temperature, the more external energy input, and the more persulfate is activated. The promotion effect of too high temperature on persulfate activation is also controversial. The

Table 2
Properties of PDS, PMS, and H_2O_2.

Properties	PDS	PMS	H_2O_2
Formula	$S_2O_8^{2-}$	HSO_5^-	H_2O_2
Molecular weight (g/mol)	192	113	34.0
Redox potential (V)	2.01	1.82	1.78
Solubility (g/L, at 25 °C)	730	298	–
O–O bond distance (Å)	1.50	1.45	1.46
O–O bond energy (kJ/mol)	140	140–213	213
Quantum yield of radical generation	1.80	0.52	1.0

The data was taken from Li et al. and Yang et al. (Yang et al., 2019b; Li et al., 2022b).

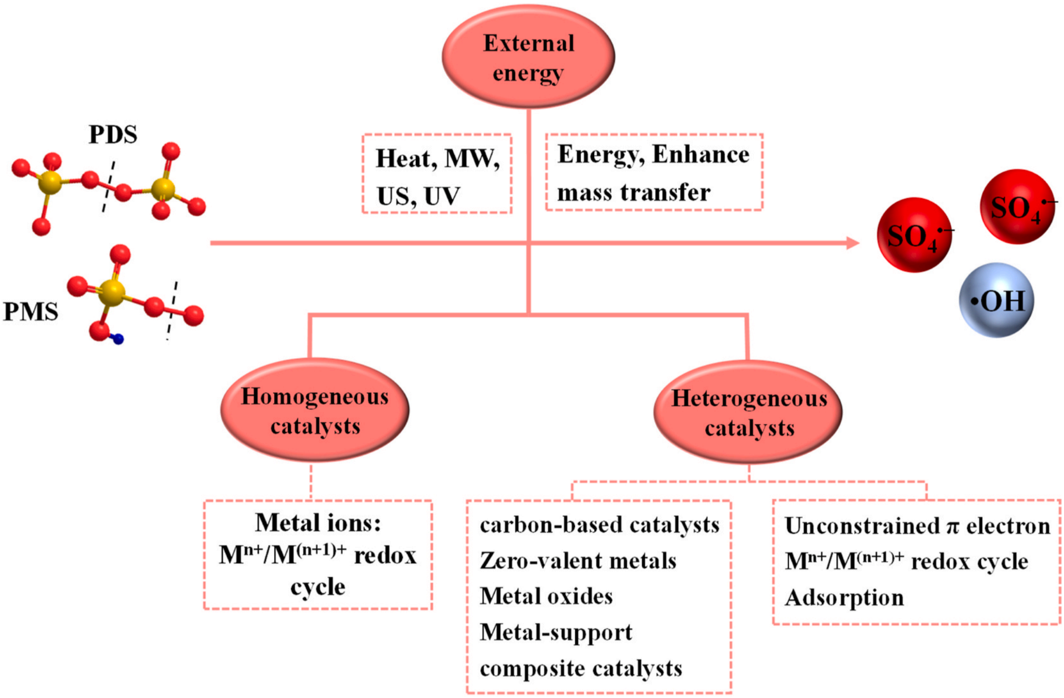

Fig. 1. Activation mechanism of persulfate.

increase of temperature (e.g., 80 °C) will accelerate the release of $SO_4^{\bullet -}$, leading to the excessive production of free radicals, which will lead to the self-quenching reaction of free radicals (Xu et al., 2016; Li et al., 2022b). In practical applications, it is necessary to reasonably set the thermal activation temperature to avoid the low utilization of oxidants due to insufficient activation efficiency and the waste of free radicals at high temperatures. In addition, studies have shown that temperature not only affects the yield of $SO_4^{\bullet -}$, but also affects the transformation pathway and product distribution of pollutants. In the heat/PDS/benzoic acid system, with the increase of thermal activation temperature, the decarboxylation of benzoic acid is gradually the main process (Zrinyi and Pham, 2017). Similarly, with the increase of temperature, the reaction mechanism of sulfate radicals on phenol will also change. At room temperature, the degradation products of sulfate radicals on phenol are mainly hydroxyl benzene and oxidized open chain products, while the thermal activation of persulfate at 70 °C will not lead to the mineralization of phenol but to the formation of polymer-type products (Mora et al., 2011). In addition, temperature also affects the proportion of iodide and bromide disinfection products in water (Chu et al., 2016).

Microwave (MW) is also an effective method to activate persulfate. The mechanism of microwave heating is to make solution molecules vibrate rapidly and violently in the alternating electric field of the microwave, thereby realizing the transformation from microwave to heat energy (Li et al., 2022b; Xia et al., 2022a). The heat is generated from the inside to the outside of the system, which is more uniform and faster than direct heat conduction. Compared with conventional heating, MW heating can well reduce the reaction activation energy and improve the utilization rate of persulfate (Hu et al., 2019). Research shows that MW can effectively activate PMS at a lower temperature than direct heating, which well demonstrates the advantages of microwave heating (Qi et al., 2017). Microwave heating is a reverse heating mode, and the microwave effect caused by it can effectively heat the solution to activate persulfate. However, the corresponding microwave equipment requires a large investment, so it is generally used as an auxiliary means in $SO_4^{\bullet -}$-AOPs water treatment.

Ultrasound (US) is a mechanical wave with a frequency of more than 20,000 Hz and a wavelength of less than 2 cm. Ultrasound activation of persulfate is achieved through the cavitation process, that is, local high temperature and pressure are formed through the formation, growth, and collapse of the cavity, thus causing the fracture of O–O bond in persulfate to produce $SO_4^{\bullet -}$ (Yang et al., 2019a). In addition to activation, the violent turbulence caused by ultrasound also accelerated the reaction process. The $SO_4^{\bullet -}$ signal detected by electron paramagnetic resonance (EPR) demonstrated the effective activation of persulfate by US (Li and Zhu, 2016). Although US can be used alone to degrade specific pollutants, the synergistic effect of US and persulfate oxidation will form a large amount of highly active $SO_4^{\bullet -}$, which is conducive to the efficient degradation of more pollutants (Rayaroth et al., 2015). Ultrasound can also be used to enhance the activation of persulfate. With the assistance of ultrasound, the concentration of $SO_4^{\bullet -}$ in the system is significantly enhanced (Chen and Huang, 2015). The US has the dual role of persulfate activation and enhanced mass transfer compared with other activation methods, but ultrasound/persulfate is more energy intensive, which hinders its large-scale application.

Ultraviolet (UV) light is an electromagnetic wave with a wavelength of 10–400 nm. Only ultraviolet with the wavelength of 254 nm (UV_{254}) can effectively activate persulfate. For UV_{254}, there are two common types of lamps: low-pressure and medium-pressure mercury vapor lamps. Low-pressure (LP) mercury lamps can only emit monochromatic UV light at 254 nm, while medium-pressure (MP) mercury lamps emit UV light in the range of 200–300 nm (Ao and Liu, 2017). The O–O bonds of PMS, PDS, and H_2O_2 can all break under UV to form $SO_4^{\bullet -}$ and/or •OH, and their combination with UV can effectively degrade pollutants. Under the irradiation of an MP mercury lamp, the activation efficiency follows UV/PMS > UV/PDS > UV/H_2O_2 (Ao and Liu, 2017). Other studies have found that PDS activation is most efficient when LP mercury lamps are used (Yang et al., 2010). This may be related to the target pollutants, some of which have a certain light absorption capacity and can be photodissociated directly. In addition, visible light (>400 nm) can also activate PDS to generate $SO_4^{\bullet -}$ through the photosensitization of some dyes. For example, Rhodamine B (RhB) will be excited to form RhB* under visible light irradiation, and further activate PDS through RhB* (Gao et al., 2017). This may inspire PDS activation under visible light.

Activating persulfate through external energy introduced above has been proven to be effective, but when the scale of pollutant treatment increases, the corresponding treatment cost will increase significantly, which is the key problem hindering its large-scale application. In the current research, heat, microwave, ultrasound, and ultraviolet are often used together with the catalyst for the activation of persulfate, which can save energy consumption and maximize the use of persulfate. We will introduce this in detail in 3.1.2 and 3.1.3.

3.1.2. *Activation of persulfate by homogeneous catalysts*

Although the homogeneous catalyst has the disadvantages of being difficult to recover and easily causing secondary pollution, when the catalyst used is non-toxic to the environment and the cost is low, the homogeneous catalyst has its unique advantages, such as fast reaction rate and high utilization rate. As a transition metal, Co^{2+} has a high redox potential ($E^0(Co^{3+}/Co^{2+}) = 1.92$ V, $E^0(Mn^{3+}/Mn^{2+}) = 1.54$ V, $E^0(Fe^{3+}/Fe^{2+}) = 0.77$ V, $E^0(Cu^{2+}/Cu^{+}) = 0.17$ V) (Anipsitakis and Dionysiou, 2004). In many studies, it has been proved to be the best metal element for PMS activation. For example, Zhang et al. synthesized a very efficient and stable persulfate activator through the incorporation of cobalt, and achieved complete removal of 10 μmol/L pollutants in 5 min (Zhang et al., 2022a). However, due to the potential carcinogenic effect of cobalt compounds, the practical application of homogeneous Co^{2+} still has some limitations (Han et al., 2022).

Iron is often used as a homogeneous catalyst to activate persulfate to generate $SO_4^{\bullet -}$ for environmental remediation due to its abundant reserves on earth and its advantages of being environmentally friendly (Xiao et al., 2020). In Fe(II/III)/PDS system, ferrous ions transfer electrons to persulfate, resulting in the breaking of peroxide bonds to generate $SO_4^{\bullet -}$ and •OH (Eqs. (1)–(3)) (Rastogi et al., 2009; Zhu et al., 2016; Xiao et al., 2020). However, there are also three unavoidable problems in this homogeneous system:(i) the scavenging effect of Fe^{2+} on sulfate radicals; (ii) it is difficult to convert Fe^{3+} into Fe^{2+}, resulting in excessive accumulation of Fe^{3+}; (iii) the system has strict pH requirements, which limits its application. Fortunately, some studies are using chelating and reducing agents to change this defect. Han et al. (2015) adjusted the accessibility between Fe^{2+} and PDS by using different kinds of chelating agents and adjusting the ratio between chelating agents and Fe^{2+}, which achieved a decomposition rate of 91.7% for PDS at an initial pH = 9. In this study, the chelating agent stabilizes Fe^{2+} by utilizing its steric hindrance effect, preventing the consumption of $SO_4^{\bullet -}$ by Fe^{2+} to a certain extent. Liang et al. (2008) studied the effect of different complexing agents such as hydroxypropyl-β-cyclodextrin, ethylenediaminetetraacetic acid, and citric acid on maintaining effective Fe^{2+} and activating PDS to degrade benzene, and the citric acid was found to be the most effective chelating agent in the system, which may be related to the moderate molecular structure and good chelating ability of citric acid. For the problem that Fe^{3+} is difficult to reduce to Fe^{2+}, the addition of a reducing agent can promote the conversion of Fe^{3+} to Fe^{2+} to achieve fast cycling between them. Studies have shown that the addition of hydroxylamine can accelerate the conversion of Fe^{3+} to Fe^{2+} in the Fe^{2+}/PMS system, thereby realizing the rapid degradation of benzoic acid (Zou et al., 2013). Similarly, Zhou et al. (2013) found that $Na_2S_2O_3$ can act as both a chelating agent and a reducing agent, to maintain the concentration of iron, and as a reducing agent to accelerate the conversion of Fe^{3+} to Fe^{2+}, respectively.

$$Fe^{2+} + S_2O_8^{2-} \rightarrow Fe^{3+} + SO_4^{\cdot -} + SO_4^{2-}, k = 3 \times 10^1 M^{-1} s^{-1} \quad (1)$$

$$Fe^{2+} + HSO_5^- \rightarrow Fe^{3+} + SO_4^{\cdot -} + OH^-, k = 3 \times 10^4 M^{-1} s^{-1} \quad (2)$$

$$Fe^{2+} + HSO_5^- \rightarrow Fe^{3+} + SO_4^{2-} + \cdot OH \quad (3)$$

3.1.3. Activation of persulfate by heterogeneous catalysts

Heterogeneous catalysts have the advantages of strong adaptability, convenient recovery, and low environmental pollution that homogeneous catalysts do not have. In this section, we will introduce the similarities and differences in the mechanism of activating persulfate to generate sulfate radicals from metal catalysts, carbon-based catalysts, and metal-supported carbon-based catalysts.

Non-metallic carbon-based catalysts can not only completely avoid the environmental pollution caused by metal dissolution, but also have the advantages of huge surface area and easy modification (Liu et al., 2015b; Oh et al., 2016; Ushani et al., 2020). Activated carbon (AC), graphene oxide (GO), carbon nanotubes (CNTs), and biochar (BC) are increasingly used to activate persulfate to degrade pollutants. AC has good adsorption and catalytic surface functional groups, so it is often used for non-metallic catalysts to activate various oxidants (H_2O_2, PMS, PDS). It was found that powdered activated carbon had the best degradation effect on phenol when PMS was used as oxidant (Saputra et al., 2013b). The mechanism of AC activation of persulfate mainly involves π electron transfer on the AC surface, and AC acts like Fe^{2+} in the Fenton reaction, acting as a carrier for electron transfer (Eq. (4) and (5)) (Liang et al., 2009b; Yang et al., 2011). However, after activating persulfate, the increase of AC surface acidity and the decrease of surface area will lead to the weakened adsorption between pollutants and oxidants, which makes AC lack good catalytic regeneration performance (Dąbrowski et al., 2005; Zhang et al., 2013a; Yang et al., 2015). In addition, combining the semiconductor material C_3N_4 with activated carbon can further improve the catalytic activity of AC. Wei et al. (2016) used an in situ thermal method to support graphitic carbon nitride on activated carbon (g-C_3N_4/AC), and the exposure of N-$(C)_3$ groups in g-C_3N_4 further enhanced the electron density and surface alkalinity of AC, thereby increasing the stability and catalytic ability of AC.

$$ACsurface - OOH + S_2O_8^{2-} \rightarrow SO_4^{\cdot -} + ACsurface - OO + HSO_4^- \quad (4)$$

$$\mathrm{ACsurface - OOH + S_2O_8^{2-} \rightarrow SO_4^{\cdot -} + ACsurface - O\cdot + HSO_4^-} \quad (5)$$

Carbon nanotubes (CNTs) are a kind of coaxial circular tubes composed of several to dozens of layers of carbon atoms arranged in a hexagonal arrangement. The surface can be greatly increased by the number of surface functional groups by chemical treatment such as acid and heat, thereby increasing the active sites (Ren et al., 2011). Defect sites such as vacancies and non-hexacarbonyl rings in carbon nanotubes, zigzag edges with unconstrained π electrons, and Lewis basic groups such as ketone and quinone (C=O) groups at the defect edges of nanocarbon are greatly reduced (Kong et al., 2014; Duan et al., 2015b). The electron transfer from CNTs to persulfate is enhanced, and eventually leads to the generation of $SO_4^{\bullet -}$ and •OH.

The doping of heteroatoms (N, S, B, etc.) also further changes the surface charge density, which creates defects and forms active sites (Zhao et al., 2013; Duan et al., 2015b; Liu et al., 2016b). Studies have shown that N-doped single-walled carbon nanotubes exhibit an astonishing reaction rate of 57.4 times faster than undoped carbon nanotubes, which is consistent with the high asymmetric spin of adjacent carbon atoms caused by N-doping with higher electronegativity and smaller covalent radius (Deng et al., 2011; Duan et al., 2015b). In addition, nitrogen doping can also significantly enhance the catalytic effect of graphene by increasing the free electron flux density and specific surface area of graphene (Liang et al., 2017). Kang et al. (2016) achieve nitrogen doping and reduction of graphene oxide by hydrothermal method, the prepared metal-free N-doped rGO can efficiently activate persulfate to generate reactive radicals to degrade antibiotics. Further, Duan et al. (2015a) prepared an N, S co-doped reduced graphene oxide with much higher catalytic activity than GO, rGO, S-doped rGO, and N-doped rGO, and using various characterization techniques and density functional theory (DFT) calculations to demonstrate that co-doped rGO can efficiently activate sp^2 hybridized carbon lattices and facilitate electron transfer from covalent graphene sheets to activate PMS.

There are also some studies using relatively inexpensive biochar (BC) to activate persulfate to degrade pollutants, whose catalytic activity is derived from the marginal pyridinic and pyrrolic N configurations in biochar (Fang et al., 2015; Wang et al., 2019b). In short, non-metallic carbon-based materials have the advantages of metal materials that are difficult to compare, that is, no metal dissolution, non-toxic, however, the decrease of activity caused by the change of surface properties after each use is still a problem to be overcome.

Metal-based catalysts have very high catalytic efficiency for persulfate, which is difficult to achieve with non-metallic carbon-based materials. The activation mechanism of zero-valent metal, mono-/bimetallic oxide, and metal-support composite catalysts for persulfate will be introduced respectively. In the current study, the active components of metal catalysts used to activate persulfate are mostly transition metal elements (Mn, Fe, Co, Ni, Cu). And their activation mechanisms are similar, that is, through the conversion between different valence states of transition metals, the peroxide bond of persulfate is broken and finally $SO_4^{\bullet -}$ are generated.

Compared with the homogeneous Fe^{2+} system in the previous section, Ji et al. (2013) developed a porous Fe_2O_3 particle to achieve high-efficiency removal of rhodamine within pH = 5–11, effectively overcoming the limitation of pH on the homogeneous system. When porous Fe_2O_3 is in contact with PMS, Fe^{3+} sites are reduced to Fe^{2+} by PMS, and $SO_5^{\bullet -}$ is generated at the same time. The generated Fe^{2+} is oxidized to Fe^{3+} while activating PMS to generate $SO_4^{\bullet -}$, and at the same time, the cycle of iron species and the generation of free radicals are realized. In addition, due to the high redox potential of $SO_4^{\bullet -}$ (2.6–3.1 V), part of $SO_4^{\bullet -}$ can oxidize water to form •OH (1.9–2.7 V). At the same time, metal oxides such as Mn_2O_3, Fe_3O_4, and Co_3O_4 also have similar catalytic activities and reaction mechanisms (Anipsitakis et al., 2005; Saputra et al., 2013a; Tan et al., 2014). In addition, for zero-valent metals (nano zero valent iron (nZVI), nano zero valent copper (nZVC), etc.), are first oxidized by O_2 and persulfate to intermediate valence ions (Fe^{2+}, Cu^+), and then activated persulfate in a similar manner to metal oxides to produce $SO_4^{\bullet -}$ and •OH (Ghanbari et al., 2014; Zhou et al., 2018b).

Bimetallic catalysts made by replacing part of the active sites in iron oxide with other metal ions have also been increasingly used in persulfate activation recently. The valence state conversion between ions accelerates the activation efficiency of persulfate. Magnetic Fe_3O_4–MnO_2 core-shell nanocomposites show higher activity compared to pure MnO_2, Fe_3O_4, and physical mixtures of Fe_3O_4 and MnO_2 (Liu et al., 2015a). Its high activity originates from a synergistic effect due to the different standard redox potentials between the two metals (Eq. (6) and (7)), which accelerate the cycling of each in activated persulfate. Similarly, a type of $CuFe_2O_4$ magnetic nanoparticles also showed excellent catalytic performance in persulfate activation, 10 mg/L tetrabromobisphenol A in the presence of 0.1 g/L $CuFe_2O_4$ magnetic nanoparticles and 0.2 mmol/L PMS was completely removed within 30 min (Ding et al., 2013), and its high activity was also related to the cooperative transformation between Cu^{2+}/Cu^+ and Fe^{3+}/Fe^{2+} (Eq. (6) and (8)). It can be seen that the use of bimetallic catalysts can not only combine the advantages of two single-metal catalysts, but also speed up the cycle between different metal valence states, and finally achieve efficient activation of persulfate. In addition, the design of electron-rich oxygen vacancies in metal active sites can also significantly promote the cycling between metals of different valence states, providing a new idea for efficient catalyst design (Bao et al., 2023).

$$Fe^{3+} + e^- \rightarrow Fe^{2+}, E^0 = 0.77V \quad (6)$$

$$Mn^{4+} + e^- \rightarrow Mn^{3+}, E^0 = 0.15V \tag{7}$$

$$Cu^{2+} + e^- \rightarrow Cu^+, E^0 = 0.17V \tag{8}$$

Non-metallic carbon-based materials solve the problem of easy dissolution of metal catalysts, but their catalytic activity and stability limit their wide-ranging applications. Therefore, combining metal materials with non-metallic carbon materials, on the one hand, carbon materials are used as carriers to stabilize and disperse metal nanoparticles to inhibit metal dissolution, and on the other hand, metals are introduced to further adjust the electronic structure of the carbon region to increase its activity and stability (Huang et al., 2021). Recently, studies have shown that the composite of metal and carbon materials can efficiently and stably activate persulfate to degrade pollutants. Liu et al. (2019) prepared carbon-borne cobalt composites by carbonizing saturated resin with cobalt ions at high temperatures, which showed good catalytic activity in activating PMS to produce $SO_4^{\bullet-}$ and •OH to degrade trimethoprim. The catalytic activity of carbon-borne cobalt originates from the mutual conversion of Co^{2+}/Co^{3+} and the electron transfer of oxygen-containing functional groups in the carbon substrate. In addition, Khan et al. (Abdul Nasir Khan et al., 2019) synthesized a hollow carbon-supported ultrafine Co_3O_4 nanoparticle with more than twice the catalytic activity of solid carbon-supported Co_3O_4 nanoparticle by etching pyrolysis of ZIF-67.

Similar to elemental cobalt, iron-containing composites are also widely used in persulfate activation. Combining nZVI with mesoporous carbon can effectively inhibit the aggregation and oxidation of zero-valent iron, thereby greatly improving the utilization of zero-valent iron (Jiang et al., 2018b; Li et al., 2020b). Biochar-loaded magnetic iron oxide (nFe_3O_4/biochar) material can also activate persulfate efficiently. Because biochar can not only better disperse Fe_3O_4 particles, but also adsorb pollutants, which has a synergistic effect (Dong et al., 2017). As mentioned before, bimetallic catalysts can accelerate the valence conversion between two metals to increase catalytic activity, so loading bimetals into carbon materials can also play a similar accelerating effect. For example, cobalt-iron nanocomposite carbon materials have been shown to have higher catalytic activity in activated persulfate, while exhibiting good durability and recyclability (Lin and Chen, 2017; Outsiou et al., 2017).

Metal-support composites can combine the advantages of metal catalysts and carbon-based materials, and have good cycling stability while possessing low metal leaching. However, compared to metal nanoparticle-support composites, single-atom catalysts (SACs) have the largest atom utilization efficiency, tunable electronic structures, superior structural stability, and high-performance metal active sites (Shang et al., 2021; Wang et al., 2023b,c). Elements such as nitrogen, phosphorus, and sulfur are easier to coordinate with transition metals with vacant orbitals because of their lone pair electrons, and on the other hand, because of their greater electronegativity, they are more likely to change the electron density on the carbon substrate and produce more active sites, so they are usually doped on the support as heteroatoms to synthesize single-atom catalysts (Wang et al., 2019a; Huang et al., 2021).

Gao et al. (2021) prepared a single-atom iron catalyst by the cascade anchoring method, which can completely degrade 100 μM of bisphenol A in 3 min. It is one of the most active catalysts in persulfate-based AOPs. The high activity of single-atom iron catalyst originates from the Fe−pyridine N_4 moiety, which can generate not only an electron-rich Fe single atom as the active site but also eight electron-deficient C atoms next to the pyridine N as the catalytic site, thereby greatly enhancing the Increase the number of active sites to activate PMS to generate $SO_4^{\bullet-}$. In addition, the regulation of metal-nitrogen coordination number in single-atom catalysts can be achieved at different calcination temperatures, and Liang et al. (2022) obtained Co–N_4 and Co–N_3 single-atom cobalt catalysts at calcination temperatures of 800 °C and 900 °C, respectively. Reducing the coordination number from 4 to 3 can significantly increase the electron density of Co single atoms, thereby improving the conversion of PDS and generating more $SO_4^{\bullet-}$.

In addition to nitrogen, B and P can also be doped into single-atom catalysts as heteroatoms to control the electron density of active sites. Zhou et al. (2022) achieved the regulation of the electronic structure of Cu–N_4 by doping electron-deficient boron or electron-rich phosphorus heteroatoms into the catalyst. Experimental results and DFT calculations showed that the electron-deficient Cu–N_4/C–B catalyst induced the best adsorption energy of PMS, while the electron-rich Cu–N_4/C and Cu–N_4/C–P showed strong PMS binding, leading to active site poisoning. SACs is an ideal candidate for Fenton-like reactions due to its high metal utilization, tunable electronic structure and excellent activity, However, there are also some drawbacks, such as reduced stability due to leaching of active metals, application limitations due to a limited pH range, and harsh synthesis methods (Xu et al., 2022). Furthermore, the specific mechanism of the influence of heteroatom doping and different coordination number on the final generation of active species is still unclear, and further research on the intrinsic activation mechanism is needed.

The introduction of electrochemical technology into persulfate-based advanced oxidation can achieve higher oxidant utilization and better pollutant removal efficiency. In the electrochemical/persulfate system, the role of electrochemistry is mainly to promote the valence cycle of active metals in the catalyst and the direct electron transfer of persulfate to generate $SO_4^{\bullet-}$. The electrochemically assisted Fe(III)-chelator-persulfate system can achieve efficient removal of pollutants at neutral pH. In this system, the Fe(III)-chelator complex can be continuously electro-reduced to Fe(II) at the cathode, which ensures efficient and continuous activation of persulfate, thereby achieving high yield of $SO_4^{\bullet-}$ and rapid removal of pollutants (Xiong et al., 2021). The electrochemical activation of persulfate with sacrificial iron anode can avoid the additional addition of iron source, and its treatment efficiency is better than that of Fe^{2+}/PMS system (Gao et al., 2022b). In addition, the catalytic electrode prepared by loading highly active catalysts on carriers with good conductivity and large specific surface area by solvothermal method or electrodeposition method also has excellent catalytic performance and stability (Xie et al., 2023). For example, Xie et al. (2022) prepared a bimetallic modified nickel foam anode, which achieved a tetracycline removal rate of 93.05% within 1 h by activating PMS. In the electrochemical/persulfate system, the current density has a great influence on the activation of persulfate. Studies have shown that with the increase of current density, the $SO_4^{\bullet-}$ and •OH generated in the system can also activate persulfate (Li et al., 2022c).

In summary, PMS and PDS can be activated in various ways to produce $SO_4^{\bullet-}$. It is worth noting that under different activation modes, the persulfate system can derive other active species (•OH, $^1O_2$, $O_2^{\bullet-}$), and these active species can be converted to each other (Li et al., 2022a; Qi et al., 2023). Between them, •OH can be generated either by the cleavage of the peroxide bond of PMS or by the reaction of $SO_4^{\bullet-}$ with H_2O. PMS sometimes loses an H atom to generate $SO_5^{\bullet-}$ under catalysis, and the generated $SO_5^{\bullet-}$ can both react with O_2 to generate $O_2^{\bullet-}$ and spin itself to generate $^1O_2$ (Wang et al., 2022a). Recent studies have shown that $^1O_2$ and $O_2^{\bullet-}$ have other production pathways. Xie et al., 2022, 2023 combined quenching experiments and the electron paramagnetic resonance (EPR) to prove that $SO_4^{\bullet-}$ is the main contributor to other reactive oxygen species, $O_2^{\bullet-}$ can be produced by the hydrolysis of $SO_4^{\bullet-}$ and the electrochemical oxygen reduction process, and $^1O_2$ is mainly produced by the disproportionation of $O_2^{\bullet-}$.

External energy can effectively activate persulfate and strengthen mass transfer at the same time, but the construction and operation cost of supporting facilities is high. The reaction rate of homogeneous catalyst activating PMS is fast and the utilization rate is high, but it is faced with the problem of excessive discharge of metal ions. Heterogeneous catalysts such as monometallic/bimetallic catalysts and metal-support composite catalysts overcome the above shortcomings, but their synthesis steps often involve high temperature, high pressure and expensive reagents. These complex operations increase the cost and risk of catalysts. Therefore, it is necessary to select relatively suitable treatment conditions and catalysts according to specific application conditions. At present, the development of metal-supported catalysts with simple synthesis steps and cost-effective is the key to the practical application of $SO_4^{\bullet-}$-AOPs.

3.2. Production from sulfite

Although PMS and PDS are often chosen as precursors of $SO_4^{\bullet-}$, There are also some studies starting to use catalysts to activate lower-cost sulfites (SO_3^{2-}) to generate sulfate radicals for pollutant degradation. The activation process of sulfite is through the formation of a metal/carbon-sulfite complex, and then in the presence of O_2, the complex decomposes to produce $SO_3^{\bullet-}$, which in turn undergoes a series of reactions to produce $SO_4^{\bullet-}$ (Figs. 2 and 3). Compared with persulfate, sulfites as a desulfurization byproduct have the advantages of low cost, low toxicity and easy preparation, which should be another important aspect of environmental remediation using $SO_4^{\bullet-}$ (Wu et al., 2021).

3.2.1. Activation of sulfite by external energy

Unlike persulfate, sulfite does not contain a peroxide bond, and the external energy cannot make it produce $SO_4^{\bullet-}$ through the bond fracture. However, sulfite has a strong ultraviolet absorption capacity. At pH 7.5, the molar absorption coefficient of UV_{254} is 15.2 $M^{-1}cm^{-1}$ (Vellanki and Batchelor, 2013). As shown in Eqs. 9–13, sulfite first decomposes into hydrated electrons (e_{aq}^-) and $SO_3^{\bullet-}$ under UV. The former is converted to •H with hydrogen-containing substances, while the latter gradually converts $SO_3^{\bullet-}$ into $SO_4^{\bullet-}$ in the presence of O_2. e_{aq}^- and •H are strong reducing species and are used for dehalogenation in advanced reduction processes.

UV/sulfite process is often used as oxidation-reduction coupling process for dehalogenation and mineralization of pollutants. Song et al. (2023) studied the reductive the dechlorination and oxidative mineralization of 2,4-dichlorophenol in the explosion-free UV/sulfite process. The reductive active species (e_{aq}^- and •H) are responsible for converting 2,4-dichlorophenol into dechlorination products, and $SO_4^{\bullet-}$ further mineralizes it. The mineralization rate is higher than that of the nitrogen aeration system. In electrode electrolysis, the anode will produce a lot of O_2, which provides a good condition for the conversion of $SO_3^{\bullet-}$ in the UV/sulfite system. The electrolysis-assisted UV/sulfite process can provide sufficient oxygen for the generation of $SO_4^{\bullet-}$ in the system. At the same time, the generated H^+ avoids acid addition, realizes the automatic adjustment of pH and dissolved oxygen, and is an environmentally friendly and low-cost water treatment process (Chen et al., 2021). It should be noted that the sulfite concentration will have a great impact on pollutant removal, and excessive sulfite will consume active species (Eq. (14)) (Cao et al., 2021). There are few studies on the production of $SO_4^{\bullet-}$ by ultraviolet-activated sulfite, and most of them study the UV/sulfite process as an advanced reduction process.

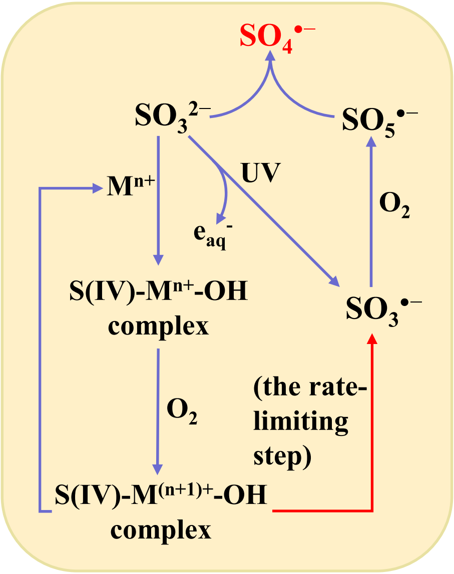

Fig. 2. Activation mechanism of sulfite by metal catalyst.

$$HSO_3^- \Big/ SO_3^{2-} + h\nu \rightarrow SO_3^{\cdot -} + e_{aq}^- \tag{9}$$

$$e_{aq}^- + HSO_3^- \Big/ H^+ \Big/ H_2O \rightarrow \cdot H + SO_3^{2-} \Big/ OH^- \tag{10}$$

$$SO_3^- + O_2 \rightarrow SO_5^-, k = 2.3 \times 10^9 M^{-1} S^{-1} \tag{11}$$

$$SO_5^- + HSO_3^- / SO_3^{2-} \rightarrow SO_4^- + SO_4^{2-}, k = 1.2 \times 10^4 M^{-1} S^{-1} \tag{12}$$

$$SO_5^- + SO_5^- \rightarrow 2SO_4^- + O_2, k = 6 \times 10^8 M^{-1} S^{-1} \tag{13}$$

$$SO_4^- + HSO_3^- / SO_3^{2-} \rightarrow SO_4^{2-} + SO_3^- \tag{14}$$

3.2.2. Activation of sulfite by homogeneous catalysts

It is difficult for sulfite to generate sulfate radicals by itself, which needs to undergo auto-oxidation under the catalysis of transition metals (Mn(II), Co(II), Ni(II), Cu(II), Cr(III/VI)) to generate oxygen-containing sulfur radicals. Specifically, when $M^{(n-1)+}$is added to the sulfite system, an M^{n+} -SO_3^{2-} complex is immediately formed, which is then oxidized by O_2 to $M^{(n+1)+}$-SO_3^{2-} complex, which undergoes electron transfer and finally decomposes into M^{n+} and $SO_3^{\bullet-}$, $SO_3^{\bullet-}$ combines with O_2 to form $SO_5^{\bullet-}$, which will further self-oxidize with sulfite to form $SO_4^{\bullet-}$ (Zhou et al., 2018a). Studies have shown that in Fe(II)/sulfite systems, the rate-limiting step is the decomposition of Fe(III)-sulfite complexes (k = 0.91 s^{-1}) (Lente and Fabian, 2002). In addition, UV–Vis as an external energy can also promote the activation of sulfite by homogeneous catalysts. Zhang et al. (2013b) studied the decolorization of Orange II by Fe (II)-sulfite system under UV–Vis irradiation and proved that UV–vis irradiation can greatly promote the decolorization of Orange II solution by Fe(II)-sulfite system. Meanwhile, the initial working pH increased from 4 to 6.1, which will greatly reduce processing costs. The key to the generation of $SO_4^{\bullet-}$ is the internal cycle of Fe^{2+}/Fe^{3+} in the Fe(II)/sulfite system. However, a part of $SO_5^{\bullet-}$ and $SO_4^{\bullet-}$ will be used for the conversion between Fe(III) and Fe(II) (Eqs. 15–19) (Yang et al., 2009; Wu et al., 2021), which reduced degradation efficiency of target pollutants. Wang et al. (2021a) also achieved 100% removal of sulfamethoxazole by utilizing $SO_4^{\bullet-}$ and •OH generated by UV/Fe^{3+}/sulfite system. In this system, NO_3^- can significantly increase the reaction rate because it can generate additional free radicals through photosensitization. However, matrix effects and pH dependence are urgent issues in the system.

$$Fe^{2+} + SO_5^- + H^+ \rightarrow Fe^{3+} + HSO_5^-, k = (4.3 \pm 2.4) \times 10^7 M^{-1} s^{-1} \tag{15}$$

$$Fe^{2+} + HSO_5^- \rightarrow Fe^{3+} + SO_4^- + OH^-, k = 1.0 \times 10^3 M^{-1} s^{-1} \tag{16}$$

$$Fe^{2+} + SO_4^- \rightarrow Fe^{3+} + SO_4^{2-}, k = 8.6 \times 10^8 M^{-1} s^{-1} \tag{17}$$

$$SO_5^- + SO_3^{2-} \rightarrow SO_4^{2-} + SO_4^-, k = 9 \times 10^6 M^{-1} s^{-1} \tag{18}$$

$$SO_5^- + HSO_3^- \rightarrow HSO_4^- + SO_4^-, k = 2.5 \times 10^4 M^{-1} s^{-1} \tag{19}$$

In addition to the use of metal-activated sulfites to degrade pollutants, the reductive removal of heavy metals can also be achieved by utilizing the metal cycle therein. Yuan et al. (2016) achieved a rapid reduction of Cr(VI) and simultaneous oxidative removal of contaminants in the Cr (VI)/sulfite system. This provides a good solution for the treatment of organic wastewater containing heavy metals (Jiang et al., 2018a). Compared with Cr(VI) or Fe(II)/sulfite system, the oxidative capacity of

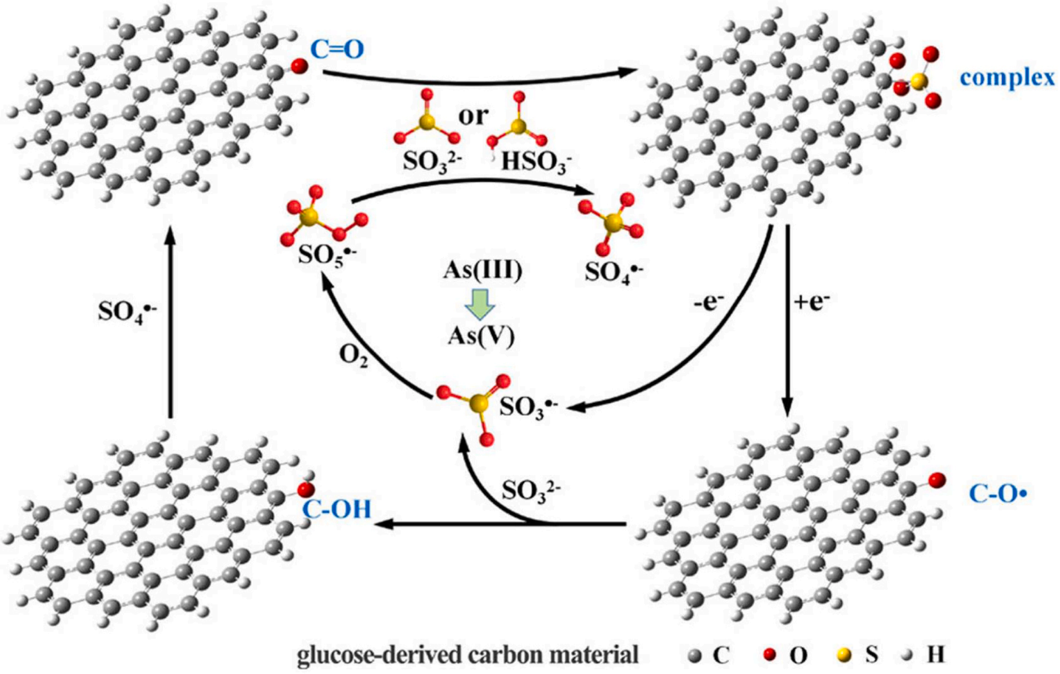

Fig. 3. Activation mechanism of sulfite by carbon catalyst. Reproduced from Ref (Zhang et al., 2021).

the Co(II)/sulfite system exhibits higher pH independence. Yuan et al. (2018) achieved rapid degradation of paracetamol by Co(II) catalyzed sulfite under alkaline pH. This is due to the different ratios of HSO_3^-/SO_3^{2-} in the solution at different pH, as shown in Eqs. (18) and (19) (Yuan et al., 2018; Wang et al., 2021a), the reaction rate of $SO_5^{\bullet -}$ and SO_3^{2-} produced by sulfite auto-oxidation is faster than that of HSO_3^-. While in neutral or alkaline conditions, sulfites always exist in the form of SO_3^{2-} (pKa = 7.2).

3.2.3. *Activation of sulfite by heterogeneous catalysts*

Homogeneous catalysts inevitably suffer from low catalyst recovery and secondary pollution due to metal leaching. Based on the above considerations, many heterogeneous catalysts (carbon materials, nanovalent iron, metal oxides, spinel, metal-carbon support composite catalysts, etc.) have been developed to activate sulfites. They have the advantages of high stability, low metal leaching rate, and easy recovery.

Recent studies have found that the defect structure and oxygen-containing functional groups (C═O, C–OH) on the surface of carbon materials contribute to the formation of $SO_4^{\bullet -}$ in sulfite activation (Zhang et al., 2021; Hung et al., 2022). On the one hand, the C element of ketonic groups in carbon materials can be complex with sulfites. On the other hand, the defective structure of carbon materials enhances its conductivity and provides a driving force for electron transfer inside the sulfite-carbon material complex, which eventually leads to the generation of ketone oxygen radicals and oxygen sulfur radicals. The latter further reacts with O_2 to form $SO_4^{\bullet -}$, which realizes the activation of sulfites (Fig. 3) (Zhang et al., 2021).

Similar to persulfates, transition metals and their oxides also play an important role in sulfite activation. Xie et al. (2017) developed an oxygen-containing Fe^0/sulfite system to achieve efficient degradation of pollutants in weakly acidic and neutral environments. In this system, the sulfate radicals that are produced by the reaction between metal-sulfite complexes and oxygen are the main active species. Studies have shown that compounding zero-valent iron with its oxide helps to improve sulfite activation efficiency, Yang et al. (2020b) prepared a $Fe@Fe_2O_3$ core-shell nanomaterial, which greatly promoted the cycling of Fe^{2+} and Fe^{3+}, thereby accelerating the generation of $SO_4^{\bullet -}$ and •OH, and achieved the efficient removal of Orange II under wide pH. Spinel ferrites (MFe_2O_4, M = Mg, Mn, Ni, Zn, Fe, Co) have also been used in sulfite activation systems as novel heterogeneous catalysts due to their unique ferromagnetic properties (Yang et al., 2009; Wu et al., 2021). Liu et al. (2017) used a $CoFe_2O_4$ nanocatalyst to activate sulfites to degrade pollutants and demonstrated that the formation of Co–OH complexes on the surface of $CoFe_2O_4$ is crucial for the generation of sulfate radicals. Additionally, studies have shown that combining external energy with spinel-type ferrite can also further improve catalytic performance. Huang et al. (2018) demonstrated that under the activation of UV–visible light, the generated photogenerated holes favored the oxidation of sulfite and accelerated the decomposition of metal-sulfite complexes on the surface of ZnCu-ferrite, thereby increasing the catalytic efficiency. However, in addition to the target pollutants, $SO_4^{\bullet -}$ also have higher reaction rates with sulfites (7.5×10^8 $M^{-1}s^{-1}$) (Zhou et al., 2018a). In the sulfite activation system, the amount of sulfite should be controlled to avoid the internal reaction of $SO_4^{\bullet -}$.

Furthermore, the metal-carbon material composite catalyst can achieve more efficient sulfite activation. Zhao et al. (2023) synthesized micron-sized iron-carbon composites to achieve efficient degradation of metronidazole. The introduction of carbon into ZVI can significantly enhance its corrosion and release more Fe^{2+} for the activation of sulfite. Similarly, the Co@NC catalyst prepared by encapsulating cobalt nanoparticles inside carbon nanotubes exhibits high efficiency, excellent repeatability, and stability for the catalytic oxidation of methyl orange in the presence of sulfite and O_2. The synergistic effect of internal cobalt nanoparticles and external carbon enhances catalytic degradation (Wu et al., 2018a).

As mentioned above, both persulfate and sulfite can be used as precursors of $SO_4^{\bullet -}$ production, Fig. 4 shows the advantages and disadvantages of the two precursors as well as their applicable ranges, which is conducive to better selection. In addition, they are different in activation mechanism, activation methods, and application scenarios. First, their activation means and $SO_4^{\bullet -}$ production mechanism are different. The details are as follows: (i) Unlike the activation of persulfate under UV, the activation of sulfite by UV is due to its strong UV absorption capacity. (ii) The catalytic effect of metal-based catalysts on persulfate and sulfite is essentially achieved by different valence transformations of metal ions. However, unlike persulfate activation, the metal-sulfite

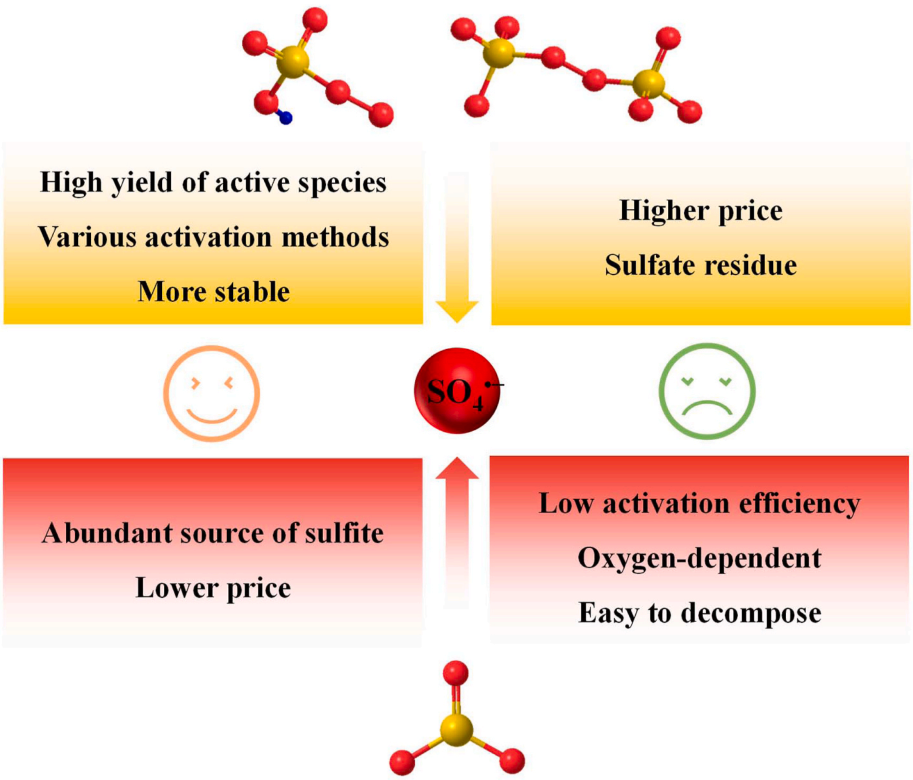

Fig. 4. Comparison of the advantages and disadvantages of persulfate and sulfite in $SO_4^{\bullet-}$-AOPs.

complex needs to be formed during sulfite activation. (iii) In sulfite activation, $SO_4^{\bullet-}$ cannot be directly generated by sulfite activation, but must first form $SO_3^{\bullet-}$ as an intermediate active species, and then oxidize to $SO_4^{\bullet-}$ under the action of O_2. Secondly, in the process of sulfite activation, reducing active species (hydrated electrons (e_{aq}^-) and hydrogen radicals (•H)) are generated at the same time. They have different degradation mechanisms and kinetics, which may lead to different degradation products and intermediates toxicity from sulfite-based $SO_4^{\bullet-}$-AOPs in environmental remediation. Finally, compared with persulfate, sulfite has a lower cost and is more conducive to the industrial application of $SO_4^{\bullet-}$-AOPs. However, the formation of $SO_4^{\bullet-}$ in sulfite activation needs to be in an aerobic environment. Therefore, sulfite-based $SO_4^{\bullet-}$-AOPs are suitable for aerated water or oxygen-rich environments.

4. Reaction mechanisms of sulfate radicals

Although the reactions of $SO_4^{\bullet-}$ with different pollutants have different intermediate products and reaction kinetics, in the process of oxidizing pollutants, the following three reactions are inseparable: (i) hydrogen atom abstraction (HAA), (ii) radical adduct formation (RAF), (iii) single electron transfer (SET) (Fig. 5) (Chen et al., 2020a; Zhang et al., 2023a). The difference is the priority of the reaction pathways and kinetics when oxidizing different kinds of pollutants. The single-electron transfer and radical adduct formation reactions of $SO_4^{\bullet-}$ with pollutants have faster second-order reaction rate constants than hydrogen atom abstraction, while •OH is more prone to radical adduct formation (Xiao et al., 2015). For different kinds of pollutants, $SO_4^{\bullet-}$ and •OH have different reaction pathways and kinetics, which leads to different

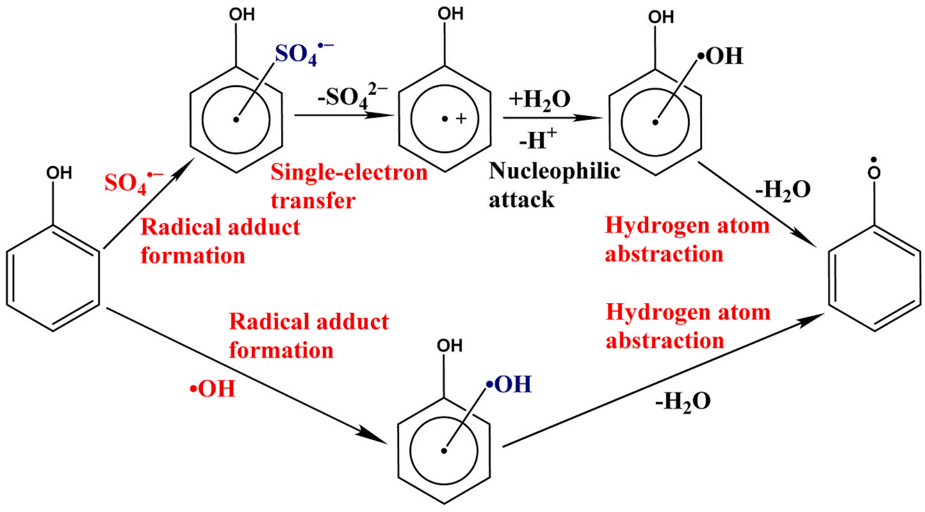

Fig. 5. Oxidation pathways of benzene ring-containing substances by hydroxyl radicals and sulfate radicals.

degradation mechanisms and the generation of intermediates (Li et al., 2020a). Recently, Zhang et al. (2023a) systematically proposed a theoretical calculation method for the dynamic analysis of the electronic structure of free radicals attacking organic pollutants in the active region for the first time. This method identifies the reactive sites of pollutants by pollutant degradation path and DFT calculation. In this section, the general rules and characteristics of the reaction of $SO_4^{\bullet-}$ with organic substances (aliphatic compounds and aromatic compounds) are introduced by comparing the reactivity similarities and differences with •OH.

4.1. Hydrogen atom abstraction

HAA reaction is the process by which free radicals extract a hydrogen atom from a pollutant molecule. Compared with the HAA reaction of $SO_4^{\bullet-}$ with corresponding compounds, the HAA reaction of •OH with pollutants is more thermodynamically feasible. Aromatic compounds and molecules containing amine and amides moieties react with $SO_4^{\bullet-}$ generally by single electron transfer, while hydrogen atom abstraction generally occurs on the C–H bond of aliphatic compounds (Xiao et al., 2015; Wojnarovits and Takacs, 2019). Li et al. (2018b) used DFT calculations to demonstrate that din-butyl phthalate catalyzed degradation was caused by HAA and RAF on the aliphatic chain, and •OH was more reactive to the H-removal reaction than $SO_4^{\bullet-}$. This conclusion is also verified in the reactions of $SO_4^{\bullet-}$ and •OH with crown ethers, which react with crown ethers through HAA to generate ether radicals, and the reaction rate constant increases linearly with the number of H atoms in crown ethers (Wan et al., 2012). For example, when crown ethers (12-crown-4 (12C4), 15-crown-5 (15C5), 18-crown-6 (18C6)) and their analogs 1,4-dioxane (6C2) reacted with $SO_4^{\bullet-}$ and •OH, their rate constants increased as the alkyl chain increased, and the rate constant of $SO_4^{\bullet-}$ is one to two orders of magnitude smaller than that of •OH. The reaction rate constants of $SO_4^{\bullet-}$ with 6C2, 12C4 and 18C6 are $6.6 \pm 0.1 \times 10^7\ M^{-1}s^{-1}$, $2.3 \pm 0.1 \times 10^8\ M^{-1}s^{-1}$ and $4.2 \pm 0.1 \times 10^8\ M^{-1}s^{-1}$, respectively, while the reaction rate constants of •OH with them are $3.4 \pm 0.2 \times 10^9\ M^{-1}s^{-1}$, $7.2 \pm 0.2 \times 10^9\ M^{-1}s^{-1}$ and $10.9 \pm 0.2 \times 10^9\ M^{-1}s^{-1}$, respectively (Wan et al., 2012).

The HAA reaction is closely related to the bond length of C–H and the charge density of H atoms. Likewise, the longer the C–H bond is, the fewer positive charges the removed hydrogen atoms carry, and the HAA reaction is more likely to occur (Wang et al., 2021b,c). In addition, due to the certain electrophilic properties of HAA channels, the presence of some electron-donating groups, such as allyl, hydroxyl, and carboxyl groups, will also facilitate the HAA reaction of $SO_4^{\bullet-}$ with organics (Lee et al., 2020; Wang et al., 2021b,c). However, in terms of the degradation of halogenated organic compounds, $SO_4^{\bullet-}$ achieves efficient dehalogenation of aliphatic halogenated compounds by removing hydrogen atoms and breaking C–C bonds, and its reaction rate is 10 times that of •OH (Hou et al., 2017).

4.2. Radical adduct formation

$SO_4^{\bullet-}$ and •OH can react with contaminants through the RAF path. In the RAF reaction, the unpaired electrons of $SO_4^{\bullet-}$ and •OH are transferred to the bonding orbital of the compound, resulting in the orbital breaking and the formation of two new σ orbitals, thereby forming a free radical adduct (Zhang et al., 2023a). Pollutants are converted into intermediates with smaller molecular weight by RAF reaction. However, $SO_4^{\bullet-}$ has a higher electrophilic index and larger steric hindrance, which makes it exhibit different addition behavior from •OH. The lower energy barrier of $SO_4^{\bullet-}$ makes RAF react faster than •OH, but the larger steric hindrance of $SO_4^{\bullet-}$ reduces the stability of the radical addition products (Zhang et al., 2023a). In the RAF reaction with aromatic rings and olefinic double bonds, the mechanisms of $SO_4^{\bullet-}$ and •OH are similar, that is, •OH can directly generate •OH adducts with it. However, when attacked by $SO_4^{\bullet-}$, it needs to overcome an additional radical adduct formation step, and then undergo a nucleophilic attack by H_2O to form •OH adducts to complete the hydroxylation process (Fig. 5) (Antoniou et al., 2010; Gu et al., 2012; Sharma et al., 2015; Li et al., 2018b). For example, in the degradation of bisphenol A (BPA), $SO_4^{\bullet-}$ undergoes RAF reaction with aromatic rings to form unstable $SO_4^{\bullet-}$ adducts. Then electron transfer occurs between the aromatic ring and $SO_4^{\bullet-}$ and leads to the release of SO_4^{2-}, the product of which is vulnerable to nucleophilic attack by H_2O due to its electron deficiency (Antoniou et al., 2010; Xie et al., 2012). This leads to the formation of •OH adducts, which are then dehydrated to form highly oxidized phenoxy-BPA radical, and the formation of phenyl radical cations can lead to various secondary reactions of functional groups (Norman et al., 1970; Sharma et al., 2015; Luo et al., 2018) (Fig. 6). In the above process, the formation of phenoxy-BPA radical can also be achieved by direct HAA reaction of $SO_4^{\bullet-}$ or •OH with BPA. As mentioned above, RAF is not the only mechanism of pollutant degradation, often accompanied by HAA reaction or SET reaction. Li et al. (2020a) systematically investigated the contribution of $SO_4^{\bullet-}$ and •OH to the removal of phenacetin, in which •OH was involved in the RAF reaction (69%) and HAA reaction (31%), while $SO_4^{\bullet-}$ was involved in RAF reaction (55%), HAA reaction (28%) and SET reaction (17%). By simulating the degradation kinetics of phenacetin, it is proved that UV/PDS can degrade the target compound more effectively than UV/H_2O_2. Similarly, some studies specifically analyzed the RAF and HAA reaction mechanism of •OH and $SO_4^{\bullet-}$ by theoretical calculation, and the results showed that the reaction induced by $SO_4^{\bullet-}$ had a lower free energy barrier than that of •OH, and the RAF takes precedence over HAA in both •OH and $SO_4^{\bullet-}$ with Acetaminophen reactions (Xu et al., 2021).

4.3. Single-electron transfer

We mentioned that compounds with amines, amides, and aryl groups tend to proceed with $SO_4^{\bullet-}$ through the single-electron transfer pathway in 4.1. Due to the electron donor effect of this electron-rich functional group, the electron cloud density of the molecules can be increased, which makes them more prone to SET reactions with $SO_4^{\bullet-}$ (Mei et al., 2019). Moreover, the reaction rate range between $SO_4^{\bullet-}$ and aromatic compounds is much larger than that of •OH. The reaction rate constant between compounds containing strong electron donor substituents and $SO_4^{\bullet-}$ is more than 4 orders of magnitude larger than that containing strong electron adsorbent. This reflects the different reaction mechanisms between $SO_4^{\bullet-}$ and •OH, that is, $SO_4^{\bullet-}$ is more selective than •OH (Wojnarovits and Takacs, 2019). The SET reaction rate of $SO_4^{\bullet-}$ and aromatic compounds (ACs) is closely related to the electron-donating properties of substituents. Luo et al., 2017, 2018 studied the Gibbs free energy of 76 ACs and $SO_4^{\bullet-}$ reactions and found that it increased with the decrease of the electron-donating properties of substituents on ACs. And $SO_4^{\bullet-}$ is more likely to react with ACs through the SET channel than •OH. However, the favorable way for •OH to interact with aromatic pollutants is the RAF reaction (Yang et al., 2017). Based on this finding, they further proposed two basic mechanisms for the SET reaction: (i) For benzoate compounds, their carboxylic acid groups may undergo decarboxylation after the SET reaction (Zemel and Fessenden, 1978). (ii) For other aromatic compounds, a phenyl cation may be formed after the SET reaction, and the subsequent reaction depends on the electronic effect of the functional group on the benzene ring. The oxidation reaction of two aniline drugs, sulfamethoxazole, and diclofenac, is initiated by the formation of N-centered phenyl radical cations by the single-electron transfer reaction with $SO_4^{\bullet-}$, followed by a series of decarboxylation, hydroxylation, and bond-breaking reactions to achieve final degradation (Mahdi Ahmed et al., 2012; Ghauch et al., 2013). $SO_4^{\bullet-}$ mediated attack on phenol is also caused by electron transfer from organic compounds to $SO_4^{\bullet-}$ to form the hydroxycyclohexadienyl radical, whose hydrolysis leads to the formation of hydroxylated radical products, which are then further reacted with O_2 to form more stable catechol and hydroquinone (Anipsitakis et al., 2006; Olmez-Hanci and

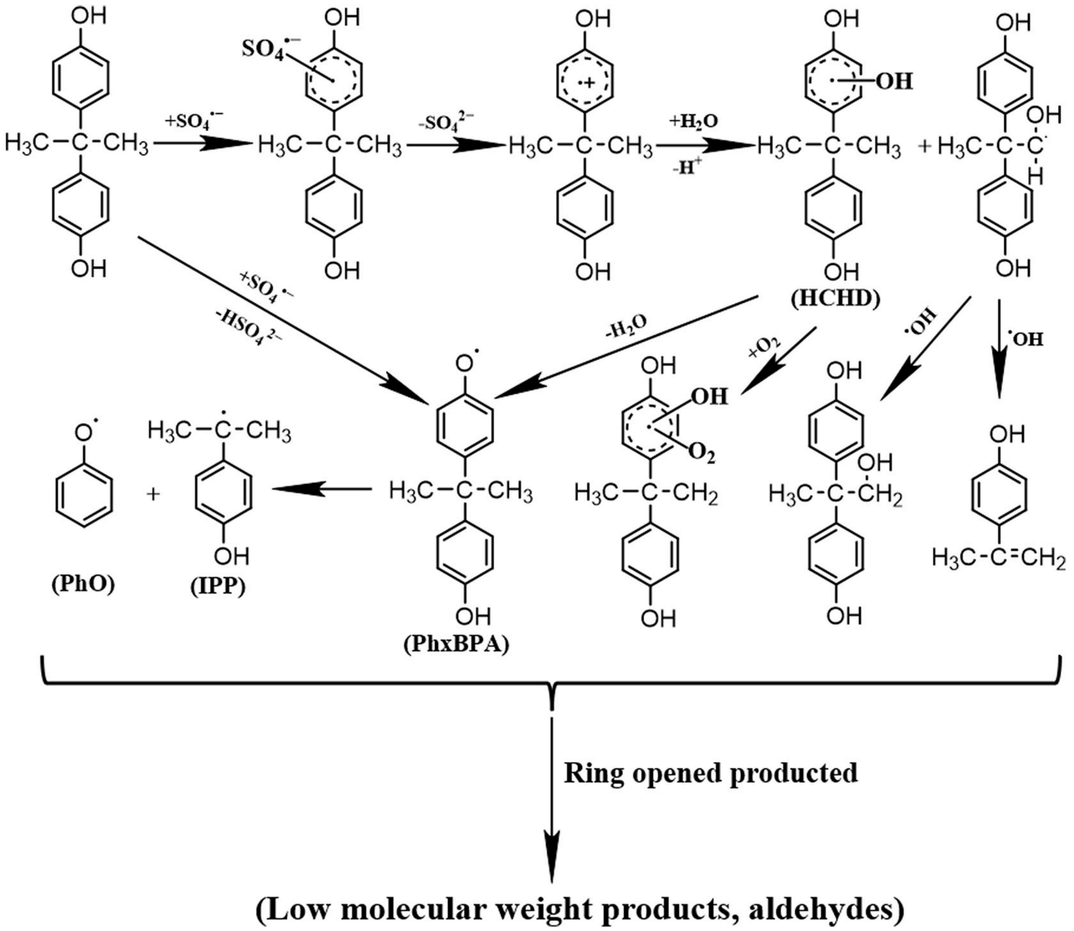

Fig. 6. The possible mechanism of BPA degradation by $SO_4^{\bullet -}$ and •OH. Reproduced from Ref. (Sharma et al., 2015).

Arslan-Alaton, 2013). The highest occupied molecular orbital energy (E_{HOMO}), a measure of electron distribution and donor capacity, is related to the electron-donating capacity of organic compounds and is commonly used to construct quantitative structure-activity relationships (QSAR) of $SO_4^{\bullet -}$ reactions with organic matter (Fang et al., 2012; Xiao et al., 2015). Since compounds with high E_{HOMO} tend to provide electrons, E_{HOMO} is a quantitative indicator that determines the degree of a free radical oxidation reaction in the SET reaction in the QSAR model, and some studies have found that ACs with high E_{HOMO} are more responsive to $SO_4^{\bullet -}$ (Fang et al., 2012; Luo et al., 2018). However, for other structurally diverse compounds, E_{HOMO} and $k_{SO4\bullet -}$ did not show this trend. This reflects that there is no major reaction path between $SO_4^{\bullet -}$ and the compound. HAA, RAF, and SET reactions are all possible, depending on the structure and functional group type of the target compound (Xiao et al., 2015).

Based on the above discussion, we obtained some rules about the reactivity of $SO_4^{\bullet -}$: (i) the HAA reaction usually occurs on the C–H bond of aliphatic compounds. The longer the C–H bond, the more likely the HAA reaction is to occur, and the reactivity of •OH to h-dehydrogenation is higher than that of $SO_4^{\bullet -}$. (ii) RAF reaction generally occurs in the aromatic ring and alkene double bond, unlike •OH, $SO_4^{\bullet -}$ adduct reaction needs to overcome an additional radical adduct formation step. (iii) The SET reaction occurs in compounds containing electron-rich functional groups such as amines, amides, and aryl groups, and their electron donor effect makes electron transfer between organic matter and $SO_4^{\bullet -}$ more likely to occur. In addition, the reaction rate range of $SO_4^{\bullet -}$ with aromatic compounds is much faster than that of •OH; (iv) The types of structure and functional group of organic compounds determine the reactivity of $SO_4^{\bullet -}$. There is no main reaction path between $SO_4^{\bullet -}$ and them, However, when the reaction of $SO_4^{\bullet -}$ with compounds is dominated by SET and RAF, the second-order rate constant is faster than that of HAA.

5. Detection methods of sulfate radicals

5.1. Probe methods combined with competitive kinetics approach

Due to the short lifetime of active species ($SO_4^{\bullet -}$, •OH, $^1O_2$, $^\bullet O_2^-$) in water, their concentrations in $SO_4^{\bullet -}$-AOPs systems are difficult to accurately measure. Therefore, it is common to use quenchers with very high reaction rates to scavenge free radicals and then compare the removal efficiency of pollutants with and without quenchers to finally obtain the relative content of each free radical (Oh et al., 2016; Zhou et al., 2018a; Gao et al., 2022a). Table 3 lists the second order rate constants for the reactions of common probe compounds/quenchers with $SO_4^{\bullet -}$ and •OH

Table 3
Rate constants for reactions between selected chemical probes and either hydroxyl radicals or sulfate radicals. Reproduced from Ref. (Liang and Su, 2009).

Chemical probes	$SO_4^{\bullet -}$ ($M^{-1}s^{-1}$)	•OH ($M^{-1}s^{-1}$)
Anisole	4.9×10^9	7.8×10^9
Benzoic acid	1.2×10^9	4.2×10^9
Benzene	$(2.4–3) \times 10^9$	7.8×10^9
Ethanol	$(1.6–7.7) \times 10^7$	$(1.2–2.8) \times 10^9$
Methanol	3.2×10^6	9.7×10^8
Nitrobenzene	$< 10^6$	$(3.0–3.9) \times 10^9$
Propanol	6.0×10^7	2.8×10^9
Phenol	8.8×10^9	6.6×10^9
Tert-butyl alcohol	$(4.0–9.1) \times 10^5$	$(3.8–7.6) \times 10^8$

(Liang and Su, 2009). Alcohols such as methanol (MeOH), ethanol (EtOH), isopropanol (IPA), and tert-butanol (TBA) are the most commonly used quenchants. Among them, MeOH and EtOH show high reactivity to •OH and $SO_4^{\bullet-}$ simultaneously, while TBA without α-hydrogen shows inconsistent reactivity to •OH and $SO_4^{\bullet-}$ ($k_{SO4\bullet-+TBA} = 4.0 \times 10^5\ M^{-1}s^{-1}$, $k_{\bullet OH+TBA} = 6.0 \times 10^8\ M^{-1}s^{-1}$) (Buxton et al., 1988; Clifton and Huie, 1989). Based on this feature, the relative contents of •OH and $SO_4^{\bullet-}$ can be obtained by comparing the removal efficiency of contaminants before and after the addition of TBA (Li et al., 2024). Some studies have also found that free radicals produced during PMS activation may stay on the surface of the catalyst and not be released into solution, i.e., "surface-bound free radicals." For such active species, it is difficult for hydrophilic substances such as methanol and tert-butanol to reach the catalyst surface to achieve quenching effect, KI and dimethyl sulfoxide (DMSO) are usually used as quenching agents to verify the existence of surface-bound free radicals. Wang et al. (2017) combined methanol, tert-butanol and potassium iodide to quenching the system and found that the main active species was surface-bound SO4•−, proposing that bisphenol A was adsorbed on the catalyst surface and degraded in situ by surface-bound SO4•−. Yao et al. (2017) also reported that in the presence of DMSO scavenger, the degradation of orange II would be greatly inhibited, while the presence of methanol had no effect on it. It is worth noting that KI will consume persulfate, while DMSO will affect the adsorption of the active site, which may affect the accuracy of the quenching results (Wang and Wang, 2020).

A recent study has questioned the usefulness of quenching in assessing the role of various active species in $SO_4^{\bullet-}$-AOPs. Researchers often believe that adding high-concentration quenchers can completely remove the target active species, but in addition, high-concentration quenchers also bring many confounding effects to the persulfate system, such as accelerating the decomposition of PMS, interfering with the generation of active substances and quenching of non-target active substances (Gao et al., 2022a). Based on this finding, the different removal efficiency of pollutants can not only be attributed to the quenching of target active species by the quencher but also related to the confounding effect caused by the high concentration of the quencher. Therefore, the explanation of the role of various active species in the persulfate system by the quenching method is controversial and worth reexamining. Besides, some catalysts also have certain adsorption to alcohols, which can lead to the coverage of active sites by alcohol quenchers (Zhang et al., 2012).

Aromatic compounds with strongly electron-withdrawing functional groups (nitrobenzene, benzoic acid, etc.) are also ideal probes to differentiate $SO_4^{\bullet-}$/•OH reactivity (Wang et al., 2023b). In $SO_4^{\bullet-}$-AOPs systems, the relative content of $SO_4^{\bullet-}$ and •OH can be obtained by calculating the reaction rate constants of chemical probes in different quenching systems under the assumption of excessive PMS (Oh et al., 2016). Specific steps are as follows:

When no quencher is added, the reaction rate of the chemical probe can be expressed as:

$$\frac{dC_P}{dt} = -\left(k_1[\cdot OH]C_p + k_2\left[SO_4^{\cdot-}\right]C_p\right) = -kC_P \tag{20}$$

when chemical probes that only react with ·OH are added, the reaction rate of the chemical probe can be expressed as:

$$\frac{dC_P}{dt} = -k_2\left[SO_4^{\cdot-}\right]C_P = -k'C_P \tag{21}$$

where C_P is the chemical probe concentration, k_1 and k_2 are the second–order rate constants of reaction between chemical probe with •OH and $SO_4^{\bullet-}$ respectively, k and k' are the apparent first–order rate constant. k_1 and k_2 can be obtained from Table 3 according to the different chemical probes used, and k and k' can be calculated from experimental data (Liang and Su, 2009). Therefore, the relative concentrations of $SO_4^{\bullet-}$ and •OH can be obtained according to the ratio of k' to k, and the steady-state concentration of $SO_4^{\bullet-}$ can be obtained according to Eqs. (20) and (21).

Using high performance liquid chromatography (HPLC) to determine the characteristic products of the reaction between the trapping agent and the active substance is also a quantitative method of free radicals. At present, there are HPLC quantitative detection methods for high valence iron species and •OH (Saha and Kumar Gupta, 2018; Wang et al., 2018). Unfortunately, there are few studies on the quantitative determination of $SO_4^{\bullet-}$ by HPLC. It is necessary to develop some trapping agents that react with $SO_4^{\bullet-}$ to quantitatively detect their concentration.

5.2. *Electron spin resonance spectroscopy*

Electron spin or paramagnetic resonance (ESR/EPR) is a technology used to qualitatively or quantitatively detect magnetic substances containing one or more unpaired electrons, which provides an effective method for detecting $SO_4^{\bullet-}$ and •OH containing unpaired electrons (Hayyan et al., 2016). However, these free radicals usually have a short life and are difficult to be detected directly. Therefore, spin traps will be used to react with free radicals to generate stable spin adducts, and the corresponding characteristic peaks will be obtained through ESR detection. The spin trap is a kind of diamagnetic organic compound including nitroso and nitrogen oxides. 5,5-Dimethyl-1-pyrroline (DMPO) and 2,2,6,6-tetramethylpiperidine (TEMP) are the most commonly used spin traps. As shown in Fig. 7, when DMPO is used as the capture agent, the characteristic peak intensity ratios of the corresponding adducts formed with $SO_4^{\bullet-}$, •OH, and ${}^{\bullet}O_2^-$ are 1:2:1:2, 1:2:2:1 and 1:1:1:1 respectively, while the capture agent of ${}^1O_2$ is TEMP, and the characteristic peak intensity ratios of the adducts are 1:1:1 (Wang and Wang, 2020). However, in $SO_4^{\bullet-}$-AOPs, DMPO-$SO_4^{\bullet-}$ and DMPO-•OH often coexist, and when 5-diethoxyphosphoryl-5-methyl-1-pyrroline-N--oxide (DEPMPO) was used as a spin trap to capture $SO_4^{\bullet-}$, it was observed that DEPMPO-$SO_4^{\bullet-}$ would undergo nucleophilic substitution with H_2O/OH^- to form DEPMPO-•OH, which affects the accuracy of the measurement results (Timmins et al., 1999). Therefore, ESR is generally used for qualitative or semi-quantitative measurement. Zhang et al. (2022c) developed and verified the qualitative and semi-quantitative capture capability of $SO_4^{\bullet-}$/•OH and ${}^1O_2$ using the soluble probe 9, 10-anthracenediyl-bis(methylene)-dimalonic acid. This method is more convenient and reliable than the electron paramagnetic resonance detection using DMPO and TEMP as spin trapping agents and the ROS quenching by alcohol, furfuryl alcohol, and L-histidine. Due to the low lifetime and high activity of ROS, and they often appear in the $SO_4^{\bullet-}$-AOPs system at the same time, their roles in pollutant degradation are often confused, and the existing detection methods are difficult to accurately quantify the content of each active species, therefore, it is necessary to develop more accurate and advanced detection techniques to gain a deeper understanding of their contributions and response mechanisms.

5.3. *Transient absorption spectroscopy*

Transient absorption spectroscopy can determine some reactive substances by comparing the spectra of photoexcited and unexcited samples, which can be used for the qualitative detection of $SO_4^{\bullet-}$ (Wang and Wang, 2020). Studies have shown that the reaction of purine and pyrimidine derivatives with •OH and $SO_4^{\bullet-}$ can obtain the maximum transient absorption spectra at different wavelengths. The former has the maximum absorption at 340 nm, while the latter has the maximum absorption at 320 nm (Pramod et al., 2006; Manoj et al., 2007). In addition, by photolysis of $S_2O_8^{2-}$ aqueous solution, it was also found that $SO_4^{\bullet-}$ can be adsorbed on the surface of suspended silica nanoparticles and form a characteristic transient adduct with $\lambda_{max} \approx 320$ nm (Caregnato et al., 2003). Unfortunately, this method has not been applied to the study of $SO_4^{\bullet-}$-AOPs, but these characteristics suggest that transient absorption spectroscopy may provide new ideas for the detection of

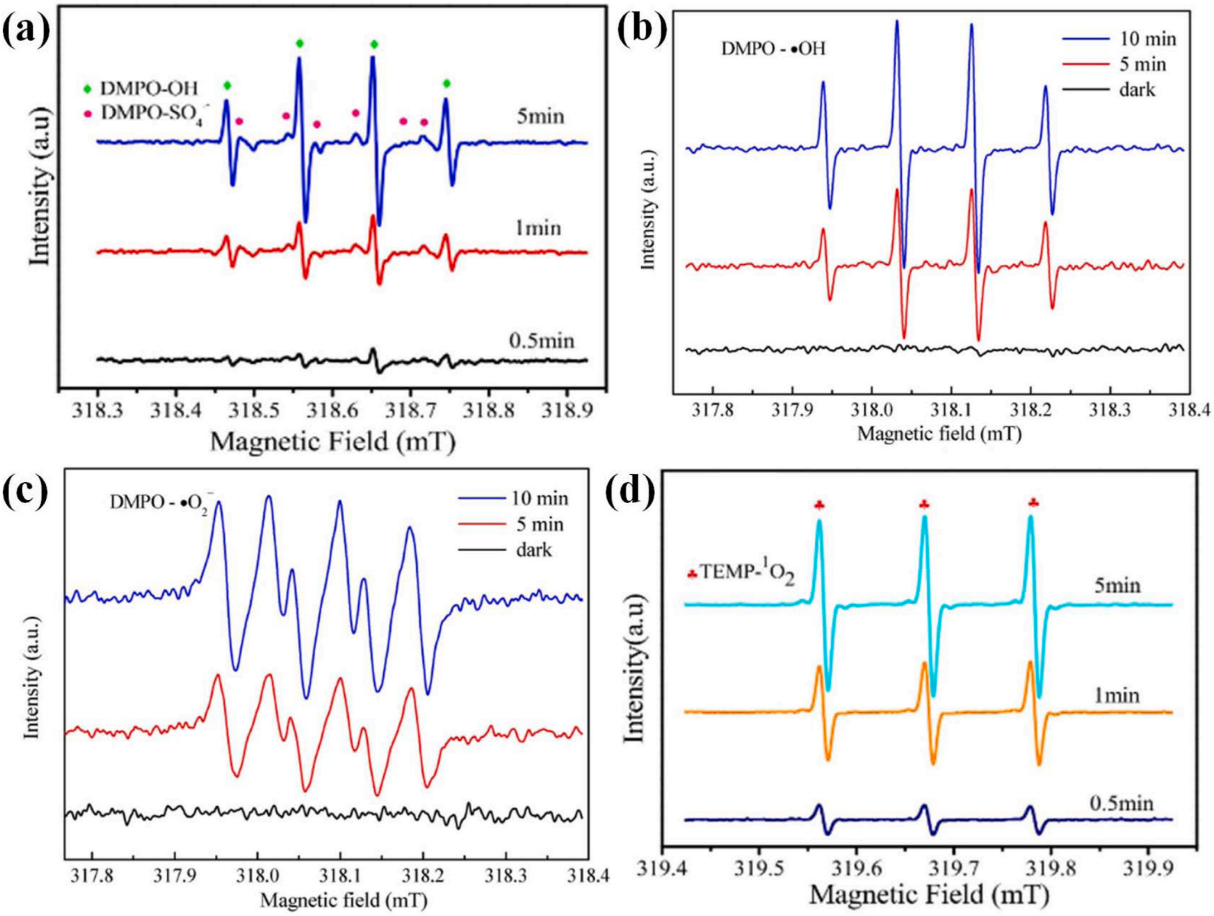

Fig. 7. Spin trapping ESR spectra of DMPO with active species. (a) DMPO-•OH and DMPO-$SO_4^{\bullet-}$; (b) DMPO-•OH; (c) DMPO-$^{\bullet}O_2^-$; (d) DMPO-$^1O_2$. Reproduced from Ref (Lin et al., 2019; Fu et al., 2022).

$SO_4^{\bullet-}$.

In $SO_4^{\bullet-}$-AOPs systems, $SO_4^{\bullet-}$ and •OH often coexist, which have different selectivity and oxidation capacity to pollutants. Therefore, it is critical to determine the presence of $SO_4^{\bullet-}$ and assess its contribution to further understand its reaction pathway. In general, the detection and identification of $SO_4^{\bullet-}$ strategies are as follows: (i) use of chemical reagents (quencher/chemical probe) to selectively react with reactive species in combination with competitive kinetic methods to determine relative/steady-state concentrations of sulfate radicals. (ii) Indirect detection of sulfate radicals using electron spin resonance spectroscopy to detect adducts formed by the reaction of spin traps with free radicals. (iii) The maximum transient absorption spectroscopy of different wavelengths generated by the reaction of $SO_4^{\bullet-}$ and •OH with the same substance are potential detection methods.

6. Applications of sulfate radicals-based AOPs

Based on the above discussion, we know that the strategy of activating sulfite or persulfate to produce $SO_4^{\bullet-}$ has been very mature, and understand its reactivity with pollutants. Although $SO_4^{\bullet-}$-AOPs have great application potential, their specific application methods (reactor design, combination strategy with other treatment methods) and practical processing variability and challenges are rarely summarized systematically. In order to make readers more clearly understand the prospects and shortcomings of $SO_4^{\bullet-}$ in practical applications, in this section, we will comprehensively explain the application of $SO_4^{\bullet-}$ in environmental remediation, focusing on its application in industrial wastewater, soil and groundwater, sludge dewatering and conditioning and membrane separation. The application status, the potential reaction mechanism, and the shortcomings of $SO_4^{\bullet-}$-AOPs in practical applications are summarized. In addition, the application prospects of $SO_4^{\bullet-}$ in water disinfection and air purification are briefly introduced.

6.1. *Wastewater treatment*

Wastewater mainly includes domestic sewage and industrial wastewater produced in the process of production and living. With the increasing use of pharmaceuticals and personal care products, many recalcitrant pollutants are beginning to appear in domestic sewage. Conventional sewage treatment facilities cannot remove them. In addition, Industrial wastewater has the characteristics of large daily discharge, variety, and toxicity, which has caused great harm to the environment and human health. The traditional biological method has some limitations for the removal of stubborn contaminants, and the toxic substances also limits its application in industrial wastewater (Zhao et al., 2006). Physical methods such as coagulation and membrane separation only transfer pollutants and are difficult to eliminate. Advanced oxidation technology is very effective for the removal of various refractory pollutants and toxic substances. Compared with •OH, the strong oxidizing property and long half-life of $SO_4^{\bullet-}$ make it more effective in wastewater treatment. Its pH independence and low reactivity with dissolved organic matter make it more suitable for the treatment of various industrial wastewater. In addition, in terms of precursors , persulfate with long life and easy transportation and storage also makes $SO_4^{\bullet-}$ consistently produced, thereby providing continuous removal of total organic carbon (TOC). On the contrary, H_2O_2 as a liquid is not easy to store and will decompose slowly, making it less efficient than persulfate. Moreover, the ineffective consumption of H_2O_2

by •OH also limits its removal of TOC (Li et al., 2009; Chen et al., 2022b).

The application of $SO_4^{\bullet -}$-AOPs in wastewater treatment mainly involves the following three aspects: (i) Completely remove stubborn pollutants that are difficult to be removed by conventional methods to reduce the toxicity of wastewater. (ii) The conversion of macromolecular organic compounds into small molecular substances to improve the biodegradability of wastewater. (iii) Reduction or adsorption precipitation of heavy metal ions to reduce heavy metal pollution. In the process of actual wastewater treatment, especially industrial wastewater,

Table 4
Performances of different $SO_4^{\bullet -}$-AOPs systems for wastewater treatment.

wastewaters	$SO_4^{\bullet -}$-AOPs	Wastewater characteristics	Operational conditions	Removal efficiency	Refs.
Landfill leachate	UV/PMS	COD = 978.69 mg/L, NH_4^+-N = 6.23 mg/L, color number (CN) = 0.328 cm^{-1}, pH = 8.05	PMS = 0.048 mol/L, pH = 7.5, Time = 60 min	37.39% COD, 95.88% CN	Guo et al. (2020)
Landfill leachate	nano-Fe_3O_4/PDS	COD = 780–1160 mg/L, color = 380–460 times, pH = 6.5–7.1, NH_3–N = 120–160 mg/L	nano-Fe_3O_4 = 1.5 g/L, PDS = 3.5 g/L, pH = 3.0, Shaking speed = 350 rpm, Time = 120 min	63% COD, 98% Color	Liu et al. (2018b)
Landfill leachate	$CuFe_2O_4$/PDS	COD = 2600 ± 130 mg/L, BOD_5 = 980 ± 50 mg/L, NH_3–N = 2560 ± 128 mg/L, Color (Pt–Co units) = 5110 ± 255.50, pH = 8 ± 0.16	$CuFe_2O_4$ = 1.5 g/L, PDS = 5 g/L, pH = 2.0, Time = 60 min	57% COD, 71% NH_3–N, 63% Color	Karimipourfard et al. (2020)
Landfill leachate	Fe_2O_3/Co_3O_4/exfoliated graphite (EG)/PDS	COD = 14,000 mg/L, NH_4^+-N = 3120 mg/L, Color = 1028°, pH = 8.98	Fe_2O_3/Co_3O_4/exfoliated graphite (EG) = 0.1 g/L, PDS = 5 g/L, pH = 0.05, Time = 60 min	67.1% COD, 90.6% NH_4^+-N	Guo et al. (2019)
Landfill leachate	Electrolysis/$FeTiO_3$/UV-LED	COD = 14,200 mg/L, TOC = 5600 mg/L, pH = 8.56, TDS = 18,860 mg/L	$FeTiO_3$ = 1 g/L, PDS = 234 mM, pH = 8.6, UV-LED = 200 mA/cm^2, Time = 480 min	90% COD, 90% mineralization	Silveira et al. (2018)
Landfill leachate	Electrolysis (Fe/C granules)/PDS	COD = 1041.38 mg/L, NH_3–N = 444.39 mg/L, pH = 7.81	Fe/C granules = 1 g/L, PDS = 28 mM, Operating voltage = 5 V, Time = 120 min	72.9% COD, 84.1% TOC, 99.3% NH_3–N	Yu et al. (2020)
Landfill leachate	MW/PDS/H_2O_2	COD = 526.58 mg/L, CN = 4.226, pH = 7.37	MW power = 450 W, H_2O_2 = PDS = 3.7 mM, pH = 3, Time = 16 min	73.5% COD, 98.1% CN	Chen et al. (2020c)
Landfill leachate	MW/ZVI/PDS	TOC = 169.25 mg/L, CN = 0.102 cm^{-1}, pH = 8.65	MW power = 320 W, PDS = 30 mM, ZVI = 0.5 g/L, pH = 3, Time = 10 min	78.63% TOC, 80.39% UV_{254}	Yang et al. (2022)
Landfill leachate	MW/PS	COD = 829.69 mg/L, chroma = 0.393 cm^{-1}, pH = 7.87, BOD_5 = 91.27 mg/L	MW power = 450 W, PDS = 8 g/L, pH = 3, Time = 20 min	65.65% COD, 84.15% UV_{254}	Chen et al. (2019)
Petrochemical wastewater	UV/PDS/Fe^{2+}	COD = 950 ± 50 mg/L, BOD_5 = 190 ± 10 mg/L, Color (absorbance at 400 nm) = 0.411 ± 0.003 cm^{-1}, pH = 7.10 ± 0.04	PDS = 4 mM, Fe^{2+} = 0.3 g/L, pH = 7, Time = 60 min	70% COD, 100% Color, BOD_5/COD: from 0.2 to 0.45	Babaei and Ghanbari (2016)
Petrochemical wastewater	UV/PDS/Fe^{2+}	Catechol = 200 mg/L, COD = 3500 mg/L, BOD_5 = 370 mg/L, TOC = 1500 mg/L, pH = 6.3	PDS = 4 mM, Fe^{2+} = 0.3 g/L, pH = 4, Time = 60 min	64.7% Catechol, 39.7% COD	Delavaran Shiraz et al. (2018)
Petrochemical wastewater	H_2O_2/PDS/Fe^{2+}	Dinitrotoluene = 603.1 ± 6 mg/L, COD = 3285 ± 40 mg/L, BOD_5 = 150 ± 20 mg/L, pH = 6.7	H_2O_2 = 0.2 g/L, PDS = 0.5 g/L, Fe^{2+} = 0.3 g/L, pH = 11, Time = 60 min	100% Dinitrotoluene, 89.1% COD	Takdastan et al. (2019)
Petrochemical wastewater	US/nZVI/PMS	COD = 1025 mg/L, BOD_5 = 250 mg/L, TOC = 275 mg/L, Total phenols = 47.6 mg/L, pH = 6.7	PMS = 1.25 mM, nZVI = 0.4 g/L, US power = 200 W, pH = 3, Time = 90 min	60% COD, 47% TOC, 61% Total phenols, BOD_5/COD: from 0.24 to 0.41	Barzegar et al. (2018)
Petrochemical wastewater	US/PMS/Ozone	COD = 825 mg/L, TDS = 748 mg/L, pH = 6.5	Ozone = 6.8 mg/L, PMS = 1.5 mM, US power = 200 W, pH = 7, Time = 60 min	85% COD, 75% TOC	Ghanbari et al. (2020)
Petrochemical wastewater	US/Electrolysis/PDS	COD = 750 mg/L, BOD_5 = 115 mg/L, TOC = 274 mg/L, pH = 7.28	Potential electrode = 10 V, PDS = 20 mM, US power = 300 W, pH = 3, Time = 120 min	82.31% COD	Yousefi et al. (2019)
Pharmaceutical wastewater	UV/MnO_2/PMS	COD = 354 mg/L, BOD_5 = 185 mg/L, TOC = 152 mg/L, Total phenol = 20.1 mg/L, pH = 5.6	PMS = 1.0 mM, MnO_2 = 0.25 g/L, Natural pH, Time = 120 min	65% COD, 60% BOD_5, 53% TOC, 74% Total phenol	Eslami et al. (2018)
Printing and dyeing wastewater	UV/US/PMS	COD = 1280 mg/L, TOC = 550 mg/L, pH = 8.9	PMS = 1.5 mM, Natural pH, Time = 90 min	64.8% COD, 50.9% TOC, 92.9% Color	Ahmadi and Ghanbari (2018)
Printing and dyeing wastewater	US/UV/ZnO/PDS	COD = 1546.2 mg/L, BOD_5 = 231.4 mg/L, TOC = 714 mg/L, pH = 8.3	PDS = 2.43 mM, ZnO = 0.88 g/L, US power density = 300 W/L, pH = 6	96.6% COD, 97.1% TOC, BOD_5/COD: from 0.15 to 0.61	Asgari et al. (2020)
Printing and dyeing wastewater	US/UV/Fe–Bi_2O_3/PMS	COD = 2612 mg/L, BOD_5 = 118 mg/L, TOC = 897 mg/L, pH = 8.01	PMS = 6 g/L, Fe–Bi_2O_3 = 0.88 g/L, pH = 8.01	91% COD, 77% TOC	Dinesh et al. (2016)
Printing and dyeing wastewater	US/UV/$CeO_2Fe_3O_4$/PMS	COD = 875 mg/L, BOD_5 = 240 mg/L, TOC = 232 mg/L, pH = 6.4	PMS = 1.5 mM, CeO_2–Fe_3O_4 = 0.3 g/L, pH = 7.0, Time = 90 min	63% COD, 44% TOC, 55% BOD_5, 78% Color	Ghanbari et al. (2019)
Winery wastewater	UV/$LaCoO_3$–TiO_2/PMS	COD = 139.25 mg/L, BOD_5 = 42.5 mg/L, TOC = 44.50 mg/L, pH = 3.43	PMS = 10 mM, $LaCoO_3$–TiO_2 = 0.5 g/L, pH = 7.0, Time = 180 min	60% COD, 95% Polyphenol	Solís et al. (2018)
Winery wastewater	UV/Fe^{2+}/PMS	COD = 513 mg/L, Total polyphenols = 33 mg/L, TOC = 143 mg/L, pH = 4.0	PMS = 2.5 mM, Fe^{2+} = 1 mM, UV_{365} = 70 W/m^2, pH = 6.5, Time = 90 min	75% COD, 56% TOC	Rodríguez-Chueca et al. (2017)

these functions often coexist. Table 4 summarizes the application status of $SO_4^{\bullet-}$-AOPs in wastewater treatment in recent years.

The most important role of $SO_4^{\bullet-}$-AOPs in practical wastewater treatment is to remove toxic pollutants and macromolecular organic compounds that are difficult to degrade by using highly oxidizing $SO_4^{\bullet-}$, to achieve detoxification and improve the biodegradability of wastewater. Chen et al. (2022b) combined experimental and computational studies to prove that PDS/Fe(II) offers better performance than H_2O_2/Fe (II) in improving the biodegradability of wastewater. However, the application of the PDS/Fe(II) process is limited by pH. At present, the catalysts used for activating persulfate in practical applications are gradually developing from a single homogeneous catalyst to a multiphase composite catalyst. Liu et al. (2018b) used nano-Fe_3O_4 as PDS catalyst to achieve 63% COD removal rate and 98% chroma removal rate of landfill leachate, and the aromatic nature and molecular structure complexity of organic matter were reduced under the strong oxidation of $SO_4^{\bullet-}$. Similarly, $FeTiO_3$, $CuFe_2O_4$ (Karimipourfard et al., 2020), and Fe_2O_3/Co_3O_4/exfoliated graphite (Guo et al., 2019) composite catalysts also have a good catalytic effect in the degradation of landfill leachate. They can effectively activate PMS/PDS to produce a large amount of highly active $SO_4^{\bullet-}$, so as to achieve a high removal rate of COD, NH_4^+-N, and color. Furthermore, the catalytic activity and surface area can be further improved by loading them on the support. Zero-valent iron nanofiber/reduced super-large graphene oxide as persulfate activator can achieve up to 80.87% COD removal rate and 72.38% NH_3–N removal rate in treating real leachate, and the biodegradability (BOD_5/COD) of leachate was also increased from 0.25 to 0.52 (Soubh et al., 2018).

To further improve the utilization of the oxidant and reduce SO_4^{2-} residue in water, combining UV (Silveira et al., 2018), electrolysis (Silveira et al., 2018; Yu et al., 2020), MW (Qi et al., 2017; Hu et al., 2020; Yang et al., 2022) with the catalyst, and simultaneously activating H_2O_2 and PDS/PMS to generate more free radicals, can realize effective purification of wastewater. Specifically, the presence of current density enhances the formation of hypochlorite and the conversion of PDS to $SO_4^{\bullet-}$, which improves the decolorization efficiency. The decolorization of landfill leachate increases the light penetration and the photoreduction of Fe(III) to Fe(II) on the $FeTiO_3$ surface, which promotes the catalytic effect of Fe(II) on PDS and H_2O_2. Yu et al. (2020) developed a three-dimensional electrode of Fe/C particles to simultaneously achieve anodic electrolysis of chlorine species and activation of PDS, which significantly promoted the removal of refractory organic pollutants from wastewater (Fig. 8a). Co–TiO_2/zeolite catalyst, on the one hand, uses the photoabsorption ability of TiO_2 to form electron-hole pairs to stimulate the decomposition of PDS to generate $SO_4^{\bullet-}$, on the other hand, cobalt doping enhances the catalytic activity of PDS, which can realize photocatalysis and co-catalysis of PDS at the same time (Eqs. 22–25) (He et al., 2019). Akbar et al. (Eslami et al., 2018) applied UV/MnO_2/PMS process to the treatment of petrochemical wastewater and pharmaceutical wastewater. Under the conditions of 1 mM PMS, 0.25 g/L MnO_2, 2 h reaction time, and natural pH, the biodegradability of the two wastewater was improved. The BOD/COD ratio increased from 0.49 to 0.52 to 0.61, respectively, and the toxicity was reduced by more than 40%.

$$\mathrm{Co-TiO_2 + hv(UVlight) \rightarrow TiO_2\left(h_{sb}^{+}\right) + TiO_2\left(e_{ob}^{-}\right)} \tag{22}$$

$$O_2 + e_{ab}^{-} \rightarrow \cdot O_2^{-} \tag{23}$$

$$H_2O + h_{vb}^{+} \rightarrow \cdot OH + H^{+} \tag{24}$$

$$S_2O_8^{-} + e_{ab}^{-} \rightarrow SO_4^{\cdot-} + SO_4^{2-} \tag{25}$$

Heavy metal pollution is also a major problem in environmental remediation, phytoremediation is considered to be the best way to remove heavy metals (Iyyappan et al., 2023). When organic pollutants and heavy metals exist in wastewater, their effective removal at the same time has special significance for environmental remediation. In a recent study, $SO_4^{\bullet-}$-AOPs were demonstrated to be an efficient process for removing organic pollutants and heavy metals from wastewater. Persulfate can not only be activated by natural sulfide metal minerals to produce $SO_4^{\bullet-}$ to remove organic pollutants, but also stimulate the catalyst itself to reduce heavy metals studies have shown that pollutant intermediates degraded by $SO_4^{\bullet-}$ can also enhance the photoreduction of Cr(VI) by minerals. Oxalic acid and formic acid, the degradation intermediates of Rhodamine B, are introduced to cooperatively promote the reduction of Cr(VI) in the chalcopyrite/PDS system through their clearance of photogenic holes (Zheng et al., 2022).

Heavy metals in industrial wastewater usually coexist with chelating agents to form a heavy metal complex, which has a stable chelating structure and is difficult to remove by chemical precipitation. $SO_4^{\bullet-}$ can directly destroy the chelating structure of heavy metals, resulting in a decomplexation reaction and metal ion precipitation, which is conducive to the removal of heavy metals in subsequent steps. Hong et al. (2022) used the highly efficient co-activation of PDS with alkali and CuO to decomplexate Cu-ethylenediamine tetraacetic acid (Cu(II)-EDTA) at the same time and precipitated Cu(II), and could completely remove 3.14 mM Cu(II) within 2 h. However, the activation process of PDS is acidic, which increases the amount of alkali required for Cu(II) precipitation, and CuO itself also has the risk of Cu(II) dissolution. Zero-valent

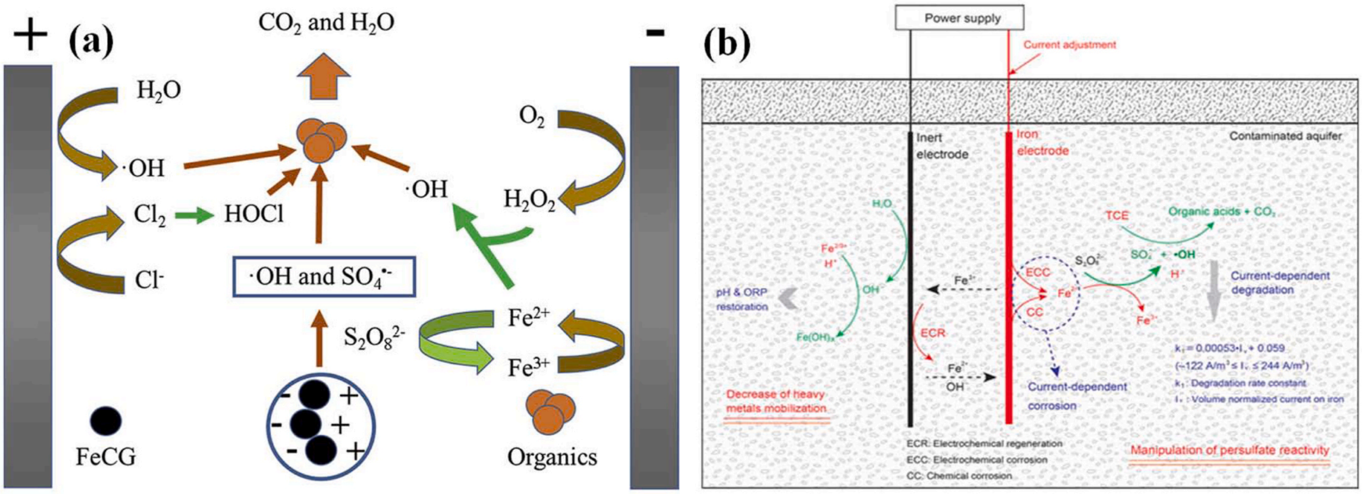

Fig. 8. Mechanism of electro-assisted $SO_4^{\bullet-}$-AOPs wastewater treatment. (a) Three-dimensional Fe/C particle electrode/PDS system. (b) Iron electrode/PDS system. Reproduced from Ref (Yuan et al., 2014; Yu et al., 2020).

iron (ZVI) can avoid the above problems. ZVI, as the activator of PDS, generates $SO_4^{\bullet -}$ which destroys the chelating structure of Cu(II)-EDTA, and the generated Fe^{3+} can replace part of Cu(II) and EDTA chelating, which synergically promotes the release of Cu(II). The released Cu(II) is finally adsorbed on the ZVI surface and further reduced to zero-valent copper (Fei et al., 2021).

As mentioned above, the application status and mechanism of $SO_4^{\bullet -}$-AOPs in wastewater treatment mainly include: using the strong oxidation of $SO_4^{\bullet -}$ to remove stubborn pollutants and convert macromolecular compounds into small molecular substances, reduce the toxicity of wastewater and improve the biodegradability of wastewater; Under the mediation of $SO_4^{\bullet -}$, heavy metal ions can be reduced or adsorbed and precipitated to reduce heavy metal pollution.

However, there are some problems that need to be noted when $SO_4^{\bullet -}$-AOPs is applied in wastewater treatment. Firstly, the addition of oxidizer will introduce a large amount of SO_4^{2-} into the treated wastewater and increase the TDS of the water body. As shown in Table 4, the dosage of persulfate in the actual wastewater treatment is mostly between several grams and tens of grams, which will eventually be converted into SO_4^{2-}, all of which are greater than the applied water sanitation standard stipulated in China (TDS $\leq$1000 mg/L). In addition, if biological treatment is carried out later, the SO_4^{2-} is likely to be converted into H_2S, increasing the risk of subsequent treatment. It is suggested that $SO_4^{\bullet -}$-AOPs be used as an auxiliary means for wastewater treatment, such as in membrane reactor for wastewater post-treatment, to give full play to the oxidation capacity of $SO_4^{\bullet -}$ and reduce its influence on water quality. Secondly, special attention should be paid to the generation of toxic byproducts in the practical application of $SO_4^{\bullet -}$-AOPs. Unlike the reversible reaction of •OH with halogen ions (Eq. (26)), $SO_4^{\bullet -}$ is prone to react with halide ions to form halogen free radicals (Eq. (27) and (30)), which can further react with organic matter in the wastewater to form toxic halide byproducts. Finally, in order to maximize persulfate utilization, researchers often use complex methods to synthesize more efficient catalysts and apply external energy or electricity to increase $SO_4^{\bullet -}$ yield, but this is often divorced from practical application. It is necessary to give full play to the advantages of the diversity of $SO_4^{\bullet -}$-AOPs activation means according to the actual situation, such as using the waste heat of industrial wastewater to activate persulfate for wastewater treatment, and using the iron-containing sludge generated in the flocculation stage to make biochar activated persulfate (Merzouk et al., 2011; Liu et al., 2012).

$$X^- + \cdot OH \rightleftarrows HOX^{\cdot -} \tag{26}$$

$$X^- + SO_4^{\cdot -} \rightarrow X^{\cdot} \tag{27}$$

$$X^{\cdot} + X^- \rightarrow X_2^{\cdot -} \tag{28}$$

$$X_2^{\cdot -} + H_2O \rightarrow HOX \tag{29}$$

$$HOX + I^- \rightarrow XO_3^- \tag{30}$$

6.2. Groundwater and soil remediation

The contamination of soil and groundwater by organic pollutants is a major threat to the supply of drinking water. Ex-situ remediation is often not widely used due to the high cost of ex situ treatment and the complexity of the site. Therefore, in situ remediation (ISCO) is increasingly used in soil and groundwater remediation as a more efficient and economical method (Tsitonaki et al., 2010; Liu et al., 2014). The oxidants used in early ISCO were permanganate (MnO_4^-) and H_2O_2, but the resulting manganese oxides (such as MnO_2) clogged soil pores and prevented the transport of oxidants underground. H_2O_2 can undergo Fenton reaction/Fenton-like reaction with underground minerals to generate •OH, and the instability of H_2O_2 and the decomposition of H_2O_2 by catalase in the underground will cause a lot of losses (Kwan and Voelker, 2003; Waldemer and Tratnyek, 2006). Persulfate has recently become a popular ISCO oxidant (Waldemer et al., 2007; Costanza et al., 2010). Compared with conventional oxidants, persulfate have greater stability in the underground environment. In the absence of an external activator, the half-life of persulfate in the aquifer is more than 2 years (Jiang et al., 2017). In the presence of natural Fe/Mn minerals, persulfate decomposition can be accelerated, but the half-life is still between a few months and a year (Liu et al., 2014). Persulfate is more stable and easier to transport in the subsurface environment, allowing for higher utilization of the oxidant.

Aquifer sediments in the subsurface environment contain large amounts of metal minerals in which transition metals can activate persulfate. Therefore, adding persulfate alone is also used in soil and groundwater remediation. Fe(II)–O complexes in in-situ underground sediments can effectively activate persulfate to produce $SO_4^{\bullet -}$ for the remediation of aniline-contaminated groundwater. Under the conditions of persulfate concentration of 10–50 mM, precipitate amount of 100–300 g/L, and aniline concentration of 0.05–1.0 mM, more than 90% of aniline can be removed within 6 h (Mustapha et al., 2021). Yan et al. (2019) used four kinds of soil and aquifer sediments to study the activation ability of underground media to in-situ chemical oxidation of 1, 4-dioxane, and proved that dissolved iron in sediments was the main reason for persulfate activation, and manganese oxide and soil organic matter also promoted to a certain extent. It is worth noting that the respiration of organic matter in the underground anoxic environment leads to the reductive dissolution of Fe-oxyhydroxides, resulting in some dissolved Fe(II) (12 μM–518 μM) in groundwater (Zhang et al., 2018). Fang et al. (2023) added PMS directly to Fe(II)-rich groundwater with high arsenic (As) to achieve in-situ immobilization of As(III). Fe(II) can activate PMS to produce active substances to oxidize As(III), and the generated Fe(III) can form colloids to flocculate and adsorb As(V). The removal efficiency of As(III) can reach 98.8% within 1 min. Environmentally friendly cysteine (Cys) can also be used in groundwater remediation. Cys can not only form complexes with Fe^{2+} to stabilize Fe^{2+} but also its reduced sulfhydryl group (-SH) can accelerate the redox cycle of Fe^{3+} to Fe^{2+}. By adding Cys to the Fe^{2+}/PS process, the higher removal efficiency of targeted contaminants over a wide pH range can be achieved (Jiang et al., 2020). Similarly, citric acid (CA) can also be used to chelate Fe(II)-activated persulfate for groundwater remediation. When the PDS/Fe(II)/CA molar ratio is 15:2:1, trichloroethylene can be completely degraded within 60 min (Wu et al., 2014). In addition to Fe^{2+}, humic acid in soil and groundwater can also play an important role in $SO_4^{\bullet -}$-AOPs. Redox-active functional groups such as quinones in humic acid can effectively activate persulfate to degrade 2,4,4′-trichlorobiphenyl. The coordination reaction of quinones with hydroquinone produces semiquinone radicals, which induce persulfate activation to generate $SO_4^{\bullet -}$ to degrade pollutants (Fang et al., 2013).

The activation of persulfate by using active components in underground environment is a unique advantage of $SO_4^{\bullet -}$-AOPs in soil and groundwater treatment, but it is difficult to achieve the expected effect in practical application, which requires the addition of artificial catalysts or combined with electrochemical treatment technology. The catalytic activity of bimetallic Fe–Mn oxides for PDS in the actual groundwater sand column is very stable and can be continuously operated for 115 days. $SO_4^{\bullet -}$ and •OH play a major role in the system, and the reaction stoichiometric efficiency of PDS is 3–5%, which is much higher than that reported in H_2O_2-based ISCO ($\leq$0.28%) (Yang et al., 2020a). Magnetite and Cu^{2+} have a synergistic effect on the activation of PDS. Cu^{2+} is adsorbed and reduced by the structural Fe(II) on the surface of magnetite under neutral or alkaline conditions to form Cu^+, which contributes to the activation of PDS (Chen et al., 2020b). It provides a new way to improve the effect of mineral activation PDS in ISCO. Dong et al. (2019) used sulfide-modified nanoscale zero-valent iron to activate persulfate to remove trichloroethylene. Compared with nZVI, sulfide-modified achieves a higher removal rate and mineralization efficiency of trichloroethylene by increasing the number of electrons and accelerating electron transfer. Combining electrochemistry with ISCO is also a very effective remediation method for soil and groundwater. In-situ electrolysis of iron electrodes is a good example of application (Fig. 8b). On the one hand, positive/negative current is applied to the iron anode to promote/inhibit the generation of Fe^{2+}, which realizes the control of the degradation reaction of underground pollutants by persulfate. On the other hand, OH^- is produced by electrolysis at the cathode to regulate pH and redox potential, which inhibits the leaching of underground heavy metals (Yuan et al., 2014). The three-dimensional electrode composed of $CuFe_2O_4$ magnetic nanoparticles as a particle electrode and catalyst of PDS can effectively remove atrazine. When the dosage of $CuFe_2O_4$ was 3.0 g/L, the concentration of PDS was 4.0 mM, the current density was 4 mA/cm^2, and the initial pH was 6.3, the degradation efficiency and TOC removal rate of atrazine were 99% and 22.1%, respectively (Li et al., 2019a).

Due to the complex nature of the soil, particular attention should be paid to the effect of water composition on the removal of target contaminants in persulfate-based ISCO. Cl^- and HCO_3^- are common substrates in water environments, and sometimes interfere with soil and groundwater remediation. However, it has been reported that Cl^- plays a positive role in the persulfate activation of iron-based catalysts. Cl^- can inhibit the corrosion of iron, improve the utilization efficiency of the catalyst and produce more $SO_4^{\bullet-}$ (Li et al., 2018a). HCO_3^- also has an activation effect on PDS. Jiang et al. (2017) demonstrated for the first time that PDS can be activated by bicarbonate to form HCO_4^- which plays a major role in the conversion of acetaminophen. In the degradation of persulfate-based phenolic compounds, nitrite can lead to the formation of nitration byproducts, which account for about 70% of phenol products (Ji et al., 2017). However, nitroaromatic compounds are carcinogenic, mutagenic, and genotoxic. The formation of nitrified organic byproducts in $SO_4^{\bullet-}$-AOPs should be carefully reviewed and possible health and ecological effects assessed. Special attention is also needed to the primary alkalinity and pH values in contaminated groundwater, which mainly affect the surface complexation of aquifer minerals. Higher alkalinity facilitates the formation of inactive surface carbonate complexes, which inhibit persulfate activation, while lower pH facilitates the formation of active surface hydroxyl complexes, which can accelerate the remediation (Li et al., 2017). The oxygen content in the underground environment also affects the type of products. For example, in the presence of O_2, about 30%–60% of benzene is converted into phenol, and the remaining benzene is converted into ring-cracking products. In the case of anoxia, the concentration of ring-cracking products increases relative to phenol (Liu et al., 2016a).

In summary, persulfate-based ISCO is very promising in the remediation of contaminated soil and groundwater. Its unique advantage is that some components in the underground environment can be used for persulfate activation, such as a large number of metal minerals in aquifer sediments and their soluble and active functional groups in humic acid (e.g., quinones). In addition, compared with $KMnO_4$ and H_2O_2, persulfate has greater stability in underground environments. In practical applications, it is more important to note that some intermediates may be more toxic than their parent compounds, especially when the nitrate content is high. Before specific applications, the potential risks of intermediates need to be carefully evaluated. In practical applications, toxicity monitoring is carried out regularly to ensure that groundwater is not subject to secondary pollution. In addition, attention should also be paid to the risk of groundwater pH reduction caused by persulfate decomposition, which may lead to the leaching of underground heavy metals.

6.3. Sludge dewatering and conditioning

With the increasing demand for sanitation and water treatment facilities, more and more sludge is produced. Sewage sludge contains various toxic substances such as pathogens, heavy metals, and organic pollutants, which can cause serious pollution risks (Wu et al., 2020). Sludge dewatering is essential to reducing sludge volume and sludge toxicity, while $SO_4^{\bullet-}$-AOPs have an irreplaceable role in regulating sludge dewaterability and removing heavy metals and organic micro-pollutants (Liu et al., 2018a). Extracellular Polymers (EPS) are macromolecular polymers secreted by microorganisms in vitro, which exist inside and on the surface of activated sludge floc, and their effects on the stability, flocculation, and metabolism of activated sludge can significantly interfere with the hydrophilicity and hydrophobicity of biological floes (Liu and Fang, 2003). EPS is the most important determinant of sludge dewatering performance.

The highly oxidizing $SO_4^{\bullet-}$ in $SO_4^{\bullet-}$-AOPs can effectively degrade EPS and destroy hydrophilic proteins and fluorescent substances in EPS, resulting in the release of bound water and the increase of zeta potential, thus improving the dehydration ability (Zhen et al., 2019; Liu et al., 2021a; Bai et al., 2022). Studies have shown that when EPS is destroyed, hydrophilic substances are exposed first, resulting in the expansion of protein structure, exposing the internal unsaturated hydrophobic structure, and resulting in the release of bound water (Li et al., 2019b; Chen et al., 2022a). In addition, $SO_4^{\bullet-}$ can also crack the cell membrane, release intracellular substances and water, and further increase the dewaterability (Liu et al., 2018a; Li et al., 2019b).

The high temperature produced by the mesophilic or thermophilic digestion process can activate persulfate and produce $SO_4^{\bullet-}$, which can oxidize toluene and other organic matter in the anaerobic digested sludge, thereby improving its dewaterability (Wacławek et al., 2016). ZVI and Fe^{2+} are the most commonly used catalysts in $SO_4^{\bullet-}$-AOPs sludge treatment. In addition to activating persulfate to produce $SO_4^{\bullet-}$, they also act as flocculants. After the sludge floc is broken into small particle size by destroying the EPS structure by $SO_4^{\bullet-}$, the oxidation products of ZVI and Fe^{2+} can reduce the electrostatic repulsion by compressing the double electric layer and neutralizing the negative charge of the sludge colloidal particles, so that the sludge particles with small particle sizes can be aggregated into large sludge particles (Fig. 9) (Xiao et al., 2017; Li et al., 2019b). The improvement effect of ZVI-activated PDS on sludge dewatering performance is lower than that of Fe^{2+}, because the iron oxide layer formed near the metal surface of ZVI can inhibit the activation of PDS (Zhen et al., 2018). Some studies have shown that the iron oxide layer on the surface of ZVI will be destroyed when ultrasonic-assisted ZVI-PDS is used (Liu et al., 2020). However, when Fe^{2+} or ZVI activated sulfites were used for sludge dewatering, the capillary suction time reduction was 73.2% and 81.7%, respectively. ZVI/sulfite system is more beneficial to improve the dewatering property of sludge. This is because of the slow-release rate of Fe^{2+} in the ZVI/sulfite system, which helps to avoid the adverse consumption of Fe^{2+} on $SO_4^{\bullet-}$ (Liu et al., 2021a,b). Shi et al. (2015) introduced phosphogypsum into the system to promote the formation of columnar dihydrate gypsum crystals in the sludge, which formed a permeable and rigid lattice structure in the sludge and enhanced sludge dewatering. In addition, introducing oxalic acid into the Fe^{2+}-PDS system can also enhance sludge dewatering. On the one hand, the Fe^{3+}-oxalic acid complex can enhance the reflocculation of sludge particles. On the other hand, the chelation of oxalic acid can also promote the dissolution of heavy metals from sludge (Zhang et al., 2023b).

Micropollutants generally have long-term persistence, and their concentration in sludge is about 100 mg/kg TS (Liu et al., 2018a). Heat-PDS, MW-PDS, and FeS-PMS have been proven to be effective in degrading micropollutants (i.e. toluene, ciprofloxacin, and triclosan) in sludge (Bilgin Oncu and Akmehmet Balcioglu, 2013; Wacławek et al., 2016; Liang et al., 2021). Heavy metals are another risk species in sludge, with a total concentration of several thousand mg/kg DS (Babel and del Mundo Dacera, 2006). $SO_4^{\bullet-}$-AOPs promote the release and dissolution of heavy metals in sludge by destroying sludge flocs and reducing pH, thus reducing the toxicity of dewatered sludge (Li et al., 2019b; Bai et al., 2022).

In summary, the role of $SO_4^{\bullet-}$-AOPs in sludge dewatering and conditioning is mainly reflected in the following aspects: (i) $SO_4^{\bullet-}$ can

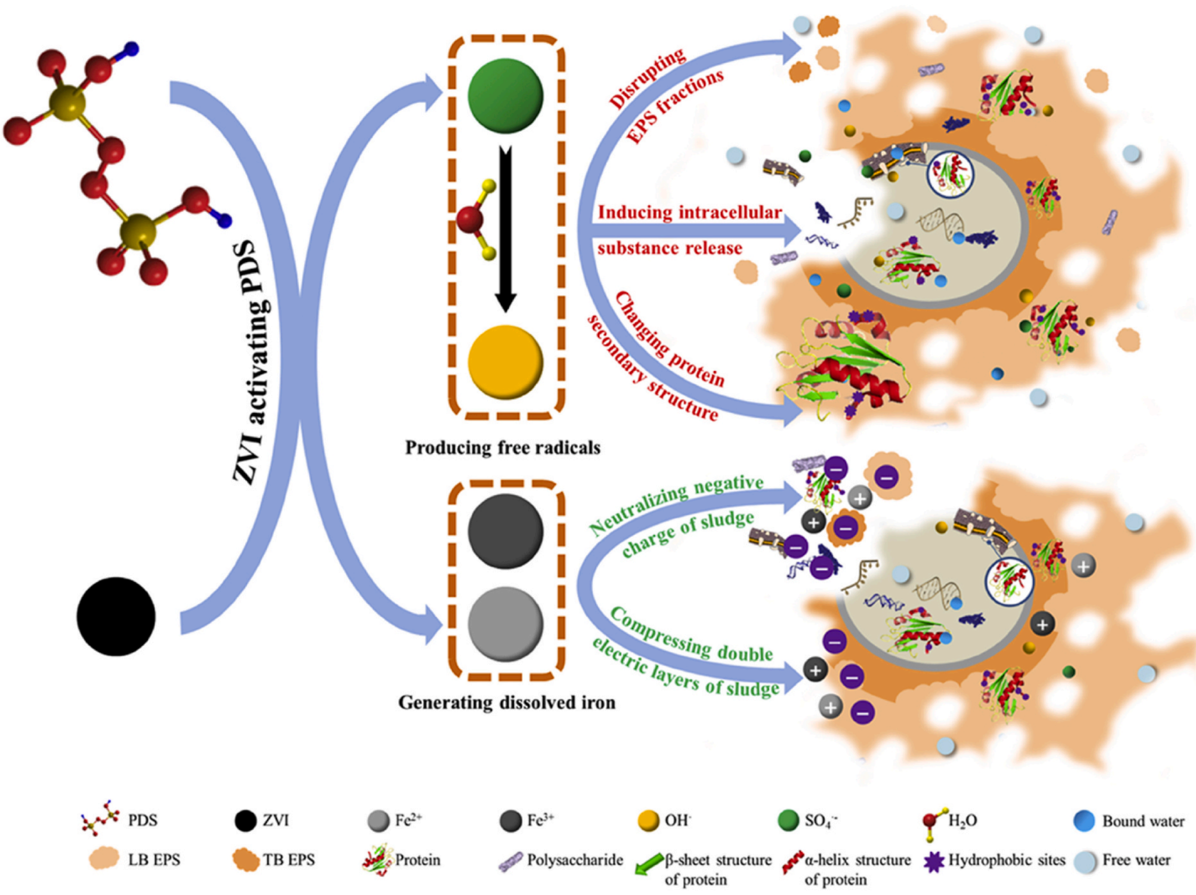

Fig. 9. The possible mechanism of ZVI/PDS treatment enhancing anaerobically digested sludge dewaterability. Reproduced from Ref (Li et al., 2019b).

effectively degrade hydrophilic proteins and fluorescent substances in EPS in sludge, so as to release the bound water and improve the dewatering performance. (ii) The iron-based catalysts used in the sludge treatment of $SO_4^{\bullet -}$-AOPs, in addition to activating persulfate, also act as flocculants to promote the reflocculation of the sludge after dehydration. (iii) $SO_4^{\bullet -}$ can also promote the release and dissolution of heavy metals in sludge by destroying sludge flocculants and reducing pH, thus reducing the toxicity of dehydrated sludge. However, the side effects of adding persulfate and catalyst on sludge treatment also lack systematic studies, such as the impact of Fe^{2+} introduction on sludge calorific value, and the impact of $SO_4^{\bullet -}$ on the transmission of antibiotic resistance genes inside and outside the sludge microorganism cells (Lu et al., 2020; Bian et al., 2021).

6.4. Membrane separation

Another application of $SO_4^{\bullet -}$-AOPs is the combination with membrane separation. On the one hand, it can improve the utilization rate of oxidant, on the other hand, it can realize self-cleaning of the membrane and improve the flux, which has a synergistic effect (Lee et al., 2022). Effluent organic matter, biopolymer, and humus will block the pores inside the membrane and form a pie structure, reducing the membrane flux and causing organic pollution of the membrane (Pramanik et al., 2019; Zhang et al., 2022a). Pramanik et al. (2019) proved that UV/PDS pretreatment could effectively alleviate organic pollution of forward osmosis membranes, and $SO_4^{\bullet -}$ generated by UV/PDS pretreatment could effectively decompose large molecular weight hydrophobic compounds into small molecular weight hydrophilic substances, thus significantly enhancing the flux of membranes. At present, more research is to combine the membrane with a catalyst with good catalytic performance as a highly active catalytic self-cleaning membrane to simultaneously achieve efficient decontamination and self-cleaning of the membrane. Ye et al. (2021a) constructed a macroporous Fe–Co@NC-CNTs/PVDF catalytic membrane. The fully exposed active site catalyzed the PMS to produce a large amount of $SO_4^{\bullet -}$, which had good catalytic and self-cleaning properties in the coexistence system of HA and BPA. 100% removal of BPA was achieved within 40 min while maintaining an extremely high flux (10464.45 L m^{-2} h^{-1}). Similarly, they also coated metal nanoparticles in N-doped microtubule composites and fixed them on polyvinylidene fluoride (PVDF) membrane, effectively avoiding membrane contamination. The unique structure not only prevented the agglomeration of nanoparticles but also suppressed metal leaching (Ye et al., 2021c). Yue et al. (Yue and Sun, 2021) specifically compared the flux retention rate of the catalytic self-cleaning membrane in the presence of PMS, and the results showed that the flux retention rate of the membrane was increased by 30% under the action of PMS. The combination of $SO_4^{\bullet -}$-AOPs and membrane separation was proved to be effective. In addition, the loading amount of the catalyst in the film can be controlled through multiple impregnation cycles to achieve the best utilization of the catalyst and film (Bao et al., 2018).

The loading of highly efficient persulfate catalysts onto the membrane to form a self-cleaning catalytic membrane is an innovative combination of $SO_4^{\bullet -}$-AOPs and membrane separation technology. The self-cleaning of the membrane can be achieved while improving the utilization rate of the oxidant. It should be noted that in the long-term operation, the catalytic activity and transmembrane pressure will deteriorate, the consumption of active sites and the accumulation of small molecular organic matter on the catalytic membrane will hinder its activation of persulfate, resulting in further damage to the catalytic membrane, especially in the treatment of actual water samples (Xia et al., 2022b). Therefore, further efforts are needed to improve the long-term stable operation ability of self-cleaning catalytic membrane in complex water matrix.

6.5. Water disinfection and air purification

In addition to the above applications, $SO_4^{\bullet -}$-AOPs also have applications in water disinfection and air purification. Water disinfection is a method of killing microbial pathogens in water to avoid waterborne diseases. It is generally divided into the physical disinfection methods, electrochemical disinfection methods, and chemical disinfection methods. The former two methods have high energy consumption and operation cost. Traditional chemical disinfectants such as free chlorine, chlorine dioxide and ozone have strong bactericidal effects on microbial pathogens (Xiao et al., 2019). However, they can produce disinfection byproducts (DBPs) and cause secondary pollution to the water body. $SO_4^{\bullet -}$ has a high redox potential and is easy to react with cell structure, resulting in microbial inactivation while producing a low level of DBPs (Lin and Xia, 2022). Under the oxidation of $SO_4^{\bullet -}$, the cell membrane/cell wall of microorganisms is first destroyed, and then the antioxidant enzymes and genetic material are induced to be inactivated, leading to cell death (Wang et al., 2019c). By contrast, Wen et al. (2017) demonstrated the effect of UV/PMS on the cell membrane and cell wall destruction in microorganisms. Under UV alone, the surface structure of microorganisms will not be damaged, while UV/PMS will damage the membrane structure, resulting in the release of intracellular substances and the inactivation of spores. The current research has proved that $SO_4^{\bullet -}$ has strong oxidation and a wide range of pH adaptation. It can effectively destroy intracellular biomolecules (lipids, carbohydrates, proteins, DNA/RNA), and has inactivation effects on microorganisms such as *Escherichia coli*, MS_2 phage and bacillus spores, which has broad application prospects in the inactivation of pathogenic microorganisms in water (Wang et al., 2021b,c). In addition, the potential risks of $SO_4^{\bullet -}$ deactivation techniques, such as the effect of SO_4^{2-} residues in water on TDS and the secondary toxicity of low-level DBPs, should be taken into account.

Persulfate can be used as an absorbent and supplemented by certain activation means to promote the absorption and oxidation of gaseous pollutants in the water phase (Zhang et al., 2015). For example, Adewuyi et al. (Adewuyi and Sakyi, 2013b, 2013a) achieved efficient removal of NO from gas-liquid contactors by using sodium persulfate solution activated simultaneously by temperature and Fe^{2+}. Furthermore, they demonstrated that the presence of SO_2 significantly enhances the absorption and oxidation of NO, while the SO_2 itself is completely removed, which may be helpful for wet flue gas desulfurization. BTEX waste gas (benzene, toluene, ethylbenzene, xylene) is a volatile petroleum organic pollutant, which is difficult to be removed by a wet washing system because of its insolubility. When the persulfate solution containing Fe^{2+} is used for wet washing, the mass transfer effect and oxidation of BTEX can be greatly improved (Liang et al., 2009a). The oxidation and mass transfer of insoluble waste gas can be achieved simultaneously by using water containing strong oxidizing $SO_4^{\bullet -}$ to wet wash the toxic waste gas (benzene, toluene, etc.) that is insoluble in water in the gas phase, which provides a new solution for the purification of harmful gases and the application of $SO_4^{\bullet -}$-AOPs in this field.

7. Conclusions and perspectives

To sum up, this review presents the state-of-art development of $SO_4^{\bullet -}$ generation and application in environmental remediation. The generation mechanism of $SO_4^{\bullet -}$ under different activation strategies is emphasized, which provides a new idea for the rational design of catalysts in practical applications. The latest application status of $SO_4^{\bullet -}$ in different fields of environmental remediation is systematically summarized, and the main challenges in the application of $SO_4^{\bullet -}$ in different fields are presented. Based on the previous review and discussion, future research needs for $SO_4^{\bullet -}$-AOPs were also proposed, as described below.

(1) The metal-support composite catalyst combines the advantages of mono-metal/bimetallic oxides and carbon materials, which has low metal leaching rate and good cycling stability. It is an ideal catalyst for activating persulfate and sulfite to produce $SO_4^{\bullet -}$. However, the synthesis process usually involves complex materials and harsh conditions, which limits their application in practical environmental remediation. Therefore, the development of simple and cost-effective metal-supported catalysts is the key to bringing $SO_4^{\bullet -}$-AOPs to practical applications.

(2) Both persulfate and sulfite can be used as precursors for the production of $SO_4^{\bullet -}$, but they are different in the specific activation mechanism, action mode, and application scenarios. Low-cost sulfites are more favorable for industrial applications of $SO_4^{\bullet -}$-AOPs, but the formation of $SO_4^{\bullet -}$ in sulfite activation requires an aerobic environment. Therefore, sulfite-based AOPs are suitable for aerated water bodies or oxygen-rich environments. In addition, in the process of sulfite activation, reducing active species (hydrated electrons (e_{aq}^-) and hydrogen radicals (•H)) are generated at the same time. They have different degradation mechanisms and kinetics, which may lead to different degradation products and intermediates toxicity from sulfite-based AOPs in environmental remediation. It needs to be further studied.

(3) When reacting with different kinds of pollutants, $SO_4^{\bullet -}$ and •OH show different reactivity, which is related to their oxidation potential, electrophilicity, and reaction energy barrier, and also related to the highest occupied molecular orbital and electrostatic potential of pollutant molecules (Zhang et al., 2023a). Combining the degradation products of pollutants and DFT calculation to analyze the active sites of target pollutants, and thus to analyze the energy evolution law of the reaction between two kinds of free radicals and pollutants through three paths, is a more in-depth understanding of the degradation mechanism of organic pollutants under the action of active species, which can greatly promote the selective degradation and directional transformation of target pollutants.

(4) Since $SO_4^{\bullet -}$ is very easy to be converted into •OH, the existing detection methods are difficult to accurately determine the content and contribution of $SO_4^{\bullet -}$. The use of HPLC to determine the characteristic products of the reaction between the capture agent and the active substance has been used as a quantitative method for high-valent iron species and •OH. Unfortunately, there are few studies on the quantitative determination of $SO_4^{\bullet -}$ by similar methods. It is necessary to develop capture agents that specifically react with $SO_4^{\bullet -}$, coupled with high-precision instruments to quantitatively detect their concentrations, so as to gain a deeper understanding of their contributions and response mechanisms.

(5) $SO_4^{\bullet -}$-AOPs are recommended as an adjunct to wastewater treatment, such as in membrane reactors for wastewater retreatment, to maximize the oxidation capacity of $SO_4^{\bullet -}$ for stubborn contaminants and reduce its impact on water quality. In addition, special attention should be paid to the production of toxic by-products. Unlike the reversible reaction of •OH with halogen ions, $SO_4^{\bullet -}$ tends to react with halogen ions to form halogen radicals, which can further react with organic matter in wastewater to form toxic halide byproducts.

(6) The potential risks of intermediates need to be carefully evaluated before specific application, as some intermediates may be more toxic than their corresponding parent compounds. In addition, attention should be paid to the risk of pH reduction in groundwater due to persulfate decomposition, which can lead to the leaching of heavy metals underground.

(7) $SO_4^{\bullet -}$ can effectively destruct the structure of sludge and make it release the bound water and heavy metals, which has a good application prospect in sludge dewatering and harmless treatment. However, the side effects of adding persulfate and catalyst

on sludge treatment also lack systematic studies, such as the impact of Fe^{2+} introduction on sludge calorific value, and the impact of $SO_4^{\bullet -}$ on the transmission of antibiotic resistance genes inside and outside the sludge microorganism cells, and the subsequent treatment of sludge dehydrated filtrate.

Author contribution statement

Jun Xie: Conceptualization, Methodology, Investigation, Writing-original draft, Writing-reviewing & editing. **Chunping Yang**: Conceptualization, Supervision, Project administration, Funding acquisition, Writing-original draft, Writing-review & editing. **Xiang Li**: Visualization, Writing-original draft, Writing-reviewing & editing. **Shaohua Wu**: Investigation, Conceptualization, Funding acquisition, Writing-review & editing, Writing-original draft. **Yan Lin**: Investigation, Writing-original draft, Writing-reviewing & editing.

Declaration of competing interest

The authors declare that they have no known competing financial interests or personal relationships that could have appeared to influence the work reported in this paper.

Data availability

Data will be made available on request.

Acknowledgements

This work was supported by the National Natural Science Foundation of China (Grant No.: 52200093, 52270064, 52100081, 51978178 and 51521006), the Department of Science and Technology of Guangdong Province of China (Contract No.: 2023A1515012062, 2022A1515010226, 2021A1515011797 and 2019A1515012044), the Department of Education of Guangdong Province of China (Contract No.: 2021KTSCX078), Hunan Provincial Natural Science Foundation of China (Contract No.: 2022JJ40036), Maoming Municipal Department of Science and Technology of Guangdong Province of China (Contract No.: 2018S0013), the Key Laboratory of Petrochemical Pollution Control of Guangdong Higher Education Institutes (KLGHEI 2017KSYS004), and the Startup Fund of Guangdong University of Petrochemical Technology (Contract No.: 2020rc041 and 2018rc63).

References

Abdul Nasir Khan, M., Kwame Klu, P., Wang, C., Zhang, W., Luo, R., Zhang, M., Qi, J., Sun, X., Wang, L., Li, J., 2019. Metal-organic framework-derived hollow Co_3O_4/carbon as efficient catalyst for peroxymonosulfate activation. Chem. Eng. J. 363, 234–246.

Adewuyi, Y.G., Sakyi, N.Y., 2013a. Removal of nitric oxide by aqueous sodium persulfate simultaneously activated by temperature and Fe^{2+} in a lab-scale bubble reactor. Ind. Eng. Chem. Res. 52, 14687–14697.

Adewuyi, Y.G., Sakyi, N.Y., 2013b. Simultaneous absorption and oxidation of nitric oxide and sulfur dioxide by aqueous solutions of sodium persulfate activated by temperature. Ind. Eng. Chem. Res. 52, 11702–11711.

Ahmadi, M., Ghanbari, F., 2018. Combination of UVC-LEDs and ultrasound for peroxymonosulfate activation to degrade synthetic dye: influence of promotional and inhibitory agents and application for real wastewater. Environ. Sci. Pollut. Control Ser. 25, 6003–6014.

Anipsitakis, G.P., Dionysiou, D.D., 2004. Radical generation by the interaction of transition metals with common oxidants. Environ. Sci. Technol. 38, 3705–3712.

Anipsitakis, G.P., Dionysiou, D.D., Gonzalez, M.A., 2006. Cobalt-mediated activation of peroxymonosulfate and sulfate radical attack on phenolic compounds. implications of chloride ions. Environ. Sci. Technol. 40, 1000–1007.

Anipsitakis, G.P., Stathatos, E., Dionysiou, D.D., 2005. Heterogeneous activation of oxone using Co_3O_4. J. Phys. Chem. B 109, 13052–13055.

Antoniou, M.G., de la Cruz, A.A., Dionysiou, D.D., 2010. Intermediates and reaction pathways from the degradation of microcystin-LR with sulfate radicals. Environ. Sci. Technol. 44, 7238–7244.

Ao, X., Liu, W., 2017. Degradation of sulfamethoxazole by medium pressure UV and oxidants: peroxymonosulfate, persulfate, and hydrogen peroxide. Chem. Eng. J. 313, 629–637.

Asgari, G., Shabanloo, A., Salari, M., Eslami, F., 2020. Sonophotocatalytic treatment of AB113 dye and real textile wastewater using ZnO/persulfate: modeling by response surface methodology and artificial neural network. Environ. Res. 184, 109367.

Babaei, A.A., Ghanbari, F., 2016. COD removal from petrochemical wastewater by UV/hydrogen peroxide, UV/persulfate and UV/percarbonate: biodegradability improvement and cost evaluation. J. Water Reuse Desalination 6, 484–494.

Babel, S., del Mundo Dacera, D., 2006. Heavy metal removal from contaminated sludge for land application: a review. Waste Manag. 26, 988–1004.

Bai, L., Wang, G., Ge, D., Dong, Y., Wang, H., Wang, Y., Zhu, N., Yuan, H., 2022. Enhanced waste activated sludge dewaterability by the ozone-peroxymonosulfate oxidation process: performance, sludge characteristics, and implication. Sci. Total Environ. 807.

Bao, C., Wang, H., Wang, C., Zhang, X., Zhao, X., Dong, C.-L., Huang, Y.-C., Chen, S., Guo, P., She, X., Sun, Y., Yang, D., 2023. Cooperation of oxygen vacancy and Fe^{III}/Fe^{II} sites in H_2-reduced Fe-MIL-101 for enhanced Fenton-like degradation of organic pollutants. J. Hazard Mater. 441, 129922.

Bao, Y., Lim, T.-T., Wang, R., Webster, R.D., Hu, X., 2018. Urea-assisted one-step synthesis of cobalt ferrite impregnated ceramic membrane for sulfamethoxazole degradation via peroxymonosulfate activation. Chem. Eng. J. 343, 737–747.

Barzegar, G., Jorfi, S., Zarezade, V., Khatebasreh, M., Mehdipour, F., Ghanbari, F., 2018. 4-Chlorophenol degradation using ultrasound/peroxymonosulfate/nanoscale zero valent iron: reusability, identification of degradation intermediates and potential application for real wastewater. Chemosphere 201, 370–379.

Bian, C., Ge, D., Wang, G., Dong, Y., Li, W., Zhu, N., Yuan, H., 2021. Enhancement of waste activated sludge dewaterability by ultrasound-activated persulfate oxidation: operation condition, sludge properties, and mechanisms. Chemosphere 262, 128385.

Bilgin Oncu, N., Akmehmet Balcioglu, I., 2013. Microwave-assisted chemical oxidation of biological waste sludge: simultaneous micropollutant degradation and sludge solubilization. Bioresour. Technol. 146, 126–134.

Buxton, G.V., Greenstock, C.L., Helman, W.P., Ross, A.B., 1988. Critical Review of rate constants for reactions of hydrated electrons, hydrogen atoms and hydroxyl radicals ($\bullet OH/O^{\bullet -}$) in Aqueous Solution. J. Phys. Chem. Ref. Data 17, 513–886.

Cao, Y., Qiu, W., Li, J., Jiang, J., Pang, S., 2021. Review on UV/sulfite process for water and wastewater treatments in the presence or absence of O_2. Sci. Total Environ. 765, 142762.

Caregnato, P., Mora, V.C., Le Roux, G.C., Mártire, D.O., Gonzalez, M.C., 2003. A kinetic study of the reactions of sulfate radicals at the silica nanoparticle−water interface. J. Phys. Chem. B 107, 6131–6138.

Chen, C., Wu, Z., Zheng, S., Wang, L., Niu, X., Fang, J., 2020a. Comparative study for interactions of sulfate radical and hydroxyl rRadical with phenol in the presence of nitrite. Environ. Sci. Technol. 54, 8455–8463.

Chen, J., Zhou, X., Zhu, Y., Zhang, Y., Huang, C.-H., 2020b. Synergistic activation of peroxydisulfate with magnetite and copper ion at neutral condition. Water Res. 186.

Chen, L., Xue, Y., Luo, T., Wu, F., Alshawabkeh, A.N., 2021. Electrolysis-assisted UV/sulfite oxidation for water treatment with automatic adjustments of solution pH and dissolved oxygen. Chem. Eng. J. 403.

Chen, M., Ling, X., Cai, A., Deng, J., Zhu, S., Zeng, H., Li, X., 2022a. Pyrite catalyzed peroxydisulfate for improving dewaterability of waste activated sludge: reaction sequence of hydrophobic/hydrophilic structures. J. Environ. Chem. Eng. 10.

Chen, W.-S., Huang, C.-P., 2015. Mineralization of aniline in aqueous solution by electro-activated persulfate oxidation enhanced with ultrasound. Chem. Eng. J. 266, 279–288.

Chen, W., Luo, Y., Ran, G., Li, Q., 2019. An investigation of refractory organics in membrane bioreactor effluent following the treatment of landfill leachate by the O_3/H_2O_2 and MW/PS processes. Waste Manag. 97, 1–9.

Chen, W., Luo, Y., Ran, G., Li, Q., 2020c. Microwave-induced persulfate-hydrogen peroxide binary oxidant process for the treatment of dinitrodiazophenol industrial wastewater. Chem. Eng. J. 382, 122803.

Chen, W., Wang, F., He, C., Li, Q., 2020d. Molecular-level comparison study on microwave irradiation-activated persulfate and hydrogen peroxide processes for the treatment of refractory organics in mature landfill leachate. J. Hazard Mater. 397, 122785.

Chen, Y., Vu, H.C., Miller, C.J., Garg, S., Pan, D., Waite, T.D., 2022b. Comparative experimental and computational studies of hydroxyl and sulfate radical-mediated degradation of simple and complex organic substrates. Environ. Sci. Technol. 56, 8819–8832.

Chu, W., Hu, J., Bond, T., Gao, N., Xu, B., Yin, D., 2016. Water temperature significantly impacts the formation of iodinated haloacetamides during persulfate oxidation. Water Res. 98, 47–55.

Clifton, C.L., Huie, R.E., 1989. Rate constants for hydrogen abstraction reactions of the sulfate radical, SO_4^-. Alcohols. Int. J. Chem. Kinet. 21, 677–687.

Costanza, J., Otaño, G., Callaghan, J., Pennell, K.D., 2010. PCE oxidation by sodium persulfate in the presence of solids. Environ. Sci. Technol. 44, 9445–9450.

Dąbrowski, A., Podkościelny, P., Hubicki, Z., Barczak, M., 2005. Adsorption of phenolic compounds by activated carbon—a critical review. Chemosphere 58, 1049–1070.

Das, T.N., Huie, R.E., Neta, P., 1999. Reduction potentials of $SO_3^{\bullet -}$, $SO_5^{\bullet -}$, and $S_4O_6^{\bullet 3-}$ radicals in aqueous solution. J. Phys. Chem. 103, 3581–3588.

Delavaran Shiraz, A., Takdastan, A., Borghei, S.M., 2018. Photo-Fenton like degradation of catechol using persulfate activated by UV and ferrous ions: influencing operational parameters and feasibility studies. J. Mol. Liq. 249, 463–469.

Deng, D., Pan, X., Yu, L., Cui, Y., Jiang, Y., Qi, J., Li, W.-X., Fu, Q., Ma, X., Xue, Q., Sun, G., Bao, X., 2011. Toward N-doped graphene via solvothermal synthesis. Chem. Mater. 23, 1188–1193.

Dinesh, G.K., Anandan, S., Sivasankar, T., 2016. Synthesis of Fe-doped Bi_2O_3 nanocatalyst and its sonophotocatalytic activity on synthetic dye and real textile wastewater. Environ. Sci. Pollut. Control Ser. 23, 20100–20110.

Ding, Y., Zhu, L., Wang, N., Tang, H., 2013. Sulfate radicals induced degradation of tetrabromobisphenol A with nanoscaled magnetic $CuFe_2O_4$ as a heterogeneous catalyst of peroxymonosulfate. Appl. Catal. B Environ. 129, 153–162.

Dong, C.-D., Chen, C.-W., Hung, C.-M., 2017. Synthesis of magnetic biochar from bamboo biomass to activate persulfate for the removal of polycyclic aromatic hydrocarbons in marine sediments. Bioresour. Technol. 245, 188–195.

Dong, H., Hou, K., Qiao, W., Cheng, Y., Zhang, L., Wang, B., Li, L., Wang, Y., Ning, Q., Zeng, G., 2019. Insights into enhanced removal of TCE utilizing sulfide-modified nanoscale zero-valent iron activated persulfate. Chem. Eng. J. 359, 1046–1055.

Duan, X., O'Donnell, K., Sun, H., Wang, Y., Wang, S., 2015a. Sulfur and nitrogen Co-doped graphene for metal-free catalytic oxidation reactions. Small 11, 3036–3044.

Duan, X., Sun, H., Wang, Y., Kang, J., Wang, S., 2015b. N-doping-induced nonradical reaction on single-walled carbon nanotubes for catalytic phenol oxidation. ACS Catal. 5, 553–559.

Eslami, A., Hashemi, M., Ghanbari, F., 2018. Degradation of 4-chlorophenol using catalyzed peroxymonosulfate with nano-MnO_2/UV irradiation: toxicity assessment and evaluation for industrial wastewater treatment. J. Clean. Prod. 195, 1389–1397.

Fang, G.-D., Dionysiou, D.D., Wang, Y., Al-Abed, S.R., Zhou, D.-M., 2012. Sulfate radical-based degradation of polychlorinated biphenyls: effects of chloride ion and reaction kinetics. J. Hazard Mater. 227–228, 394–401.

Fang, G., Gao, J., Dionysiou, D.D., Liu, C., Zhou, D., 2013. Activation of persulfate by quinones: free radical reactions and implication for the degradation of PCBs. Environ. Sci. Technol. 47, 4605–4611.

Fang, G., Liu, C., Gao, J., Dionysiou, D.D., Zhou, D., 2015. Manipulation of persistent free radicals in biochar to activate persulfate for contaminant degradation. Environ. Sci. Technol. 49, 5645–5653.

Fang, Y., Liu, Q., Song, Y., Cai, H., Yang, Y., Yang, Z., Li, H., 2023. Highly efficient in-situ purification of Fe(II)-rich high-arsenic groundwater under anoxic conditions: promotion mechanisms of PMS on oxidation and adsorption. Chem. Eng. J. 453, 139915.

Fei, L., Ren, S., Xijun, M., Ali, N., Jing, Z., Yi, J., Bilal, M., 2021. Efficient removal of EDTA-chelated Cu(II) by zero-valent iron and peroxydisulfate: mutual activation process. Separ. Purif. Technol. 279, 119721.

Fu, X., Lin, Y., Yang, C., Wu, S., Wang, Y., Li, X., 2022. Peroxymonosulfate activation via CoP nanoparticles confined in nitrogen-doped porous carbon for enhanced degradation of sulfamethoxazole in wastewater with high salinity. J. Environ. Chem. Eng. 10, 107734.

Gao, L., Guo, Y., Zhan, J., Yu, G., Wang, Y., 2022a. Assessment of the validity of the quenching method for evaluating the role of reactive species in pollutant abatement during the persulfate-based process. Water Res. 221, 118730.

Gao, Y.-Q., Zhou, J.-Q., Ning, H., Rao, Y.-Y., Gao, N.-Y., 2022b. Electrochemically activated peroxymonosulfate for the abatement of chloramphenicol in water: performance and mechanism. Environ. Sci. Pollut. Control Ser. 29, 17866–17877.

Gao, Y., Li, Y., Yao, L., Li, S., Liu, J., Zhang, H., 2017. Catalyst-free activation of peroxides under visible LED light irradiation through photoexcitation pathway. J. Hazard Mater. 329, 272–279.

Gao, Y., Zhu, Y., Li, T., Chen, Z., Jiang, Q., Zhao, Z., Liang, X., Hu, C., 2021. Unraveling the high-activity origin of single-atom iron catalysts for organic pollutant oxidation via peroxymonosulfate activation. Environ. Sci. Technol. 55, 8318–8328.

Ghanbari, F., Ahmadi, M., Gohari, F., 2019. Heterogeneous activation of peroxymonosulfate via nanocomposite CeO_2-Fe_3O_4 for organic pollutants removal: the effect of UV and US irradiation and application for real wastewater. Separ. Purif. Technol. 228, 115732.

Ghanbari, F., Khatebasreh, M., Mahdavianpour, M., Lin, K.-Y.A., 2020. Oxidative removal of benzotriazole using peroxymonosulfate/ozone/ultrasound: synergy, optimization, degradation intermediates and utilizing for real wastewater. Chemosphere 244, 125326.

Ghanbari, F., Moradi, M., Manshouri, M., 2014. Textile wastewater decolorization by zero valent iron activated peroxymonosulfate: compared with zero valent copper. J. Environ. Chem. Eng. 2, 1846–1851.

Ghauch, A., Ayoub, G., Naim, S., 2013. Degradation of sulfamethoxazole by persulfate assisted micrometric Fe^0 in aqueous solution. Chem. Eng. J. 228, 1168–1181.

Giannakis, S., Lin, K.-Y.A., Ghanbari, F., 2021. A review of the recent advances on the treatment of industrial wastewaters by sulfate radical-based advanced oxidation processes (SR-AOPs). Chem. Eng. J. 406, 127083.

Gu, X., Lu, S., Qiu, Z., Sui, Q., Miao, Z., Lin, K., Liu, Y., Luo, Q., 2012. Comparison of photodegradation performance of 1,1,1-trichloroethane in aqueous solution with the addition of H_2O_2 or $S_2O_8^{2-}$ Oxidants. Ind. Eng. Chem. Res. 51, 7196–7204.

Guo, R., Meng, Q., Zhang, H., Zhang, X., Li, B., Cheng, Q., Cheng, X., 2019. Construction of Fe_2O_3/Co_3O_4/exfoliated graphite composite and its high efficient treatment of landfill leachate by activation of potassium persulfate. Chem. Eng. J. 355, 952–962.

Guo, S., Wang, Q., Luo, C., Yao, J., Qiu, Z., Li, Q., 2020. Hydroxyl radical-based and sulfate radical-based photocatalytic advanced oxidation processes for treatment of refractory organic matter in semi-aerobic aged refuse biofilter effluent arising from treating landfill leachate. Chemosphere 243, 125390.

Han, D., Wan, J., Ma, Y., Wang, Y., Li, Y., Li, D., Guan, Z., 2015. New insights into the role of organic chelating agents in Fe(II) activated persulfate processes. Chem. Eng. J. 269, 425–433.

Han, X., Zhang, W., Li, S., Cheng, C., Zhou, L., Jia, Q., Xiu, G., 2022. Efficient activation of peroxymonosulfate by MnS/Fe-MOF hybrid catalyst for sulfadiazine degradation: synergistic effects and mechanism. Separ. Purif. Technol. 287, 120509.

Hayyan, M., Hashim, M.A., AlNashef, I.M., 2016. Superoxide ion: generation and chemical implications. Chem. Rev. 116, 3029–3085.

He, Q., Si, S., Song, L., Yan, H., Yao, Y., Zhao, D., Cai, Q., 2019. Refractory petrochemical wastewater treatment by $K_2S_2O_8$ assisted photocatalysis. Saudi J. Biol. Sci. 26, 849–853.

Hong, Y., Luo, Z., Zhang, N., Qu, L., Zheng, M., Suara, M.A., Chelme-Ayala, P., Zhou, X., Gamal El-Din, M., 2022. Decomplexation of Cu(II)-EDTA by synergistic activation of persulfate with alkali and CuO: kinetics and activation mechanism. Sci. Total Environ. 817, 152793.

Hou, S., Ling, L., Shang, C., Guan, Y., Fang, J., 2017. Degradation kinetics and pathways of haloacetonitriles by the UV/persulfate process. Chem. Eng. J. 320, 478–484.

Hu, L., Wang, P., Shen, T., Wang, Q., Wang, X., Xu, P., Zheng, Q., Zhang, G., 2020. The application of microwaves in sulfate radical-based advanced oxidation processes for environmental remediation: a review. Sci. Total Environ. 722, 137831.

Hu, L., Zhang, G., Wang, Q., Wang, X., Wang, P., 2019. Effect of microwave heating on persulfate activation for rapid degradation and mineralization of p-Nitrophenol. ACS Sustain. Chem. Eng. 7, 11662–11671.

Huang, W., Xiao, S., Zhong, H., Yan, M., Yang, X., 2021. Activation of persulfates by carbonaceous materials: a review. Chem. Eng. J. 418, 129297.

Huang, Y., Han, C., Liu, Y., Nadagouda, M.N., Machala, L., O'Shea, K.E., Sharma, V.K., Dionysiou, D.D., 2018. Degradation of atrazine by $Zn_xCu_1{-}xFe_2O_4$ nanomaterial-catalyzed sulfite under UV–vis light irradiation: green strategy to generate $SO_4^{\bullet-}$. Appl. Catal. B Environ. 221, 380–392.

Hung, C.-M., Chen, C.-W., Huang, C.-P., Dong, C.-D., 2022. Bioremediation pretreatment of waste-activated sludge using microalgae spirulina platensis derived biochar coupled with sodium sulfite: performance and microbial community dynamics. Bioresour. Technol. 362.

Iyyappan, J., Baskar, G., Deepanraj, B., Anand, A.V., Saravanan, R., Awasthi, M.K., 2023. Promising strategies of circular bioeconomy using heavy metal phytoremediated plants–A critical review. Chemosphere 313, 137097.

Ji, F., Li, C., Wei, X., Yu, J., 2013. Efficient performance of porous Fe_2O_3 in heterogeneous activation of peroxymonosulfate for decolorization of Rhodamine B. Chem. Eng. J. 231, 434–440.

Ji, Y., Wang, L., Jiang, M., Lu, J., Ferronato, C., Chovelon, J.-M., 2017. The role of nitrite in sulfate radical-based degradation of phenolic compounds: an unexpected nitration process relevant to groundwater remediation by in-situ chemical oxidation (ISCO). Water Res. 123, 249–257.

Jiang, B., Xin, S., Liu, Y., He, H., Li, L., Tang, Y., Luo, S., Bi, X., 2018a. The role of thiocyanate in enhancing the process of sulfite reducing Cr(VI) by inhibiting the formation of reactive oxygen species. J. Hazard Mater. 343, 1–9.

Jiang, F., Li, Y., Zhou, W., Yang, Z., Ning, Y., Liu, D., Tang, Z., Yang, S., Huang, H., Wang, G., 2020. Enhanced degradation of monochlorobenzene in groundwater by ferrous iron/persulfate process with cysteine. Chem. Eng. J. 387.

Jiang, M., Lu, J., Ji, Y., Kong, D., 2017. Bicarbonate-activated persulfate oxidation of acetaminophen. Water Res. 116, 324–331.

Jiang, X., Guo, Y., Zhang, L., Jiang, W., Xie, R., 2018b. Catalytic degradation of tetracycline hydrochloride by persulfate activated with nano Fe^0 immobilized mesoporous carbon. Chem. Eng. J. 341, 392–401.

Kang, J., Duan, X., Zhou, L., Sun, H., Tadé, M.O., Wang, S., 2016. Carbocatalytic activation of persulfate for removal of antibiotics in water solutions. Chem. Eng. J. 288, 399–405.

Karimipourfard, D., Eslamloueyan, R., Mehranbod, N., 2020. Heterogeneous degradation of stabilized landfill leachate using persulfate activation by $CuFe_2O_4$ nanocatalyst: an experimental investigation. J. Environ. Chem. Eng. 8, 103426.

Kong, X.-K., Chen, C.-L., Chen, Q.-W., 2014. Doped graphene for metal-free catalysis. Chem. Soc. Rev. 43, 2841–2857.

Kwan, W.P., Voelker, B.M., 2003. Rates of hydroxyl radical generation and organic compound oxidation in mineral-catalyzed Fenton-like systems. Environ. Sci. Technol. 37, 1150–1158.

Lee, J., von Gunten, U., Kim, J.-H., 2020. Persulfate-based advanced oxidation: critical assessment of opportunities and roadblocks. Environ. Sci. Technol. 54, 3064–3081.

Lee, W.J., Bao, Y., Liangdy, A., Hu, X., Lim, T.-T., 2022. Insights into the synergistic role of catalytic ceramic membranes for ozone and peroxymonosulfate activation towards effective recalcitrant micropollutant degradation and mineralization. Chem. Eng. J. 430.

Lente, G., Fabian, I., 2002. Kinetics and mechanism of the oxidation of sulfur(IV) by iron (III) at metal ion excess. J. Chem. Soc. Dalton Trans. 778–784.

Li, A., Wu, Z., Wang, T., Hou, S., Huang, B., Kong, X., Li, X., Guan, Y., Qiu, R., Fang, J., 2018a. Kinetics and mechanisms of the degradation of PPCPs by zero-valent iron (Fe degrees) activated peroxydisulfate (PDS) system in groundwater. J. Hazard Mater. 357, 207–216.

Li, B., Zhu, J., 2016. Simultaneous degradation of 1,1,1-trichloroethane and solvent stabilizer 1,4-dioxane by a sono-activated persulfate process. Chem. Eng. J. 284, 750–763.

Li, H., Zhang, Y., Wan, J., Xiao, H., Chen, X., 2018b. Theoretical investigation on the oxidation mechanism of dibutyl phthalate by hydroxyl and sulfate radicals in the gas and aqueous phase. Chem. Eng. J. 339, 381–392.

Li, J., Yan, J., Yao, G., Zhang, Y., Li, X., Lai, B., 2019a. Improving the degradation of atrazine in the three-dimensional (3D) electrochemical process using $CuFe_2O_4$ as both particle electrode and catalyst for persulfate activation. Chem. Eng. J. 361, 1317–1332.

Li, J., Zhu, W., Gao, Y., Lin, P., Liu, J., Zhang, J., Huang, T., 2022a. The catalyst derived from the sulfurized Co-doped metal–organic framework (MOF) for peroxymonosulfate (PMS) activation and its application to pollutant removal. Separ. Purif. Technol. 285, 120362.

Li, M., Sun, J., Han, D., Wei, B., Mei, Q., An, Z., Wang, X., Cao, H., Xie, J., He, M., 2020a. Theoretical investigation on the contribution of •OH, $SO_4^{\bullet-}$ and $CO_3^{\bullet-}$ radicals to the degradation of phenacetin in water: mechanisms, kinetics, and toxicity evaluation. Ecotoxicol. Environ. Saf. 204, 110977.

Li, N., Wu, S., Dai, H., Cheng, Z., Peng, W., Yan, B., Chen, G., Wang, S., Duan, X., 2022b. Thermal activation of persulfates for organic wastewater purification: heating modes, mechanism and influencing factors. Chem. Eng. J. 450, 137976.

Li, R., Yang, C., Chen, H., Zeng, G., Yu, G., Guo, J., 2009. Removal of triazophos pesticide from wastewater with Fenton reagent. J. Hazard Mater. 167, 1028–1032.

Li, S., Tang, J., Liu, Q., Liu, X., Gao, B., 2020b. A novel stabilized carbon-coated nZVI as heterogeneous persulfate catalyst for enhanced degradation of 4-chlorophenol. Environ. Int. 138, 105639.

Li, W., Orozco, R., Camargos, N., Liu, H., 2017. Mechanisms on the impacts of alkalinity, pH, and chloride on persulfate-based groundwater remediation. Environ. Sci. Technol. 51, 3948–3959.

Li, X., Wu, L., Zhang, A., Wu, S., Lin, Y., Yang, C., 2024. Cobalt doping amount determines dominant reactive species in peroxymonosulfate activation via porous carbon catalysts co-doped by cobalt and nitrogen. J. Environ. Sci. 138, 212–226.

Li, Y., Pan, L., Zhu, Y., Yu, Y., Wang, D., Yang, G., Yuan, X., Liu, X., Li, H., Zhang, J., 2019b. How does zero valent iron activating peroxydisulfate improve the dewatering of anaerobically digested sludge? Water Res. 163.

Li, Y., Yang, Z., Yang, K., Wei, J., Li, Z., Ma, C., Yang, X., Wang, T., Zeng, G., Yu, G., Yu, Z., Zhang, C., 2022c. Removal of chloride from water and wastewater: removal mechanisms and recent trends. Sci. Total Environ. 821, 153174.

Liang, C., Chen, Y.-J., Chang, K.-J., 2009a. Evaluation of persulfate oxidative wet scrubber for removing BTEX gases. J. Hazard Mater. 164, 571–579.

Liang, C., Huang, C.-F., Chen, Y.-J., 2008. Potential for activated persulfate degradation of BTEX contamination. Water Res. 42, 4091–4100.

Liang, C., Lin, Y.-T., Shih, W.-H., 2009b. Treatment of trichloroethylene by adsorption and persulfate oxidation in batch Studies. Ind. Eng. Chem. Res. 48, 8373–8380.

Liang, C., Su, H.-W., 2009. Identification of sulfate and hydroxyl radicals in thermally activated persulfate. Ind. Eng. Chem. Res. 48, 5558–5562.

Liang, J., Zhang, L., Zhou, Y., 2021. Pyrite assisted peroxymonosulfate sludge conditioning: uncover triclosan transformation during treatment. J. Hazard Mater. 413.

Liang, P., Zhang, C., Duan, X., Sun, H., Liu, S., Tade, M.O., Wang, S., 2017. An insight into metal organic framework derived N-doped graphene for the oxidative degradation of persistent contaminants: formation mechanism and generation of singlet oxygen from peroxymonosulfate. Environ. Sci.: Nano 4, 315–324.

Liang, X., Wang, D., Zhao, Z., Li, T., Chen, Z., Gao, Y., Hu, C., 2022. Engineering the low-coordinated single cobalt atom to boost persulfate activation for enhanced organic pollutant oxidation. Appl. Catal. B Environ. 303.

Lin, K.-Y.A., Chen, B.-J., 2017. Prussian blue analogue derived magnetic carbon/cobalt/iron nanocomposite as an efficient and recyclable catalyst for activation of peroxymonosulfate. Chemosphere 166, 146–156.

Lin, Y., Wu, S., Yang, C., Chen, M., Li, X., 2019. Preparation of size-controlled silver phosphate catalysts and their enhanced photocatalysis performance via synergetic effect with MWCNTs and PANI. Appl. Catal. B Environ. 245, 71–86.

Lin, M., Xia, D., 2022. Sulfate radical-based advanced oxidation processes for water disinfection. Environ. Chem. 41, 2813–2822.

Lin, Y., Yang, C., Niu, Q., Luo, S., 2022. Interfacial charge transfer between silver phosphate and W_2N_3 induced by nitrogen vacancies enhances removal of beta-Lactam antibiotics. Adv. Funct. Mater. 32.

Liu, C., Chen, D., Chen, X.e., Wu, B., 2021a. Application of zero-valent iron/sulfite system for aerobically digested sludge conditioning. Chem. Eng. J. (Amsterdam, Neth.) 420.

Liu, C., Wu, B., Chen, X.e., 2018a. Sulfate radical-based oxidation for sludge treatment: a review. Chem. Eng. J. 335, 865–875.

Liu, C., Wu, B., Chen, X.e., 2020. Ultrasound enhanced zero-valent iron-activated peroxymonosulfate oxidation for improving dewaterability of aerobically digested sludge. Chem. Eng. J. (Amsterdam, Neth.) 392.

Liu, H., Bruton, T.A., Doyle, F.M., Sedlak, D.L., 2014. In situ chemical oxidation of contaminated groundwater by persulfate: decomposition by Fe(III)- and Mn(IV)-containing oxides and aquifer materials. Environ. Sci. Technol. 48, 10330–10336.

Liu, H., Bruton, T.A., Li, W., Van Buren, J., Prasse, C., Doyle, F.M., Sedlak, D.L., 2016a. Oxidation of benzene by persulfate in the presence of Fe(III)- and Mn(IV)-containing oxides: stoichiometric efficiency and transformation products. Environ. Sci. Technol. 50, 890–898.

Liu, H., Sun, P., Feng, M., Liu, H., Yang, S., Wang, L., Wang, Z., 2016b. Nitrogen and sulfur co-doped CNT-COOH as an efficient metal-free catalyst for the degradation of UV filter BP-4 based on sulfate radicals. Appl. Catal. B Environ. 187, 1–10.

Liu, J., Zhao, Z., Shao, P., Cui, F., 2015a. Activation of peroxymonosulfate with magnetic Fe_3O_4–MnO_2 core–shell nanocomposites for 4-chlorophenol degradation. Chem. Eng. J. 262, 854–861.

Liu, L., Zhu, Y.-P., Su, M., Yuan, Z.-Y., 2015b. Metal-free carbonaceous materials as promising heterogeneous catalysts. ChemCatChem 7, 2765–2787.

Liu, Q., Wang, Y., Hu, Z., Zhang, Z., 2021b. Iron-based single-atom electrocatalysts: synthetic strategies and applications. RSC Adv. 11, 3079–3095.

Liu, X., Li, X.-M., Yang, Q., Yue, X., Shen, T.-T., Zheng, W., Luo, K., Sun, Y.-H., Zeng, G.-M., 2012. Landfill leachate pretreatment by coagulation-flocculation process using iron-based coagulants: optimization by response surface methodology. Chem. Eng. J. 200, 39–51.

Liu, Y., Fang, H.H.P., 2003. Influences of extracellular polymeric substances (EPS) on flocculation, settling, and dewatering of activated sludge. Crit. Rev. Environ. Sci. Technol. 33, 237–273.

Liu, Y., Guo, H., Zhang, Y., Cheng, X., Zhou, P., Deng, J., Wang, J., Li, W., 2019. Highly efficient removal of trimethoprim based on peroxymonosulfate activation by carbonized resin with Co doping: performance, mechanism and degradation pathway. Chem. Eng. J. 356, 717–726.

Liu, Z., Li, X., Rao, Z., Hu, F., 2018b. Treatment of landfill leachate biochemical effluent using the nano-Fe_3O_4/$Na_2S_2O_8$ system: oxidation performance, wastewater spectral analysis, and activator characterization. J. Environ. Manag. 208, 159–168.

Liu, Z., Yang, S., Yuan, Y., Xu, J., Zhu, Y., Li, J., Wu, F., 2017. A novel heterogeneous system for sulfate radical generation through sulfite activation on a $CoFe_2O_4$ nanocatalyst surface. J. Hazard Mater. 324, 583–592.

Lu, Y., Xiao, Y., Zheng, G., Lu, J., Zhou, L., 2020. Conditioning with zero-valent iron or Fe^{2+} activated peroxydisulfate at an acidic initial sludge pH removed intracellular antibiotic resistance genes but increased extracellular antibiotic resistance genes in sewage sludge. J. Hazard Mater. 386.

Luo, C., Lin, Y., Zhang, Y., Zhang, S., Tong, S., Wu, S., Yang, C., 2023. S-scheme heterojunction between MOFs and Ag_3PO_4 leads to efficient photodegradation of antibiotics in swine wastewater. Separ. Purif. Technol. 320, 124052.

Luo, S., Wei, Z., Dionysiou, D.D., Spinney, R., Hu, W.-P., Chai, L., Yang, Z., Ye, T., Xiao, R., 2017. Mechanistic insight into reactivity of sulfate radical with aromatic contaminants through single-electron transfer pathway. Chem. Eng. J. 327, 1056–1065.

Luo, S., Wei, Z., Spinney, R., Villamena, F.A., Dionysiou, D.D., Chen, D., Tang, C.-J., Chai, L., Xiao, R., 2018. Quantitative structure–activity relationships for reactivities of sulfate and hydroxyl radicals with aromatic contaminants through single–electron transfer pathway. J. Hazard Mater. 344, 1165–1173.

Lutze, H.V., Bircher, S., Rapp, I., Kerlin, N., Bakkour, R., Geisler, M., von Sonntag, C., Schmidt, T.C., 2015. Degradation of chlorotriazine pesticides by sulfate radicals and the influence of organic matter. Environ. Sci. Technol. 49, 1673–1680.

Mahdi Ahmed, M., Barbati, S., Doumenq, P., Chiron, S., 2012. Sulfate radical anion oxidation of diclofenac and sulfamethoxazole for water decontamination. Chem. Eng. J. 197, 440–447.

Manoj, P., Mohan, H., Mittal, J.P., Manoj, V.M., Aravindakumar, C.T., 2007. Charge transfer from 2-aminopurine radical cation and radical anion to nucleobases: a pulse radiolysis study. Chem. Phys. 331, 351–358.

Mei, Q., Sun, J., Han, D., Wei, B., An, Z., Wang, X., Xie, J., Zhan, J., He, M., 2019. Sulfate and hydroxyl radicals-initiated degradation reaction on phenolic contaminants in the aqueous phase: mechanisms, kinetics and toxicity assessment. Chem. Eng. J. 373, 668–676.

Merzouk, B., Gourich, B., Madani, K., Vial, C., Sekki, A., 2011. Removal of a disperse red dye from synthetic wastewater by chemical coagulation and continuous electrocoagulation. A comparative study. Desalination 272, 246–253.

Mora, V.C., Rosso, J.A., Mártire, D.O., Gonzalez, M.C., 2011. Phenol depletion by thermally aChuctivated peroxydisulfate at 70°C. Chemosphere 84, 1270–1275.

Mustapha, N.A., Liu, H., Ibrahim, A.O., Huang, Y., Liu, S., 2021. Degradation of aniline in groundwater by persulfate with natural subsurface sediment as the activator. Chem. Eng. J. 417.

Norman, R.O.C., Storey, P.M., West, P.R., 1970. Electron spin resonance studies. Part XXV. Reactions of the sulphate radical anion with organic compounds. J. Chem. Soc. B Phys. Org. 1087–1095.

Oh, W.-D., Dong, Z., Lim, T.-T., 2016. Generation of sulfate radical through heterogeneous catalysis for organic contaminants removal: current development, challenges and prospects. Appl. Catal. B Environ. 194, 169–201.

Olmez-Hanci, T., Arslan-Alaton, I., 2013. Comparison of sulfate and hydroxyl radical based advanced oxidation of phenol. Chem. Eng. J. 224, 10–16.

Outsiou, A., Frontistis, Z., Ribeiro, R.S., Antonopoulou, M., Konstantinou, I.K., Silva, A. M.T., Faria, J.L., Gomes, H.T., Mantzavinos, D., 2017. Activation of sodium persulfate by magnetic carbon xerogels (CX/CoFe) for the oxidation of bisphenol A: process variables effects, matrix effects and reaction pathways. Water Res. 124, 97–107.

Pramanik, B.K., Hai, F.I., Roddick, F.A., 2019. Ultraviolet/persulfate pre-treatment for organic fouling mitigation of forward osmosis membrane: possible application in nutrient mining from dairy wastewater. Separ. Purif. Technol. 217, 215–220.

Pramod, G., Mohan, H., Manoj, P., Manojkumar, T.K., Manoj, V.M., Mittal, J.P., Aravindakumar, C.T., 2006. Redox chemistry of 8-azaadenine: a pulse radiolysis study. J. Phys. Org. Chem. 19, 415–424.

Qi, C., Liu, X., Lin, C., Zhang, H., Li, X., Ma, J., 2017. Activation of peroxymonosulfate by microwave irradiation for degradation of organic contaminants. Chem. Eng. J. 315, 201–209.

Qi, M., Lin, P., Shi, Q., Bai, H., Zhang, H., Zhu, W., 2023. A metal-organic framework (MOF) and graphene oxide (GO) based peroxymonosulfate (PMS) activator applied in pollutant removal. Process Saf. Environ. Protect. 171, 847–858.

Rastogi, A., Al-Abed, S.R., Dionysiou, D.D., 2009. Effect of inorganic, synthetic and naturally occurring chelating agents on Fe(II) mediated advanced oxidation of chlorophenols. Water Res. 43, 684–694.

Rayaroth, M.P., Aravind, U.K., Aravindakumar, C.T., 2015. Sonochemical degradation of Coomassie Brilliant Blue: effect of frequency, power density, pH and various additives. Chemosphere 119, 848–855.

Ren, X., Chen, C., Nagatsu, M., Wang, X., 2011. Carbon nanotubes as adsorbents in environmental pollution management: a review. Chem. Eng. J. 170, 395–410.

Rodríguez-Chueca, J., Amor, C., Silva, T., Dionysiou, D.D., Li Puma, G., Lucas, M.S., Peres, J.A., 2017. Treatment of winery wastewater by sulphate radicals: HSO_5^-/transition metal/UV-A LEDs. Chem. Eng. J. 310, 473–483.

Saha, J., Kumar Gupta, S., 2018. The production and quantification of hydroxyl radicals at economically feasible tin-chloride modified graphite electrodes. J. Environ. Chem. Eng. 6, 3991–3998.

Saputra, E., Muhammad, S., Sun, H., Ang, H.-M., Tadé, M.O., Wang, S., 2013a. Manganese oxides at different oxidation states for heterogeneous activation of peroxymonosulfate for phenol degradation in aqueous solutions. Appl. Catal. B Environ. 142–143, 729–735.

Saputra, E., Muhammad, S., Sun, H., Wang, S., 2013b. Activated carbons as green and effective catalysts for generation of reactive radicals in degradation of aqueous phenol. RSC Adv. 3, 21905–21910.

Schwarz, H.A., Dodson, R.W., 1984. Equilibrium between hydroxyl radicals and thallium (II) and the oxidation potential of hydroxyl(aq). J. Phys. Chem. 88, 3643–3647.

Shang, Y., Xu, X., Gao, B., Wang, S., Duan, X., 2021. Single-atom catalysis in advanced oxidation processes for environmental remediation. Chem. Soc. Rev. 50, 5281–5322.

Sharma, J., Mishra, I.M., Dionysiou, D.D., Kumar, V., 2015. Oxidative removal of Bisphenol A by UV-C/peroxymonosulfate (PMS): kinetics, influence of co-existing chemicals and degradation pathway. Chem. Eng. J. 276, 193–204.

Shi, Y., Yang, J., Yu, W., Zhang, S., Liang, S., Song, J., Xu, Q., Ye, N., He, S., Yang, C., Hu, J., 2015. Synergetic conditioning of sewage sludge via Fe^{2+}/persulfate and skeleton builder: effect on sludge characteristics and dewaterability. Chem. Eng. J. 270, 572–581.

Silveira, J.E., Zazo, J.A., Pliego, G., Casas, J.A., 2018. Landfill leachate treatment by sequential combination of activated persulfate and Fenton oxidation. Waste Manag. 81, 220–225.

Solís, R.R., Rivas, F.J., Ferreira, L.C., Pirra, A., Peres, J.A., 2018. Integrated aerobic biological–chemical treatment of winery wastewater diluted with urban wastewater. LED-based photocatalysis in the presence of monoperoxysulfate. J. Environ. Sci. Health, Part A 53, 124–131.

Song, G., Su, P., Zhang, Q., Wang, X., Zhou, M., 2023. Revisiting UV/sulfite exposed to air: a redox process for reductive dechlorination and oxidative mineralization. Sci. Total Environ. 859, 160246.

Soubh, A.M., Baghdadi, M., Abdoli, M.A., Aminzadeh, B., 2018. Zero-valent iron nanofibers (ZVINFs) immobilized on the surface of reduced ultra-large graphene oxide (rULGO) as a persulfate activator for treatment of landfill leachate. J. Environ. Chem. Eng. 6, 6568–6579.

Stanbury, D.M., 1989. Reduction potentials involving inorganic free radicals in aqueous solution. In: Sykes, A.G. (Ed.), Advances in Inorganic Chemistry. Academic Press, pp. 69–138.

Takdastan, A., Ravanbakhsh, M., Hazrati, M., Safapour, S., 2019. Removal of dinitrotoluene from petrochemical wastewater by Fenton oxidation, kinetics and the optimum experiment conditions. SN Appl. Sci. 1, 794.

Tan, C., Gao, N., Deng, Y., Deng, J., Zhou, S., Li, J., Xin, X., 2014. Radical induced degradation of acetaminophen with Fe_3O_4 magnetic nanoparticles as heterogeneous activator of peroxymonosulfate. J. Hazard Mater. 276, 452–460.

Timmins, G.S., Liu, K.J., Bechara, E.J.H., Kotake, Y., Swartz, H.M., 1999. Trapping of free radicals with direct in vivo EPR detection: a comparison of 5,5-dimethyl-1-pyrroline-N-oxide and 5-diethoxyphosphoryl-5-methyl-1-pyrroline-N-oxide as spin traps for HO• and $SO_4^{\bullet-}$. Free Radic. Biol. Med. 27, 329–333.

Tsitonaki, A., Petri, B., Crimi, M., Mosbaek, H., Siegrist, R.L., Bjerg, P.L., 2010. In situ chemical oxidation of contaminated soil and groundwater using persulfate: a review. Crit. Rev. Environ. Sci. Technol. 40, 55–91.

Ushani, U., Lu, X., Wang, J., Zhang, Z., Dai, J., Tan, Y., Wang, S., Li, W., Niu, C., Cai, T., Wang, N., Zhen, G., 2020. Sulfate radicals-based advanced oxidation technology in various environmental remediation: a state-of-the-art review. Chem. Eng. J. 402.

Vellanki, B.P., Batchelor, B., 2013. Perchlorate reduction by the sulfite/ultraviolet light advanced reduction process. J. Hazard Mater. 262, 348–356.

Wacławek, S., Grübel, K., Dennis, P., Vinod, V.T.P., Černík, M., 2016. A novel approach for simultaneous improvement of dewaterability, post-digestion liquor properties and toluene removal from anaerobically digested sludge. Chem. Eng. J. 291, 192–198.

Waldemer, R.H., Tratnyek, P.G., 2006. Kinetics of contaminant degradation by permanganate. Environ. Sci. Technol. 40, 1055–1061.

Waldemer, R.H., Tratnyek, P.G., Johnson, R.L., Nurmi, J.T., 2007. Oxidation of chlorinated ethenes by heat-activated persulfate: kinetics and products. Environ. Sci. Technol. 41, 1010–1015.

Wan, L.K., Peng, J., Lin, M.Z., Muroya, Y., Katsumura, Y., Fu, H.Y., 2012. Hydroxyl radical, sulfate radical and nitrate radical reactivity towards crown ethers in aqueous solutions. Radiat. Phys. Chem. 81, 524–530.

Wang, A., Jiang, Y., Yan, Y., Bu, L., Wei, Z., Spinney, R., Dionysiou, D.D., Xiao, R., 2023a. Mechanistic and quantitative profiling of electro-Fenton process for wastewater treatment. Water Res. 235, 119838.

Wang, C., Wang, X., Wang, H., Zhang, L., Wang, Y., Dong, C.-L., Huang, Y.-C., Guo, P., Cai, R., Haigh, S.J., Yang, X., Sun, Y., Yang, D., 2023b. Low-coordinated Co-N_3 sites induce peroxymonosulfate activation for norfloxacin degradation via high-valent cobalt-oxo species and electron transfer. J. Hazard Mater. 455, 131622.

Wang, G., Nie, X., Ji, X., Quan, X., Chen, S., Wang, H., Yu, H., Guo, X., 2019a. Enhanced heterogeneous activation of peroxymonosulfate by Co and N codoped porous carbon for degradation of organic pollutants: the synergism between Co and N. Environ. Sci. Nano 6, 399–410.

Wang, H., Guo, W., Liu, B., Wu, Q., Luo, H., Zhao, Q., Si, Q., Sseguya, F., Ren, N., 2019b. Edge-nitrogenated biochar for efficient peroxydisulfate activation: an electron transfer mechanism. Water Res. 160, 405–414.

Wang, J., Wang, S., 2020. Reactive species in advanced oxidation processes: formation, identification and reaction mechanism. Chem. Eng. J. 401, 126158.

Wang, S., Wang, G., Fu, Y., Liu, Y., 2021a. Sulfamethoxazole degradation by UV-Fe^{3+} activated hydrogen sulfite. Chemosphere 268.

Wang, W., Chen, M., Wang, D., Yan, M., Liu, Z., 2021b. Different activation methods in sulfate radical-based oxidation for organic pollutants degradation: catalytic mechanism and toxicity assessment of degradation intermediates. Sci. Total Environ. 772.

Wang, W., Wang, H., Li, G., An, T., Zhao, H., Wong, P.K., 2019c. Catalyst-free activation of persulfate by visible light for water disinfection: efficiency and mechanisms. Water Res. 157, 106–118.

Wang, X., Tang, P., Ding, C., Cao, X., Yuan, S., Zuo, X., Deng, X., 2017. Simultaneous enhancement of adsorption and peroxymonosulfate activation of Nitrogen-doped reduced graphene oxide for bisphenol A removal. J. Environ. Chem. Eng. 5, 4291–4297.

Wang, Y., Lin, Y., Yang, C., Wu, S., Fu, X., Li, X., 2023c. Calcination temperature regulates non-radical pathways of peroxymonosulfate activation via carbon catalysts doped by iron and nitrogen. Chem. Eng. J. 451, 138468.

Wang, Y., Zeng, X., Meng, Y., 2021c. Aqueous oxidation degradation of ciprofloxacin involving hydroxyl and sulfate radicals: a computational investigation. Comput. Theoret. Chem. 1204, 113427.

Wang, Z., Almatrafi, E., Wang, H., Qin, H., Wang, W., Du, L., Chen, S., Zeng, G., Xu, P., 2022a. Cobalt Single Atoms Anchored on Oxygen-doped Tubular Carbon Nitride for Efficient Peroxymonosulfate Activation: Simultaneous Coordination Structure and Morphology Modulation. Angewandte Chemie International Edition.

Wang, Z., Jiang, J., Pang, S., Zhou, Y., Guan, C., Gao, Y., Li, J., Yang, Y., Qiu, W., Jiang, C., 2018. Is sulfate radical really generated from peroxydisulfate activated by iron(II) for environmental decontamination? Environ. Sci. Technol. 52, 11276–11284.

Wang, Z., Qiu, W., Pang, S.-y., Guo, Q., Guan, C., Jiang, J., 2022b. Aqueous Iron(IV)–Oxo Complex: an emerging powerful reactive oxidant formed by iron(II)-based advanced oxidation processes for oxidative water treatment. Environ. Sci. Technol. 56, 1492–1509.

Wei, M., Gao, L., Li, J., Fang, J., Cai, W., Li, X., Xu, A., 2016. Activation of peroxymonosulfate by graphitic carbon nitride loaded on activated carbon for organic pollutants degradation. J. Hazard Mater. 316, 60–68.

Wen, G., Xu, X., Zhu, H., Huang, T., Ma, J., 2017. Inactivation of four genera of dominant fungal spores in groundwater using UV and UV/PMS: efficiency and mechanisms. Chem. Eng. J. 328, 619–628.

Wojnarovits, L., Takacs, E., 2019. Rate constants of sulfate radical anion reactions with organic molecules: a review. Chemosphere 220, 1014–1032.

Wood, P.M., 1988. The potential diagram for oxygen at pH 7. Biochem. J. 253, 287–289.

Wu, B., Dai, X., Chai, X., 2020. Critical review on dewatering of sewage sludge: influential mechanism, conditioning technologies and implications to sludge re-utilizations. Water Res. 180, 115912.

Wu, D., Ye, P., Wang, M., Wei, Y., Li, X., Xu, A., 2018a. Cobalt nanoparticles encapsulated in nitrogen-rich carbon nanotubes as efficient catalysts for organic pollutants degradation via sulfite activation. J. Hazard. Mater. 352, 148–156.

Wu, S., Li, H., Li, X., He, H., Yang, C., 2018b. Performances and mechanisms of efficient degradation of atrazine using peroxymonosulfate and ferrate as oxidants. Chem. Eng. J. 353, 533–541.

Wu, S., Shen, L., Lin, Y., Yin, K., Yang, C., 2021. Sulfite-based advanced oxidation and reduction processes for water treatment. Chem. Eng. J. 414.

Wu, S., Yang, C., Lin, Y., Cheng, J.J., 2022. Efficient degradation of tetracycline by singlet oxygen-dominated peroxymonosulfate activation with magnetic nitrogen-doped porous carbon. J. Environ. Sci. 115, 330–340.

Wu, X., Gu, X., Lu, S., Xu, M., Zang, X., Miao, Z., Qiu, Z., Sui, Q., 2014. Degradation of trichloroethylene in aqueous solution by persulfate activated with citric acid chelated ferrous ion. Chem. Eng. J. 255, 585–592.

Xia, H., Li, C., Yang, G., Shi, Z., Jin, C., He, W., Xu, J., Li, G., 2022a. A review of microwave-assisted advanced oxidation processes for wastewater treatment. Chemosphere 287.

Xia, X., Luo, J., Liu, D., Liu, T., Wu, C., Qian, F., 2022b. Metal-free graphene-based catalytic membranes for persulfate activation toward organic pollutant removal: a review. Environ. Sci. Pollut. Control Ser. 29, 75184–75202.

Xiao, K., Chen, Y., Jiang, X., Yang, Q., Seow, W.Y., Zhu, W., Zhou, Y., 2017. Variations in physical, chemical and biological properties in relation to sludge dewaterability under Fe (II) - oxone conditioning. Water Res. 109, 13–23.

Xiao, R., Liu, K., Bai, L., Minakata, D., Seo, Y., Goktas, R.K., Dionysiou, D.D., Tang, C.-J., Wei, Z., Spinney, R., 2019. Inactivation of pathogenic microorganisms by sulfate radical: present and future. Chem. Eng. J. 371, 222–232.

Xiao, R., Ye, T., Wei, Z., Luo, S., Yang, Z., Spinney, R., 2015. Quantitative structure–activity relationship (QSAR) for the oxidation of trace organic contaminants by sulfate radical. Environ. Sci. Technol. 49, 13394–13402.

Xiao, S., Cheng, M., Zhong, H., Liu, Z., Liu, Y., Yang, X., Liang, Q., 2020. Iron-mediated activation of persulfate and peroxymonosulfate in both homogeneous and heterogeneous ways: a review. Chem. Eng. J. 384, 123265.

Xie, F., Shi, Q., Bai, H., Liu, M., Zhang, J., Qi, M., Zhang, J., Li, Z., Zhu, W., 2023. An anode fabricated by Co electrodeposition on ZIF-8/CNTs/CF for peroxymonosulfate (PMS) activation. Chemosphere 313, 137384.

Xie, F., Zhu, W., Lin, P., Zhang, J., Hao, Z., Zhang, J., Huang, T., 2022. A bimetallic (Co/Fe) modified nickel foam (NF) anode as the peroxymonosulfate (PMS) activator: characteristics and mechanism. Separ. Purif. Technol. 296, 121429.

Xie, P., Guo, Y., Chen, Y., Wang, Z., Shang, R., Wang, S., Ding, J., Wan, Y., Jiang, W., Ma, J., 2017. Application of a novel advanced oxidation process using sulfite and zero-valent iron in treatment of organic pollutants. Chem. Eng. J. 314, 240–248.

Xie, X., Zhang, Y., Huang, W., Huang, S., 2012. Degradation kinetics and mechanism of aniline by heat-assisted persulfate oxidation. J. Environ. Sci. 24, 821–826.

Xiong, L., Ren, W., Lin, H., Zhang, H., 2021. Efficient removal of bisphenol A with activation of peroxydisulfate via electrochemically assisted Fe(III)-nitrilotriacetic acid system under neutral condition. J. Hazard Mater. 403, 123874.

Xu, M., Yao, J., Sun, S., Yan, S., Sun, J., 2021. Theoretical calculation on the reaction mechanisms, kinetics and toxicity of acetaminophen degradation initiated by hydroxyl and sulfate radicals in the aqueous phase. Toxics 9.

Xu, X., Pliego, G., Zazo, J.A., Casas, J.A., Rodriguez, J.J., 2016. Mineralization of naphtenic acids with thermally-activated persulfate: the important role of oxygen. J. Hazard Mater. 318, 355–362.

Xu, X., Zhan, F., Pan, J., Zhou, L., Su, L., Cen, W., Li, W., Tian, C., 2022. Engineering single-atom Fe-Pyridine N_4 sites to boost peroxymonosulfate activation for antibiotic degradation in a wide pH range. Chemosphere 294, 133735.

Yan, N., Zhong, H., Brusseau, M.L., 2019. The natural activation ability of subsurface media to promote in-situ chemical oxidation of 1,4-dioxane. Water Res. 149, 386–393.

Yang, L., Xue, J., He, L., Wu, L., Ma, Y., Chen, H., Li, H., Peng, P., Zhang, Z., 2019a. Review on ultrasound assisted persulfate degradation of organic contaminants in wastewater: influences, mechanisms and prospective. Chem. Eng. J. 378.

Yang, Q., Choi, H., Al-Abed, S.R., Dionysiou, D.D., 2009. Iron–cobalt mixed oxide nanocatalysts: heterogeneous peroxymonosulfate activation, cobalt leaching, and ferromagnetic properties for environmental applications. Appl. Catal. B Environ. 88, 462–469.

Yang, Q., Ma, Y., Chen, F., Yao, F., Sun, J., Wang, S., Yi, K., Hou, L., Li, X., Wang, D., 2019b. Recent advances in photo-activated sulfate radical-advanced oxidation process (SR-AOP) for refractory organic pollutants removal in water. Chem. Eng. J. 378.

Yang, S., Wang, P., Yang, X., Shan, L., Zhang, W., Shao, X., Niu, R., 2010. Degradation efficiencies of azo dye Acid Orange 7 by the interaction of heat, UV and anions with common oxidants: persulfate, peroxymonosulfate and hydrogen peroxide. J. Hazard Mater. 179, 552–558.

Yang, S., Xiao, T., Zhang, J., Chen, Y., Li, L., 2015. Activated carbon fiber as heterogeneous catalyst of peroxymonosulfate activation for efficient degradation of Acid Orange 7 in aqueous solution. Separ. Purif. Technol. 143, 19–26.

Yang, S., Yang, J., Tang, J., Zhang, X., Ma, J., Zhang, A., 2022. A comparative study of the degradation of refractory organic matter in MBR effluent from landfill leachate treatment by the microwave-enhanced iron-activated hydrogen peroxide and peroxydisulfate processes. Process Saf. Environ. Protect. 162, 955–964.

Yang, S., Yang, X., Shao, X., Niu, R., Wang, L., 2011. Activated carbon catalyzed persulfate oxidation of Azo dye acid orange 7 at ambient temperature. J. Hazard. Mater. 186, 659–666.

Yang, X., Cai, J., Wang, X., Li, Y., Wu, Z., Wu, W.D., Chen, X.D., Sun, J., Sun, S.-P., Wang, Z., 2020a. A bimetallic Fe-Mn oxide-activated oxone for in situ chemical oxidation (ISCO) of trichloroethylene in groundwater: efficiency, sustained activity, and mechanism investigation. Environ. Sci. Technol. 54, 3714–3724.

Yang, Y., Lu, X., Jiang, J., Ma, J., Liu, G., Cao, Y., Liu, W., Li, J., Pang, S., Kong, X., Luo, C., 2017. Degradation of sulfamethoxazole by UV, UV/H_2O_2 and UV/persulfate (PDS): formation of oxidation products and effect of bicarbonate. Water Res. 118, 196–207.

Yang, Y., Sun, M., Zhou, J., Ma, J., Komarneni, S., 2020b. Degradation of orange II by Fe@Fe_2O_3 core shell nanomaterials assisted by $NaHSO_3$. Chemosphere 244, 125588.

Yao, Y., Lian, C., Wu, G., Hu, Y., Wei, F., Yu, M., Wang, S., 2017. Synthesis of "sea urchin"-like carbon nanotubes/porous carbon superstructures derived from waste biomass for treatment of various contaminants. Appl. Catal. B Environ. 219, 563–571.

Ye, J., Dai, J., Wang, L., Li, C., Yan, Y., Yang, G., 2021a. Investigation of catalytic self-cleaning process of multiple active species decorated macroporous PVDF membranes through peroxymonosulfate activation. J. Colloid Interface Sci. 586, 178–189.

Ye, J., Dai, J., Yang, D., Li, C., Yan, Y., Wang, Y., 2021b. 2D/2D confinement graphene-supported bimetallic Sulfides/g-C_3N_4 composites with abundant sulfur vacancies as highly active catalytic self-cleaning membranes for organic contaminants degradation. Chem. Eng. J. 418.

Ye, J., Li, C., Wang, L., Wang, Y., Dai, J., 2021c. Synergistic multiple active species for catalytic self-cleaning membrane degradation of persistent pollutants by activating peroxymonosulfate. J. Colloid Interface Sci. 587, 202–213.

Yousefi, N., Pourfadakari, S., Esmaeili, S., Babaei, A.A., 2019. Mineralization of high saline petrochemical wastewater using Sonoelectro-activated persulfate: degradation mechanisms and reaction kinetics. Microchem. J. 147, 1075–1082.

Yu, D., Cui, J., Li, X., Zhang, H., Pei, Y., 2020. Electrochemical treatment of organic pollutants in landfill leachate using a three-dimensional electrode system. Chemosphere 243, 125438.

Yuan, S., Liao, P., Alshawabkeh, A.N., 2014. Electrolytic manipulation of persulfate reactivity by iron electrodes for trichloroethylene degradation in groundwater. Environ. Sci. Technol. 48, 656–663.

Yuan, Y., Yang, S., Zhou, D., Wu, F., 2016. A simple Cr(VI)–S(IV)–O_2 system for rapid and simultaneous reduction of Cr(VI) and oxidative degradation of organic pollutants. J. Hazard. Mater. 307, 294–301.

Yuan, Y., Zhao, D., Li, J., Wu, F., Brigante, M., Mailhot, G., 2018. Rapid oxidation of paracetamol by Cobalt(II) catalyzed sulfite at alkaline pH. Catal. Today 313, 155–160.

Yue, R., Sun, X., 2021. A Self-cleaning, catalytic titanium carbide (MXene) membrane for efficient tetracycline degradation through peroxymonosulfate activation: performance evaluation and mechanism study. Separ. Purif. Technol. 279.

Zemel, H., Fessenden, R.W., 1978. The mechanism of reaction of sulfate radical anion with some derivatives of benzoic acid. J. Phys. Chem. 82, 2670–2676.

Zhang, B.-T., Zhang, Y., Teng, Y., Fan, M., 2015. Sulfate radical and its application in decontamination technologies. Crit. Rev. Environ. Sci. Technol. 45, 1756–1800.

Zhang, G., Yang, X., Wu, Z., Wu, W.D., Wang, X., Chen, X.D., Sun, S.-P., 2022a. Fe-Mn bimetallic oxide-enabled facile cleaning of microfiltration ceramic membranes for effluent organic matter fouling mitigation via activation of oxone. ACS ES T Water 2, 1234–1246.

Zhang, H., Xie, C., Chen, L., Duan, J., Li, F., Liu, W., 2023a. Different reaction mechanisms of $SO_4^{\bullet-}$ and •OH with organic compound interpreted at molecular orbital level in Co(II)/peroxymonosulfate catalytic activation system. Water Res. 229.

Zhang, J., Shao, X., Shi, C., Yang, S., 2013a. Decolorization of Acid Orange 7 with peroxymonosulfate oxidation catalyzed by granular activated carbon. Chem. Eng. J. 232, 259–265.

Zhang, K., Parker, K.M., 2018. Halogen radical oxidants in natural and engineered aquatic systems. Environ. Sci. Technol. 52, 9579–9594.

Zhang, L., Chen, L., Xiao, M., Zhang, L., Wu, F., Ge, L., 2013b. Enhanced decolorization of orange II solutions by the Fe(II)-sulfite system under xenon lamp irradiation. Ind. Eng. Chem. Res. 52, 10089–10094.

Zhang, T., Li, W., Croué, J.-P., 2012. A non-acid-assisted and non-hydroxyl-radical-related catalytic ozonation with ceria supported copper oxide in efficient oxalate degradation in water. Appl. Catal. B Environ. 121–122, 88–94.

Zhang, X., Jia, S., Song, J., Wu, S., Han, X., 2018. Highly efficient utilization of soluble Fe in the removal of arsenic during oxidative flocculation of Fe(II). Bull. Chem. Soc. Jpn. 91, 998–1007.

Zhang, X., Zhang, H., Wang, Z., Liu, T., Guo, D., Hu, Z., 2023b. Enhanced paper sludge dewatering and in-depth mechanism by oxalic acid/Fe^{2+}/persulfate process. Chemosphere 311, 136966.

Zhang, Y.-J., Chen, J.-J., Yu, H.-Q., 2022c. Semi-quantitative probing of reactive oxygen species in persulfate-based heterogeneous catalytic oxidation systems for elucidating the reaction mechanism. Chem. Eng. J. 446, 137237.

Zhang, Y., Yang, W., Zhang, K., Kumaravel, A., Zhang, Y., 2021. Sulfite activation by glucose-derived carbon catalysts for As(III) oxidation: the role of ketonic functional groups and conductivity. Environ. Sci. Technol. 55, 11961–11969.

Zhao, X., Wang, Y., Ye, Z., Borthwick, A.G.L., Ni, J., 2006. Oil field wastewater treatment in biological aerated filter by immobilized microorganisms. Process Biochem. 41, 1475–1483.

Zhao, Y., Yang, L., Chen, S., Wang, X., Ma, Y., Wu, Q., Jiang, Y., Qian, W., Hu, Z., 2013. Can boron and nitrogen Co-doping improve oxygen reduction reaction activity of carbon nanotubes? J. Am. Chem. Soc. 135, 1201–1204.

Zhao, Z., Li, Y., Zhou, Y., Hou, Y., Sun, Z., Wang, W., Gou, J., Cheng, X., 2023. Activation of sulfite by micron-scale iron-carbon composite for metronidazole degradation: theoretical and experimental studies. J. Hazard Mater. 448, 130873.

Zhen, G., Lu, X., Su, L., Kobayashi, T., Kumar, G., Zhou, T., Xu, K., Li, Y.-Y., Zhu, X., Zhao, Y., 2018. Unraveling the catalyzing behaviors of different iron species (Fe_{2+} vs. Fe) in activating persulfate-based oxidation process with implications to waste activated sludge dewaterability. Water Res. 134, 101–114.

Zhen, G., Tan, Y., Wu, T., Wang, J., Lu, X., Zhao, Y., Zhu, X., Niu, J., Xiong, J., 2019. Strengthened dewaterability of coke-oven plant oily sludge by altering extracellular organics using Fe(II)-activated persulfate oxidation. Sci. Total Environ. 688, 1155–1161.

Zheng, R., Li, J., Zhu, R., Wang, R., Feng, X., Chen, Z., Wei, W., Yang, D., Chen, H., 2022. Enhanced Cr(VI) reduction on natural chalcopyrite mineral modulated by degradation intermediates of RhB. J. Hazard Mater. 423, 127206.

Zhou, D., Chen, L., Li, J., Wu, F., 2018a. Transition metal catalyzed sulfite auto-oxidation systems for oxidative decontamination in waters: a state-of-the-art minireview. Chem. Eng. J. 346, 726–738.

Zhou, L., Zheng, W., Ji, Y., Zhang, J., Zeng, C., Zhang, Y., Wang, Q., Yang, X., 2013. Ferrous-activated persulfate oxidation of arsenic(III) and diuron in aquatic system. J. Hazard Mater. 263, 422–430.

Zhou, P., Zhang, J., Zhang, Y., Zhang, G., Li, W., Wei, C., Liang, J., Liu, Y., Shu, S., 2018b. Degradation of 2,4-dichlorophenol by activating persulfate and peroxomonosulfate using micron or nanoscale zero-valent copper. J. Hazard Mater. 344, 1209–1219.

Zhou, X., Ke, M.-K., Huang, G.-X., Chen, C., Chen, W., Liang, K., Qu, Y., Yang, J., Wang, Y., Li, F., Yu, H.-Q., Wu, Y., 2022. Identification of Fenton-like active Cu sites by heteroatom modulation of electronic density. Proc. Natl. Acad. Sci. U. S. A. 119, e2119492119.

Zhu, C., Fang, G., Dionysiou, D.D., Liu, C., Gao, J., Qin, W., Zhou, D., 2016. Efficient transformation of DDTs with persulfate activation by zero-valent iron nanoparticles: a mechanistic study. J. Hazard Mater. 316, 232–241.

Zou, J., Lin, Y., Yang, C., 2023. Covalency triggers high catalytic activity of amorphous molybdenum oxides for oxidative desulfurization. Sci. China Chem. 66, 1211–1220.

Zou, J., Ma, J., Chen, L., Li, X., Guan, Y., Xie, P., Pan, C., 2013. Rapid acceleration of ferrous iron/peroxymonosulfate oxidation of organic pollutants by promoting Fe (III)/Fe(II) cycle with hydroxylamine. Environ. Sci. Technol. 47, 11685–11691.

Zrinyi, N., Pham, A.L.-T., 2017. Oxidation of benzoic acid by heat-activated persulfate: effect of temperature on transformation pathway and product distribution. Water Res. 120, 43–51.